POLITECNICO DI TORINO

Master's Degree in Mathematical Engineering

Mathematical Modeling and Numerical Simulation

Master's Degree Thesis

A mathematical model for neuron reorientation and axonal outgrowth on a cyclically stretched substrate

Supervisors

Prof. Chiara GIVERSO

Prof. Luigi PREZIOSI

Dr. Annachiara COLOMBI

Candidate

Andrea BATTAGLIA

October 2023

Abstract

Throughout their lifetime, neurons are constantly exposed to a large variety of mechanical stimuli in many physiological circumstances. In this regard, experimental evidence demonstrated how mechanical cues play a central role in determining the direction and velocity of axonal outgrowth. In particular, neurons seeded on planar substrates undergoing periodic stretches have been shown to reorient almost perpendicularly to the main stretching direction, reaching a stable equilibrium orientation in correspondence with angles within the interval [60°, 90°]. The entire reorientation and outgrowth process is guided by a highly motile structure at the axon tip: the growth cone. In this Thesis, we present a new model for the reorientation and growth of neurons in response to cyclic stretching. A linear viscoelastic model for the growth cone reorientation with the addition of a stochastic term is merged with a moving-boundary model for tubulin-driven neurite growth to simulate the axonal pathfinding process. Various combinations of stretching frequencies and strain amplitudes have been tested, through the numerical simulation of the proposed model. Specifically, simulations show that neurons tend to reorient almost perpendicularly to the stretching direction in great agreement with biological evidence. Moreover, the model captures the relation between the stretching condition and the velocity of reorientation. Indeed, numerical results show that as the frequency and amplitude of oscillation increase, neurons tend to reorient themselves more rapidly.

Table of Contents

List of Tables

List of Figures

Chapter 1

Introduction

The significance of electrochemical signals in numerous cellular processes has been acknowledged and under investigation for several years. Nevertheless, only recently, more focus has been directed towards the cellular response to mechanical stimuli coming from the surrounding environment. There are many biological circumstances in which mechanical cues are relevant such as growth, differentiation, embryogenesis, and motility [1–3]. In addition, understanding the mechanical interactions of cells with the environment can be fundamental in providing insights into various pathologies and in developing new methods for tissue engineering applications. Various types of cells, including fibroblasts, myofibroblasts, cardiomyocytes, and endothelial cells, have been studied for their mechanical sensitivity. However, in this work, we are going to focus on how the neuron cells respond to mechanical actions, specifically on the importance of mechanical cues in the axonal growth mechanism which comprehends both the elongation and guidance phases. The study will examine the reorientation of neurons under cyclic stretch conditions, with a particular emphasis on the biological observations reported in [4].

So far, the development of the nervous system has been mainly studied in the context of biochemistry, molecular biology and genetics. However, there is a growing recognition of the importance of mechanical information in shaping the evolution and development of the neuronal network. It has been shown through experimental evidence that processes like neural migration, axon extension and neural stem cell differentiation are influenced by mechanical forces and cues [5–7].

Understanding the mechanism involved in the above-mentioned phenomena is fundamental and of great interest nowadays because neurons, both in the central and peripheral nervous system, undergo constant mechanical loading during their life cycle. For example, some peripheral nerves adapt continuously during the extension and flexion of joints. The nerves must sustain and rapidly adapt to the tension generated by the high rate of growth of some big mammalians. Indeed, the blue whale's spinal chord is reported to increase its length by 2 cm/day and its

spinal axons can reach a total length of 10 m-30 m [8–10]. A similar axon growth rate is peculiar of the giraffe's neck nerves [8]. The centrality role of forces has also been discovered in the gyrification. During the brain folding process, the brain size increases and numerous active and passive forces act in and on the cortex over different length and time scales. The cortical neurons must adapt to the tension exerted on them during this process, depending on the region they are placed. However, recent studies have shown how neurons could play an active role in the process as generators of tension. This gives an enlightening explanation of how the brain cortex folds [5, 7]. Some *in vitro* experiments demonstrate how different stiffness of the culture substrate, different mechanical stimuli and different substratum topographies affect the gene expression and protein synthesis in neural stem cells [7]. This leads us to think that mechanics plays a central role during embryogenesis. All these experiments, show how mechanical cues have an important role throughout all scales in nervous system development, from the molecular assembly in a single neuron to the final configuration of the whole nervous system.

Among all these phenomena, our aim is to investigate the neurite outgrowth in response to a dynamic mechanical stimulation. In particular, we are interested in studying how the neurites' shape and outgrowth direction can be controlled by an applied cyclic stretch. The morphology of neuron cells and the different mechanisms involved in the axonal growth will be presented in Section 1.1 followed by a more detailed list of experimental evidence on how mechanical cues affect the neurites' growth. In this section, particular attention will be put on the neurons' response to cyclic stress. Section 1.2 is devoted to a short review of the mathematical models for the axonal elongation and reorientation. Finally, the aim and the structure of this dissertation are stated in Section 1.3.

1.1 Biological background

1.1.1 Neuron morphology

Neurons are the basic unit cells of the nervous system. They are among the most complex cells of the animal kingdom because of their peculiar morphology and their ability to communicate with other excitable cells through electrochemical signalling pathways. Neurons are cells with a distinct polarity and they are morphologically divided into: *soma*, *dendrites*, *axon* and the *axon tip* (Fig. 1.1). The dendrites and the axon are globally identified as *neurites*. The soma, also known as *cell body*, is the central part of the neuron containing the nucleus and most of the cellular organelles. It processes incoming signals from the dendrites and generates outgoing signals. The dendrites are branching structures extending from the cell body that receive signals from other neurons or sensory receptors. The axon is the longest

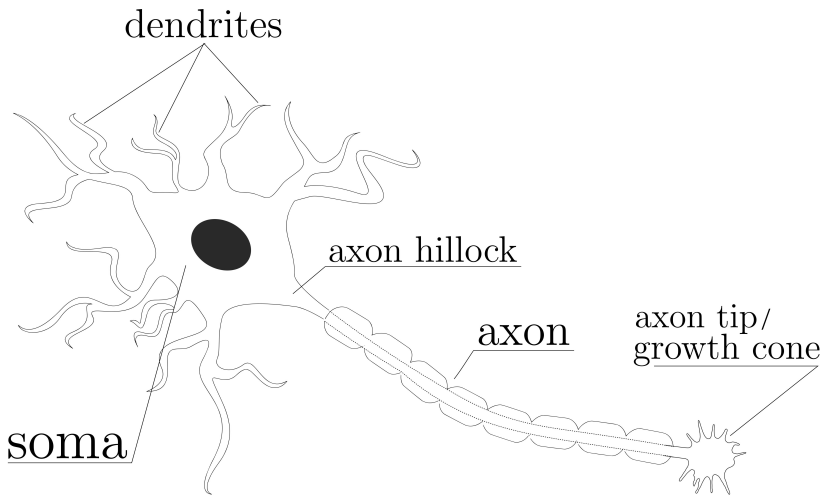

Figure 1.1: Morphology of a neuron. Once the neuron is settled, the growth cone transforms into a series of synaptic boutons.

neurite of the neuron and it carries the electrochemical signals from the soma to the axon terminals which are connected to other neurons or tissues. The axon tip is a highly motile structure, also known as *growth cone*. The growth cone has an important role during the axonal pathfinding process in the early stages of axonal growth. It serves as a guide for the axon and it determines the speed and direction of the axon outgrowth. Once the axon establishes contact with a targeted neuron or another tissue cell, the growth cone loses most of its motility by transitioning to a series of branched terminations. Each of these terminations ends with a *synapse* [5, 11, 12].

As we will see, the growth cone plays a central role in the early stage of axonal development. For this reason, it is necessary to take a look at its specific morphology in order to better understand how neuron development works. The growth cone is a highly dynamic hand-shaped termination of a neurite. It presents a very dense cytoskeleton structure shown in Fig. 1.2. The peripheral domain, also called *P-domain*, consists of finger-like filopodia made of F-actin bundles. These bundles are also known as *stress fibers*. Then, there is a transitional zone (*T-domain*) made of actomyosin contractile structures which form sort of arcs perpendicular to the F-actin filaments. Finally, the *C-domain* is the inner part of the growth cone. Here we have all the microtubules (MTs) that enter the growth cone from the axonal shaft.

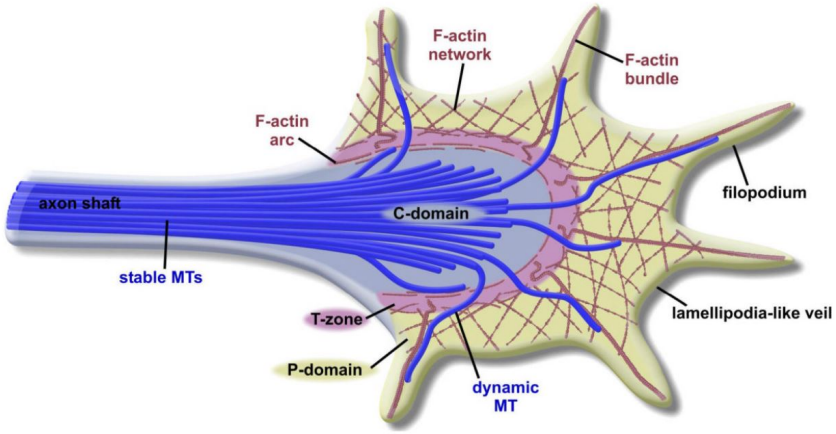

Figure 1.2: Cytoskeleton of the growth cone. Taken with permission from [13].

1.1.2 Axonal elongation

Neuronal growth is the key process necessary to establish the neuronal network during neurogenesis. The most relevant process for neuronal growth is the axonal elongation, i.e. the addition of new cellular material to the axon. This phenomenon has been proven to happen in two consecutive stages, both driven by mechanical tension [8, 14]. The first phase is called *tip-growth*, while the second stage is known as *stretch growth* or *towed axon* phase.

Tip-growth

The newly born axon is guided by the growth cone (GC) through a pool of chemo-mechanical cues and obstacles to reach its final target. The GC is able to move in a spatially biased way to translate environmental signals into directional movement towards the target cell. This entire process is known as *axonal pathfinding*. Growth cones can integrate a large variety of stimuli such as chemotropic molecules, electric signals, mechanical triggers, topography and stiffness of the substrate. Once the GC has identified the preferred direction of growth, a complex cytoskeletal remodelling process starts and leads to the axonal elongation in the growth cone's preferred direction. The GC advancement pulls the axon and the tension generated on it leads to the axonal elongation. This has been first proven by Lamoureux in 1989 and presented in [15]. During this phase the new cellular material is added in correspondence with the axon tip [12, 13].

In more details, the axon outgrowth process is divided into three stages, said *protrusion*, *engorgement* and *consolidation* [12, 13] which are represented in Fig. 1.3 and described in the following.

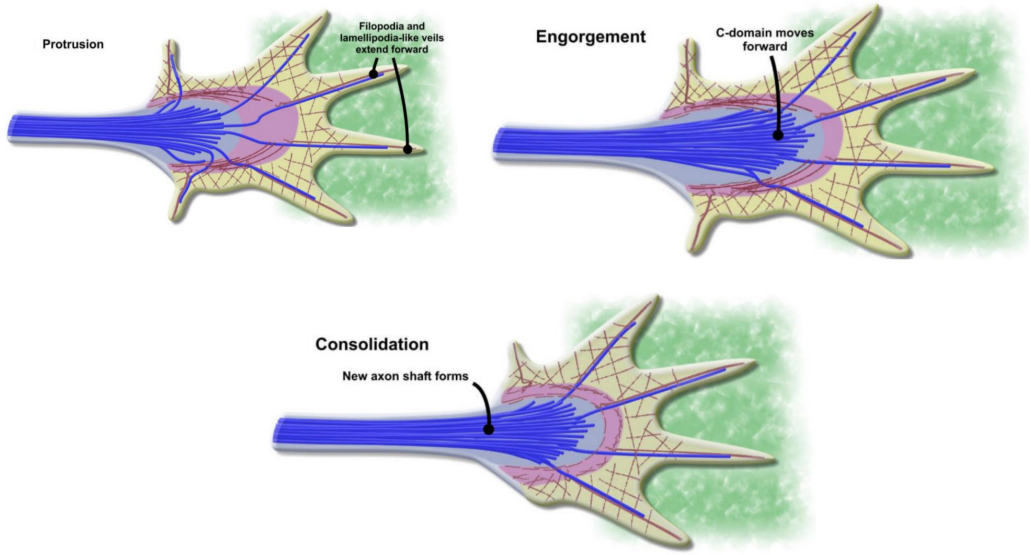

Figure 1.3: Phases of axon outgrowth. Adapted with permission from [13].

Protrusion. The actin bundles couple to the substrate via focal adhesion points. This happens thanks to cells-adhesion molecules that serve to create a clutch between the cytoskeleton and the extracellular matrix. This leads to a decrease of the F-actin retrograde flow rate enhancing the polymerization of the actin filaments against the GC external membrane. As a consequence, the filopodia and lamellopodia move forward to extend the leading edge of the growth cone. This process pulls the axonal shaft and provokes the axonal elongation. The higher the pulling magnitude, the more space is generated for the development of new microtubules. Hence, the higher is the pulling force, the longer will be the resulting axon.

Engorgement. The actin in the T-domain is removed and the arc myosin-II structures let the microtubules grow and invade the P-domain. In this phase, new cell material is added to the axon tip by the polymerization of tubulin at the free ends of the MTs. The quantity of free tubulin present in the growth cone and its assembly rate determines the magnitude of axonal outgrowth.

Consolidation. The myosin-II arcs compact the newly formed MTs in a new localized C-domain advanced with respect to the previous position. The F-actin polymerization slows down and goes back to an equilibrium with the actin retrograde flow. Filopodia retract and the whole process is ready to start again along a new preferred direction.

Our current understanding of how the axonal pathfinding phenomenon works is

far from complete. However, we can firmly state that the asymmetrical distribution of traction forces in the remodelling process of GC's cytoskeleton leads the axon to change its growing direction [12]. If the resulting force is not aligned with the previous growth direction, the GC's base is pulled toward the side of higher tension, which thus determines the area that the microtubules can invade and toward which they bend. To summarize, neurite growth depends on the complex interplay of active pushing and pulling forces mediated by the growth cone traction, the tubulin transportation and the microtubules assembly.

Stretch growth

Once the growth cone reaches the targeted cell, the axon is established and the synaptic connection is created. At this point, we step into the second stage of the axonal elongation: the *stretch growth* or *towed axon* phase. This phase is still poorly understood and it has received less attention than the tip-growth process. Nevertheless, it is well known that axon elongation happens because of the tension generated by the migration of the target cells which pull the neuron. This second stage of elongation allows neurons to adapt in cases such as the growth of an organism. During the stretch growth process, new material is no longer added to the axon tip. It is although added in various spots along the axon, most probably in correspondence with the axon hillock, i.e. in the proximity of the soma (see Fig. 1.1). The towed axon elongation phase was first theorized and presented in [16] by Weiss in 1941. Then experiments conducted by Bray [17] and Dennerll [18] biologically validated the theory.

1.1.3 Experimental results

We will now discuss some experiments that have been carried out to study neurons' responses to different types of mechanical stimuli. It is important to note that these studies were carried out on various types of neuronal cells, including those in the peripheral and central nervous systems of different organisms. Certain mechanical properties may not be universally applicable to all neurons, but are rather specific to the experimental model being used. Therefore, some experimental results may appear contradictory and inconsistent with one another.

As already stated, the ability of cultured neurites to elongate under the application of tension was first demonstrated by Bray in [17]. He also showed that the initiation and elongation of neurites could be regulated by tension and that the role of the cellular cytoskeleton is fundamental for the stabilization of neurons. Bray's work has been validated and extended by Dennerll et al. in [18] and Zheng et al. in [19]. They both recreated the condition of stretch growth by pulling the axon tip of different neurons with glass needles in order to increase the tension

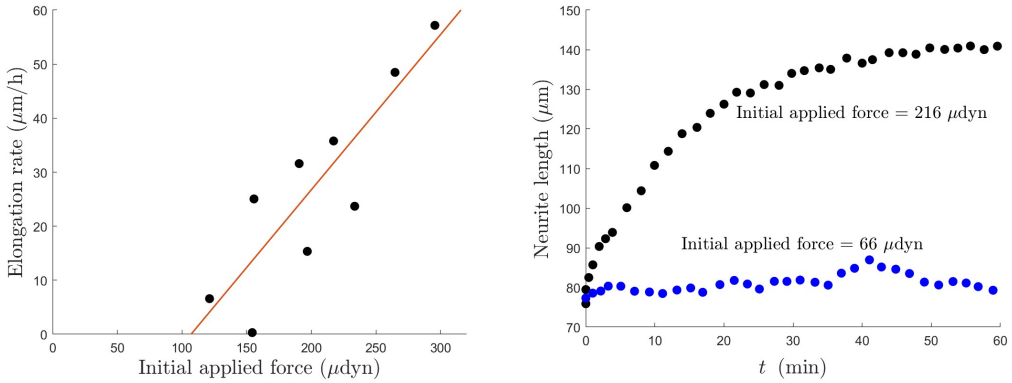

(a) Elongation rate of PC12 neurites as function of applied tension

(b) Response of two PC12 neurites to applied forces greater and less than 100 µdyn

Figure 1.4: Plots created from the experimental data collected by Dennerll in [18]. In (a) the elongation rate of PC12 neurites as a function of the initial applied tension is plotted. In this experiment, the minimum threshold value to have axonal elongation is 100 µdyn. In (b) is shown the response of two PC12 neurites to applied forces greater and less than 100 µdyn identified as the minimum threshold value to have axonal elongation.

on the neurite. They found the existence of a linear relation between the growth rate and the tension applied, with surprisingly high sensitivity (see Fig. 1.4a). An increase in tension of 1 µdyn leads to an average increase of the elongation rate equal to 1.5 µdyn/h. However, there exists a minimum tension threshold below which axon elongation does not happen (see Fig. 1.4b). For chick sensory neurons, this critical value has been reported to vary from 50 µdyn to 150 µdyn in most cases[20]. However, this value can vary and it is peculiar of each neuron. There has also been identified a lower limit tension value, called *rest tension*, which is the minimum tension that the axon tends to maintain in physiological conditions. Each neuron has its own rest tension and its value usually spans from 2 nN to 5 nN[21]. Furthermore, nerves are naturally subject to tension even in homeostatic conditions, as they are interconnected with other tissues characterized by the ability to contract and relax, such as motor muscles or the heart. The continuous change in configuration of such tissues forces neurons to constantly regulate the internal tension along the axon in order to prevent damage to their cellular functions. In the case of axonal slackening, when the tension along the axon is below the rest value, the axon starts to actively regulate its internal tension and undergo a straightening process. That's the reason why neurons generally tend to assume a straight-line configuration. This phenomenon has recently been explored in depth

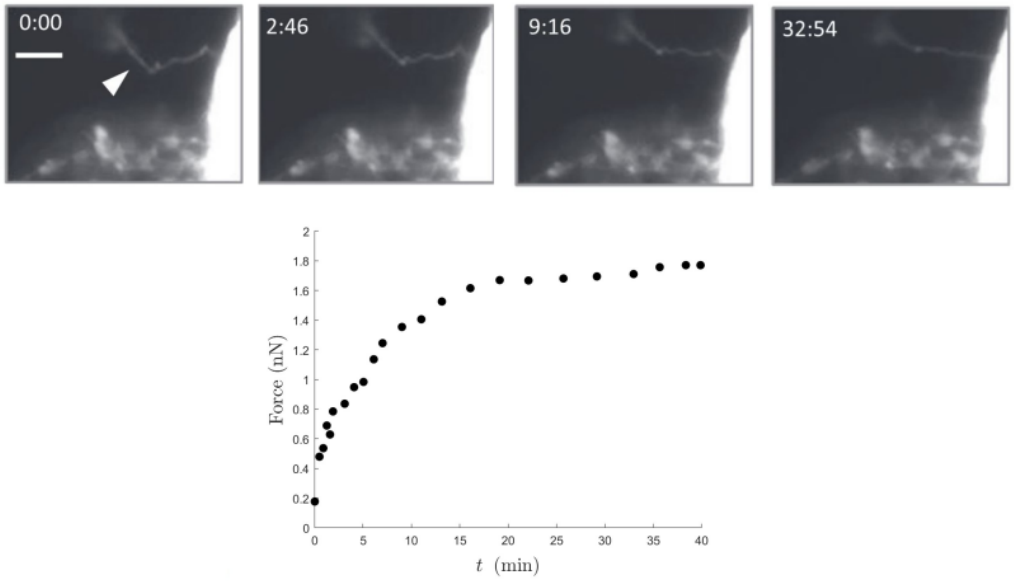

Figure 1.5: Experimental results taken with permission from [21] are presented. The sequence on the top shows the straightening process of a neuron after the axonal slackening (scale bar: 40 µm). The graph below shows how the tension along the axon is gradually restored to its rest value (around 2 nN in this case).

by Rajagopalan et al. in [21]. In addition to the straightening process, in order to maintain a constant tension as the axon length increases, the cross-sectional area of the axonal shaft grows by the addition of new cellular material [18]. These biological observations provide a simple control mechanism for axons to accommodate tissue enlargement in growing animals.

Further investigations on stretch growth phenomena have been carried out by Pfister et al. in [8]. They used a microstepper motor system to evaluate the effects of escalating rates of stretch on integrated axon tracts over days to weeks in culture. The *in vitro* experiments showed how mechanical stimuli can induce extreme axonal growth and even exceed every previously observed limit of neurite growth. Indeed, under ideal conditions, an 8 mm/day rate of stretch growth has been reached. Extreme growth occurs with a gradual increase in the strain rate of the applied deformation. The strain rate step should be small and spaced with acclimation periods otherwise neurons undergo disconnection with damages to their internal structure.

Other studies have been addressed on the importance of substrate compliance in neuron development. Since axonal tension is modulated by the nature of neuronal anchorage to its substrate, substrate stiffness has been shown to have a strong influence on the axonal growth mechanism. Neuronal cells physiologically grow

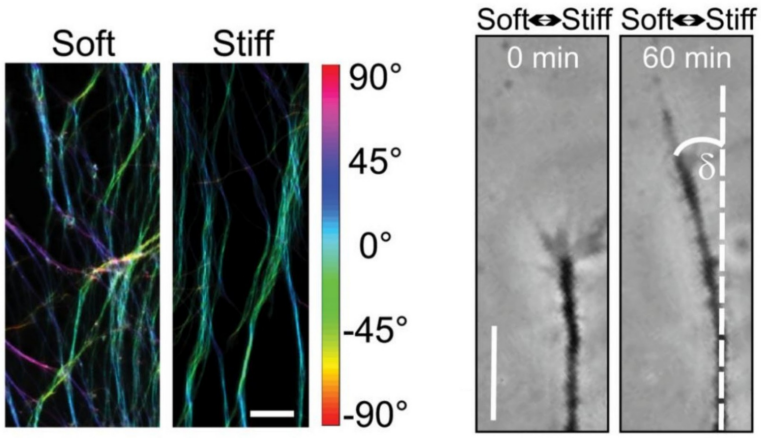

Figure 1.6: Some results from the experiments conducted in [23]. On the left panel, the different directionality of growth between the softer and the stiffer substrate is visible (scale bar: 20 µm). On the right panel, the negative durotaxis of a nerve can be observed (scale bar: 15 µm). The images are taken with permission from [23].

on substrates that are softer than those where other types of cells develop. That holds true in particular for the neurons of the central nervous system. Indeed the physiological stiffness of the brain tissue stands around 0.1 kPa [7]. In this regard, Koch et al. [22] conducted a study on the distinct behaviour of neurons belonging to the CNS (central nervous system) and PNS (peripheral nervous system) on substrates with varying levels of stiffness. Substrates ranging from 150 Pa to 5000 Pa have been used. Hippocampal neurons, part of the central nervous system, have shown an outgrowth independence on the substrate stiffness. On the contrary, dorsal root ganglion cells (part of the peripheral nervous system) displayed robust outgrowth on stiffer substrates ($\sim$ 1000 Pa) and difficulties in growing on the softer ones. The same topic has been investigated by Koser et al. in [23]. They observed the growth of *Xenopus* retinal ganglion axons *in vivo*. Growth on a stiffer (1 kPa) and a softer (0.1 kPa) substrate has been analysed. The average extension velocity of axons was significantly higher on stiff than on soft substrates. Also, the directionality of growth has been influenced by substrate compliance (see Fig. 1.6, left panel). While on stiffer substrates, axons grew rather straight and parallel to each other, on softer substrates axons grew less coherently. Another astonishing result observed is the negative durotaxis the nerves undergo (see Fig. 1.6, right panel). Indeed, fascicles of neurons in the presence of a stiffness gradient in the substrate tend to bend and grow towards the softer part of the substrate.

Lately, many works in literature have headed the attention on the role of the

geometrical features of the substrate on the axonal outgrowth. Many types of micropatterned substrates have been tested in order to screen if the substrate topography can effectively promote different aspects of neuronal development. Usually, the nano-imprinted patterns consist of parallel grooves with various depths, widths and distances between adjacent ridges. The size of such grooves usually spans from 1 µm to 100 µm as in [20, 24–26], up to 500 µm as in [27, 28]. In most of the experiments, axons grew in the longitudinal direction of grooves, even though their behaviour changes in relation to the topography dimensions and the neuron cell characteristics. The maximum alignment along the patterns happens when the spacing of the grooves matches the linear dimension of the growth cone (2 µm-10 µm) [25, 26]. Moreover, the nerve cells prefer to grow on ridge edges and elevations rather than in grooves [27]. The experiments in [29] show how neurons can potentially assume every shape by following the substrate topography, i.e. circular, squared and hexagonal grooves. However, in some cases, neurons show the ability to cross the grooves and do not follow the pattern alignment by growing perpendicularly to the ridges. This behaviour is observed to depend on the diameter and Young's modulus of axons [20].

Cyclic stretch

By now, it is recognized and experimentally proven that several types of cells align along a precise direction in response to a deformation applied on the substrate they are attached to. When a monolayer of cells experiences cyclic deformation, the cells positioned on the substrate tend to adjust their orientation in a specific manner. This adjustment continues until they achieve a stable configuration characterized by a clearly defined angle between their axis and the direction of principal stretching [1, 3, 30–33]. However, whether neurons have a similar response to cyclic stretching remains an elusive issue even though the directional alignment and outgrowth of neurons is a critical step of nerve regeneration engineering and functional recovery of nerve systems. Most mechanobiological studies in neuroscience focus on cellular responses to static strain, as reported in the previous subsection, and there has been very limited effort to reveal the role of dynamic mechanical stimulation on neurogenesis. Throughout their lifetime, neuronal cells are constantly exposed to cyclic strain. For instance, the brain tissue is highly vascularized. Brain perfusion is demonstrated to provoke a cyclic tissue deformation in the range of 2% [34]. Also, the movements of the head can induce mild accelerations that deform the brain matter with strains up to 5% with peaks of 10%-15% in some extreme sports activities [34]. Deformation may reach much higher rates during embryogenesis. Another example is the case in which nerves should sustain high levels of strain caused by the tissues they are interconnected with, such as the skin, the heart and

the muscles. Skeletal muscle cells are reported to reach levels of strain around 25%-35% [35]. The normal myocardial strain in humans falls into the 16%-22% interval, but if we consider the radial strain the values are much higher (35%-59%) [36]. Finally, the shoulder skin can reach strain levels from 40% to 60% [37]. Therefore, cyclic stretch is a physiological condition that the nervous system experiences on a daily basis.

One of the first attempts at studying how periodic stretching can promote neurite outgrowth has been performed by Higgins et al. in [38]. They had stimulated for 7 days SH-SY5Y human neuroblastoma cells with a cyclic uniaxial stretch with of 10% strain rate and 0.25 Hz frequency. They actually found out that cell stretching alone induced noticeable neurite outgrowth with respect to the control group. Ishibashi et al. presented a similar work in [39]. Dorsal root ganglion neurons have been triggered with a uniaxial cyclic stretch with 10% strain rate and frequencies in the 0.25 Hz-1 Hz range. Experiments showed how frequency has little impact on enhancing neurite outgrowth, while time is an essential parameter. The longer neurons were stretched, the higher their extension rate was. A more accurate study has been delivered by Haq et al. in [35]. They investigated the combined effect of strain rate and frequency on PC12 cells development. The considered deformations with 4%, 8%, 16% strain rates and 0.1 Hz, 0.5 Hz, 1 Hz frequencies. The influence of a micro-textured substrate has been also analysed. Strain rate and frequency have been discovered to have an interrelated relationship. Specifically, at high strain levels, increasing the frequency decreases the development of neurite extensions, whereas at low strain rates, increasing the frequency increases the development of neurites. For what concerns the directionality of axon growth, the high strain condition (16% at 1.0 Hz) caused most of the neurites to orient away from the direction of the applied strain. The other stretch conditions tested (4% and 8% amplitudes with different frequencies) led to a more uniform distribution of the axon directions. Embryonic rat cortical neurons' have been exposed to relatively high strain rate values (7%, 15% and 28%) with a 0.3 Hz frequency in [34]. Despite the high deformation imposed, neural cells showed high resilience and they all survived. All the tests displayed directed outgrowth of neurites with a preferred branch direction away from the main strain direction. The steered neuronal outgrowth effect became more pronounced with increasing amplitudes to ultimately reach average axon orientations nearly perpendicular to the deformation direction. In this experimental setting, strain rate has been discovered to be more influential on the axonal orientation process than the frequency. This result is in contrast with experimental findings on other cell types where frequency has been demonstrated to have a stronger influence on the reorientation process than the strain amplitude [1, 3, 30]. In [35], where PC12 neuron cells have been tested, the frequency seems to be just an accelerator of the orientation process, but it does not influence the final stable angle orientation.

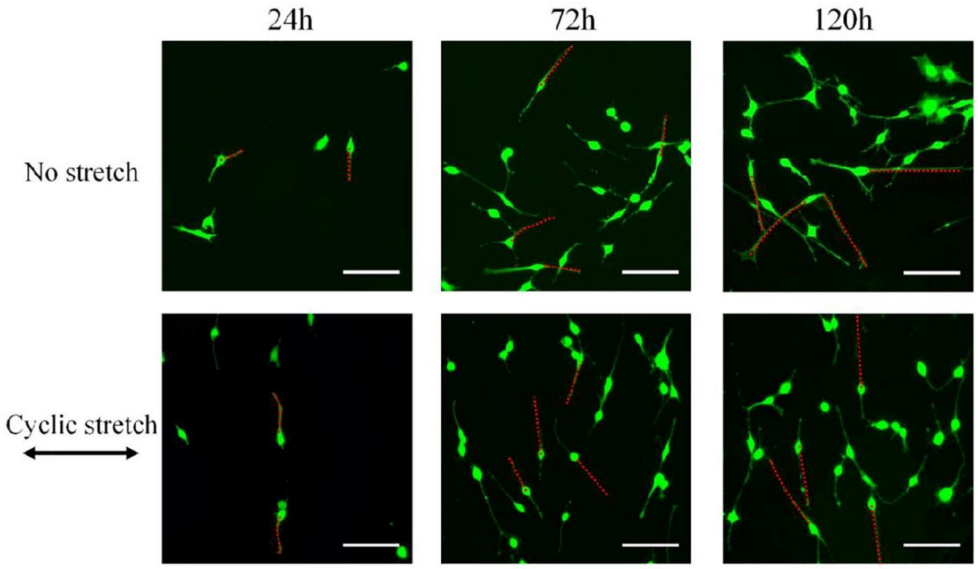

Figure 1.7: Images of the tests conducted in [4] on PC12 cells after 24, 72, and 120 h. The upper row is the control sample. In the lower row a cyclic stretch with 10% amplitude and 0.25 Hz frequency has been applied. Scale bar: 100 µm. Images taken with permission from [4].

In this dissertation, we are going to focus on the results delivered by Lin et al. in [4]. We are going to use it as the main reference because of its completeness in reporting experimental evidence on the effects of cyclic stretch on neuron reorientation and axon outgrowth. The article will be used to validate the mathematical model we will develop in the next sections by comparing our numerical results to the biological observations reported in the literature. In this work [4], a stretching device has been used to impose a cyclic uniaxial deformation to a PDMS substrate on which PC12 cells were cultured. Polydimethylsiloxane (PDMS) is a silicone elastomer widely used in micro and nanotechnology applications, microfluidic devices, optical systems and sensors. Thanks to its high biocompatibility, this material is widely used in biological experiments as well. Usually, the PDMS samples are coated with collagen or fibronectin to favour cell attachment; poly-L-lysine may be added to increase the biocompatibility level. PDMS usually offers high elasticity and its properties remain stable in time if subjected to temperature fluctuations [40]. However, the mechanical characteristics of this material are easily tunable by varying the samples-making process, i.e. the curing temperature or the mixing ratio of the base polymer and the cross-linking curing agent [41–43]. In particular, in [4] they used 20×60×1 mm PDMS strips (Sylgard 184, 10:1) that were cured for 2 h at 80 °C. For what concerns the experimental stretching condition of the substrate,

relatively low values of stretching amplitudes (2–10%) and frequencies (0.05–0.25 Hz) have been adopted. Results have been collected after 24h, 72h and 120h of stretching period (see Fig. 1.7). It was observed that neurons tend to align away from the stretch direction when stretching amplitude and frequency are sufficiently large. In particular, stretch amplitude seems to be relevant in provoking neurons' reorientation. For low strain values (2%) axons do not align along a particular direction even though maximum frequency is applied. With higher strain values (5% - 10%) neurons align almost perpendicularly to the main stretch direction. Frequency has more influence on the timing of the reorientation phenomenon. The higher is the frequency, the faster it happens. In addition, experiments show that the axon elongation rate is hardly affected by cyclic stretch. More details on the results present in [4] will be delivered in Section 4.

1.2 Mathematical modelling background

Formalizing biological processes to create mathematical models allows for a comprehensive understanding of the fundamental aspects of such phenomena and offers a direct way to test hypotheses. In this section, we will present some mathematical models developed to understand the underlying mechanisms responsible for neuron development. A complete review of such models can be found in [14].

The first attempt at modelling axons and their mechanical behaviour has been made by Dennerll in [18]. After discovering the relationship existing between tension and axon growth rate, he proposed a way to mechanically model the axon. In order to best reproduce the viscoelastic behaviour of neurites, he has proposed a combination of three classical mechanical elements: a relatively stiff spring in series with a Voigt element, in parallel with a dashpot, corresponding to a standard linear solid (see Fig. 1.8a). Considering then the fact that over a certain tension threshold axon undergoes elongation, a further dashpot has been added to the model giving the so-called Burgers element (see Fig. 1.8a). The results in [18] have been later deepened in [44] where an investigation into the mechanical properties of neurons has been conducted. More recently, Dennerll's work has been extended by O'Toole et al. in [45] with the inclusion in the model of the adhesion between the axon and the substrate. They treated the neurite under tension as a series of dashpots, while the attachments to the substrate have been represented as friction dashpots (Fig. 1.8b).

For what concerns the neurite growth process, several models exist. The first approach consists in modelling the neurite by compartmental models. Each compartment proposed in [46–51] is associated with one chemical concentration and exchanges material with other compartments via diffusion and/or active transport by motor proteins. In [50] the simplest situation is modelled, considering two

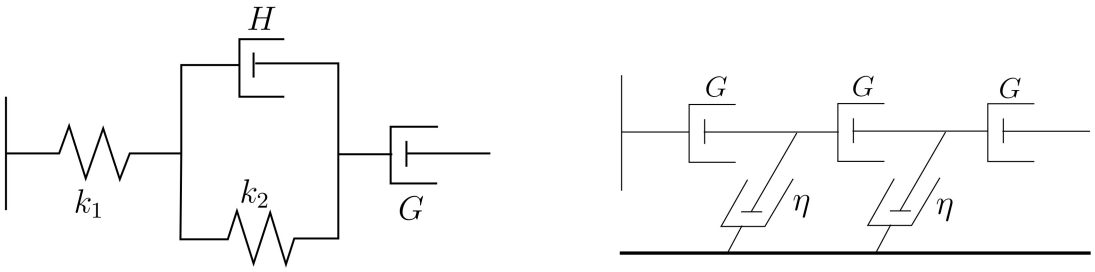

(a) Burgers element **(b)** Model for axon and substrate interaction

Figure 1.8: In (a) k_1 and k_2 are the spring constants. H is the constant of the first free dashpot while G is the growth dashpot constant. In (b) the axon modelled as in [45]: a series of growing dashpots with constant G. The attachments to the substrate are friction dashpots with constant η.

compartments: the soma and the growth cone. Growth relies on the concentration of tubulin in the axon tip and it is supplied by the soma through diffusion and active transport. The model has been extended in [51] by introducing a limiting growth factor. Afterwards, the previous compartmental models have been refined by considering the value of the concentration at every point along the neurite, thus one-dimensional continuum models of axonal elongation have been developed in [46–49]. In particular, the model given in [48] is a one-dimensional moving-boundary model for tubulin-driven axonal growth made up of a coupled system of three differential equations. The first PDE describes the time and spatial evolution of tubulin along the axonal shaft following a classical convection-diffusion problem. The other ODEs describe the evolution in time of the axonal length and the free tubulin concentration in the GC. This model will be completely reported in Section 2.4 because it will be part of the model proposed in the current dissertation.

Some models in the literature aim to reproduce more complex phenomena than simple axon growth, such as axon turning, beading, and changes in the axons' cross-sectional area. For example, in a recent study [52], a three-dimensional continuum mechanical model was presented for axonal shaft development. The model represents the neurite as a stress-free cylinder with a given initial cross-sectional area and length, fixed in correspondence with the soma end. The shaft's mechanical behaviour is based on the morphoelasticity theory, which successfully reproduces growth, retraction, and axonal turning in response to guidance cues. Similarly, another study [53] used a similar morphoelastic approach to model and reproduce the negative durotactic response observed in nerves [23]. Axon bundles are modelled as morphoelastic rods with motion analogous to that of optic rays. Interestingly, Snell's law proves to be an excellent mechanism for reproducing the peculiar durotactic response of neurons [53].

Lately, some models have been addressed to reproduce the dynamics of neuronal cells cultured on patterned surfaces. In [54] a general stochastic approach is used. The growth cone movement is described by Langevin and Fokker-Planck equations with both deterministic and stochastic contributions. Growth alignment is determined by surface geometry, and it is quantified by the deterministic part of the Langevin equation. A physical approach has instead been used in [20]. A 3D physical model of axonal outgrowth was developed. In this model, axon shafts are simulated as elastic 3D beams with focal contacts with the substrate. The bending direction of axon tips is governed by the energy minimization principle. The model predicts both axonal groove ridge crossing and alignment in relation to the geometrical and mechanical properties of the axons.

As mentioned before, there is a lack of investigations on the effects of cyclic stretch on neuron reorientation. Thus, very few mathematical models have been developed to better understand and reproduce the phenomenon. This is surprising considering the fact that there are, instead, numerous models aimed at explaining the phenomenon of reorientation in other cell types than neurons [1, 3, 10, 30–33]. Usually, these works focused on creating models in which the equilibrium orientation angle of the cells coincides with the minimum strain, the minimum stress or the minimum energy configuration. In particular, models that are based on the minimization of energy have shown a high accuracy in reproducing the biological evidence of the cell reorientation process. So far, the only theoretical framework aimed at explaining the neuron alignment under dynamical stretch is the one proposed by Lin et al. in [4]. In this article, in addition to the experiments that have been already discussed, they propose a mathematical model for neuron reorientation and axonal outgrowth. The idea of such model is to connect the evolution of neuron orientation and configuration to the microscopic dynamics of subcellular structures, such as stress fibers, focal adhesions, and microtubules. The numeric results are finally compared to the biological observations they made resulting in a model that well reproduces the experimental evidences.

1.3 Aim and structure of the Thesis

As mentioned earlier, it is clear that there is still a lot to be learned about the complex mechanisms that govern the development of neuronal cells. In particular, the way in which these cells respond to mechanical stimuli is an area that has not been extensively studied in the literature. This is particularly true when it comes to understanding how these cells react to cyclic stretching. Consequently, the development of mathematical models in this regard has significant potential for advancement, even though it is quite challenging.

The aim of this Thesis is to introduce a new model for the reorientation and

growth of neurons in response to cyclic stretching. We plan to model the neuron by dividing it into three main parts: soma, axon, and growth cone. Afterwards, we will simulate the tip growth phase and axonal guidance in response to dynamic mechanical stimuli. The soma is supposed fixed, while an ODE gives the equation of motion of the GC in the Lagrangian frame. The GC position depends on its orientation and speed. The orientations will be given by an adaptation of the linear viscoelastic model presented in [1] that has been originally developed for other cell types' reorientation phenomenology. The speed of the axon tip will be instead derived by the diffusion tubulin-driven model for axonal growth presented in [48].

The rest of the Thesis is organized as it follows. In Chapter 2 the mathematical model is fully presented. First, we report some continuum mechanics basic notations. Then, we formulate the hypothesis on the substrate's mechanical behaviour and the equation of motion for the growth cone is given. Afterwards, we infer the reorientation model equations for the growth cone by adapting the work done in [1] and then we add the one-dimensional model for the axonal growth given in [48].

In Chapter 3 the numerical implementation of the whole model is delivered. The equations are discretized by using an explicit Euler scheme for the time derivatives and finite differences schemes for the spatial terms. The integral terms are as well approximated by using explicit numerical schemes. The discretized equations are numerically solved using MATLAB ®.

In Chapter 4 we set all the parameters and conditions involved in the model. We then show the results of the numerical simulations, showing that they both qualitatively and quantitively agree with the experimental observations given in [4].

In Chapter 5, we will conclude the dissertation by summarizing the results obtained, recalling the assumptions we made and discussing the limitations of the proposed model. Lastly, some possible modifications and expansions of the model for possible future works will be presented.

Chapter 2

Mathematical model

In this Chapter, the mathematical model for neuron growth and reorientation in response to the cyclic stretch of the underlying substrate is presented. Our model combines the linear viscoelastic model for cell reorientation given in [1] with the one-dimensional axon growth model delivered in [48].

In Section 2.1 we recall some notions of continuum mechanics [55, 56]. Then, in Section 2.2 a short review of the main model assumptions is presented. The general frame to describe and quantify the axon morphology is delivered, as well as the hypothesis on the substrate behaviour. We then focus on the growth cone axonal pathfinding process. Afterwards, we present in Section 2.3 an adaptation of the linear viscoelastic model for cell reorientation given in [1]. We define an elastic energy and by its minimization the equilibrium angles are computed. To model the randomness in the living beings' behaviour, a stochastic term is added to the reorientation equation in Section 2.3.2. Finally, in Section 2.4, we follow what is done in [48] to develop a one-dimensional moving-boundary model for tubulin-driven axonal growth.

2.1 Mechanical framework

Let $\mathcal{B}_*$ be the *reference configuration*, namely the substrate when no stretch is applied. A particle in this configuration can be identified by the *Lagrangian coordinates* $\mathbf{X} = (X_K)$. Then, once the deformation has been applied, we can identify the *current configuration* $\mathcal{B}_t$ at time t (see Fig. 2.1). We denote the coordinates of a particle in the deformed configuration by the *Eulerian coordinates* $\mathbf{x} = (x_i)$. The two configurations are linked by a smooth map χ, called *finite deformation*, which assigns to a general material point $\mathbf{X}$ a spatial point $\mathbf{x}$ as follows

$$\mathbf{x} = \chi(\mathbf{X}, t) \in \mathcal{B}_t \quad \forall (\mathbf{X}, t) \in \mathcal{B}_* \times [0, T]. \tag{2.1}$$

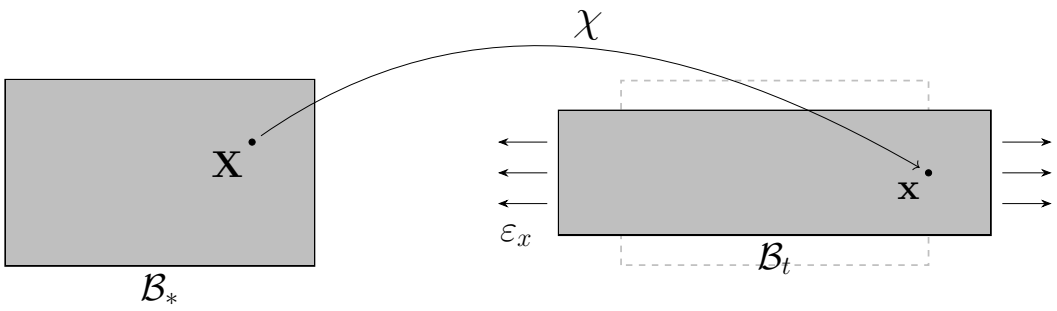

Figure 2.1: Reference configuration and current configuration in the case of a uniaxial stretch.

We can now introduce the *deformation gradient tensor* $\mathbb{F}$, a linear application that associates each infinitesimal vector $d\mathbf{X}$ in $\mathcal{B}_*$ with the correspondent infinitesimal vector $d\mathbf{x}$ in $\mathcal{B}_t$:

$$d\mathbf{x} = \mathbb{F}(\mathbf{X}, t)\, d\mathbf{X}. \tag{2.2}$$

The representative matrix of this tensor is

$$\mathbb{F} = (F_{iK}) = \left(\frac{\partial x_i}{\partial X_K}\right), \tag{2.3}$$

We require that $\det \mathbb{F} > 0$ in every point of the continuum media and at any instant time.

The vector that links the position of a material point $\mathbf{X}$ in the reference configuration to its correspondent position in the deformed configuration is called *displacement*:

$$\mathbf{u} \coloneqq \chi(\mathbf{X}, t) - \mathbf{X} = \mathbf{x} - \mathbf{X}. \tag{2.4}$$

The gradient of $\mathbf{u}$ allows us to rewrite the deformation gradient in the following form

$$\mathbb{F} = \mathbb{I} + \operatorname{Grad} \mathbf{u}, \quad \text{where} \quad (\operatorname{Grad} \mathbf{u})_{iK} = \frac{\partial u_i}{\partial X_K}, \tag{2.5}$$

where $\mathbb{I}$ is the *second order identity tensor*.

There are other mathematical entities that will be useful for our purposes. The first one is the *right Cauchy-Green deformation tensor*

$$\mathbb{C} \coloneqq \mathbb{F}^\top \mathbb{F}. \tag{2.6}$$

The aforementioned tensor measures how much the deformed body differs from the undeformed one.

The other mechanical definition that will be useful in our dissertation is the *Cauchy stress tensor* $\mathbb{T}$. Let us first consider the general tension $\mathbf{t}$ defined as the

surface load per surface unit considered on the body $\mathcal{B}_t$. The *Cauchy hypothesis of simple continuum* states that

$$\mathbf{t} = \mathbf{t}(\mathbf{x}, t, \mathbf{n}), \tag{2.7}$$

where $\mathbf{x}$ is a point on the surface we are considering and $\mathbf{n}$ is its outward normal vector with respect to the control volume one is considering. The *Cauchy's theorem* assures the existence and uniqueness of the second-order stress tensor $\mathbb{T}$, such that the surface load may be written as

$$\mathbf{t} = \mathbb{T}\mathbf{n}. \tag{2.8}$$

We now take into account the case in which the displacement $\mathbf{u}$ of every material point is relatively small. We can define a deformation as *infinitesimal* when the gradient of the displacement is very small, i.e. $\|\mathrm{Grad}\,\mathbf{u}\| \ll 1$ or $\|\mathrm{Grad}\,\mathbf{u}\| \sim \delta$ where δ is an infinitesimal parameter. In this setting, we define the *infinitesimal strain tensor* as

$$\mathbb{E} \coloneqq \frac{1}{2}\left[\mathrm{Grad}\,\mathbf{u} + (\mathrm{Grad}\,\mathbf{u})^{\top}\right]. \tag{2.9}$$

The tensor $\mathbb{E}$ coincides with the symmetrical part of $\mathrm{Grad}\,\mathbf{u}$ and it can be interpreted as a first approximation of $\mathbb{C}$. Indeed, by neglecting all the terms of a higher order than the linear one, we can write

$$\mathbb{C} = \mathbb{I} + 2\mathbb{E} + o(\epsilon). \tag{2.10}$$

Then, the infinitesimal strain tensor provides all the information needed to characterize the deformation applied to the body.

Let us now consider a generic unit vector $\mathbf{d}$ along whose direction we take a segment of infinitesimal length dS in the Lagrangian configuration. We define the *longitudinal strain*, with respect to the direction $\mathbf{d}$, in the following way

$$\varepsilon(\mathbf{d}) \coloneqq \frac{ds - dS}{dS} = \mathbf{d} \cdot \mathbb{E}\mathbf{d}, \tag{2.11}$$

where ds is the length of the segment after the deformation, i.e. in the current configuration. The longitudinal strain is simply the ratio between the length variation of an infinitesimal segment, due to a given deformation, and its initial length in the reference configuration. The general matrix form of the infinitesimal strain tensor can thus be expressed as

$$\mathbb{E} = \begin{bmatrix} \varepsilon_1 & \gamma_{12}/2 & \gamma_{13}/2 \\ \gamma_{12}/2 & \varepsilon_2 & \gamma_{23}/2 \\ \gamma_{13}/2 & \gamma_{23}/2 & \varepsilon_3 \end{bmatrix}, \tag{2.12}$$

where $\varepsilon_i = \varepsilon(\mathbf{d}_i)$ are the longitudinal strains (or normal strains) along the directions $\mathbf{d}_i$ and $\gamma_{ik} = \gamma(\mathbf{d}_i, \mathbf{d}_k)$ are the shear strains. These types of strains represent the change in angle between two perpendicular elements of the body undergoing the deformation. The directions along which the shear strains are null are called *principal directions* and the relative strains applied in these directions are named *principal strains*. Recalling that $\mathbb{E}$ is symmetric, it is always possible to find an orthogonal coordinate system with axes oriented along the principal directions and such that Eq. (2.12) thus writes

$$\mathbb{E} = \begin{bmatrix} \varepsilon_x & 0 & 0 \\ 0 & \varepsilon_y & 0 \\ 0 & 0 & \varepsilon_z \end{bmatrix}, \tag{2.13}$$

where x, y and z denote the principal directions. In this work, we will set the x axis in the direction of the maximum applied stretch which is a principal direction and z orthogonal to the substrate.

2.2 Model assumptions

2.2.1 Neuron model and substrate mechanics

In this section, some considerations about the mechanical properties of the substrate and the mathematical representation of the neuron.

Substrate mechanical properties. The first thing to point out is that neurons are attached to the substrate, hence the whole cell body perceives the deformation that is externally imposed on it. In fact, thanks to the presence of focal adhesion (FAs) and stress fibers in the cell, the PDMS deformation is transferred to the soma, the axon and the growth cone. We do not explicitly model FAs and the process of force transmission and we will assume that the deformation of the substrate is completely transferred to the neuron. Then, for simplicity, we suppose that the traction forces generated by all the cellular structures don't modify the mechanical behaviour of the substrate. Considering the range of strain amplitudes experimentally tested in [4] and that we are going to numerically reproduce in our model, we decide to treat the substrate as linear, elastic and isotropic [41].

As mentioned in the previous Chapter, the particular experimental set-up used to study cell reorientation phenomena consists of a thin strip of PDMS on which cells are seeded. It allows us to apply the *plane strain* approximation, i.e. the substrate is treated as a 2D layer and every deformation along the z axis is neglected. In addition, the experimental data are usually reported for cells located in the

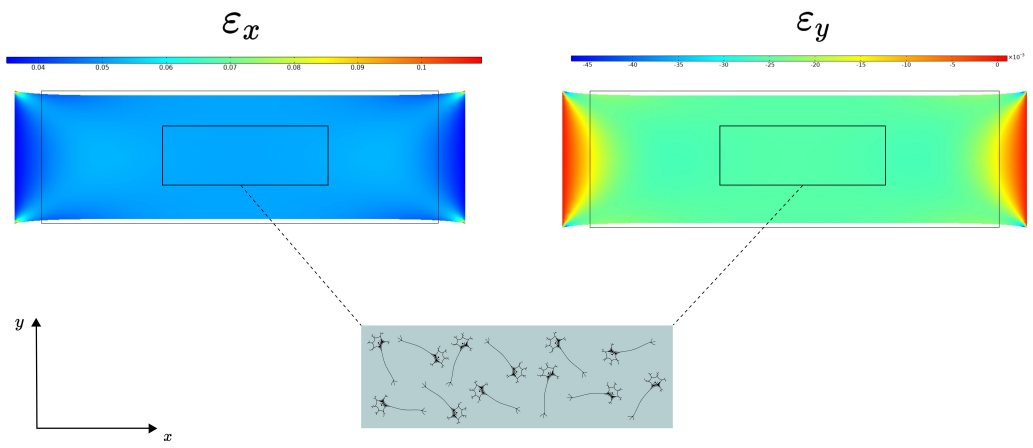

Figure 2.2: COMSOL simulation of the stretched substrate. The strains along the principal directions are plotted considering a deformation with $\varepsilon = 5\%$.

central portion of the substrate as reported in Fig. 2.2. In that area, we can assume that the stress and the strain are homogeneous, as also shown in Fig. 2.2 obtained using COMSOL. Then, the principal directions coincide with the axis along which the stretch is applied and the orthogonal one. Then Eq. (2.13) becomes

$$\mathbb{E} = \begin{bmatrix} \varepsilon_x & 0 \\ 0 & \varepsilon_y \end{bmatrix}, \tag{2.14}$$

whereas the deformation gradient takes the form

$$\mathbb{F} \approx \mathbb{I} + \mathbb{E} = \begin{bmatrix} 1+\varepsilon_x & 0 \\ 0 & 1+\varepsilon_y \end{bmatrix}. \tag{2.15}$$

In the majority of experiments, the applied strain along the x direction is usually a waveform function like

$$\varepsilon_x(t) = \frac{1}{2}\varepsilon\left[1 - \cos(\omega t)\right] = \frac{1}{2}\varepsilon\left[1 - \cos(2\pi f t)\right] \tag{2.16}$$

where ε is the maximum strain amplitude, ω is the angular frequency expressed in rad/s and f is the frequency expressed in Hz. The strain along the y axis ε_y can be either controlled externally (biaxial stretching) or freely determined by the mechanical characteristics of the substrate (uniaxial stretching). In both cases, it is useful to introduce the *biaxiality ratio* r that represents the percentage of contraction in the y direction with respect to the strain applied along the x axis. In formula, the definition reads

$$r := \max_{\forall t \in T} \frac{\varepsilon_y(t)}{\varepsilon}. \tag{2.17}$$

and in our dissertation, its value will remain constant over time. The strain along the y axis can be consequently expressed as $\varepsilon_y = -r\varepsilon_x$. We will see in Section 2.3 that parameter r is fundamental for the determination of the final cells orientation. Finally, we point out that all the variables of our model are computed and reported in the Lagrangian configuration. As a remark, when the applied deformation is null the Lagrangian frame and the Eulerian one coincide.

Axon representation. We will divide the neuron into soma, axonal shaft and growth cone (see Fig. 1.1). In order to model the axonal pathfinding process, the soma is assumed to be fixed and we consider the axon as the only neurite by neglecting other branches possibly developing from the soma. The axonal growth is thus characterized by the evolution of the position of the growth cone. The position of the growth cone is identified by a material point located at the axon tip and provided with a direction of orientation $\mathbf{N}$. This direction is determined by the preferred direction assumed by the stress fibers (SFs) making up the growth cone cytoskeleton (see Fig. 2.3). The cone's direction $\mathbf{N}$ depends on the angle $\theta(t)$ measured with respect to the main stretch direction and defined as follows

$$\mathbf{N}(t) = \Big[\cos\theta(t),\, \sin\theta(t)\Big]^\top. \tag{2.18}$$

All the SFs are linked by proteins arranged orthogonally to the fibre bundles (see Fig. 2.3) whose direction is this

$$\mathbf{N}_\perp = \Big[-\sin\theta(t),\, \cos\theta(t)\Big]^\top. \tag{2.19}$$

Moreover, stress fibers are reported to be up to ten times stiffer than the binding proteins [2]. For this reason, locally, the presence of the growth cone gives a natural anisotropic mechanical response to the GC-substratum material. In addition, we disregard the influence of the axonal shaft and the soma on the mechanical behaviour of the material, since we assume that the axon can instantaneously adapt its shape to follow the position of the growth cone. We finally assume that in the growth cone region, the material has an orthotropic linear viscoelastic response.

We identify the growth cone position in the undeformed configuration at a certain time t with $\mathbf{X}_{\mathrm{GC}}(t)$. The corresponding position in the Eulerian frame is $\mathbf{x}_{\mathrm{GC}}(t) = \chi(\mathbf{X}_{\mathrm{GC}}(t))$. We take track of the axon tip trajectory by solving the following ODE in the Lagrangian configuration

$$\frac{\mathrm{d}\mathbf{X}_{\mathrm{GC}}(t)}{\mathrm{d}t} = V(t)\mathbf{N}(t) \tag{2.20}$$

where $V(t)$ is the Lagrangian axon growth speed. This quantity will be first considered as constant with a value equal to the mean axon growth velocity reported

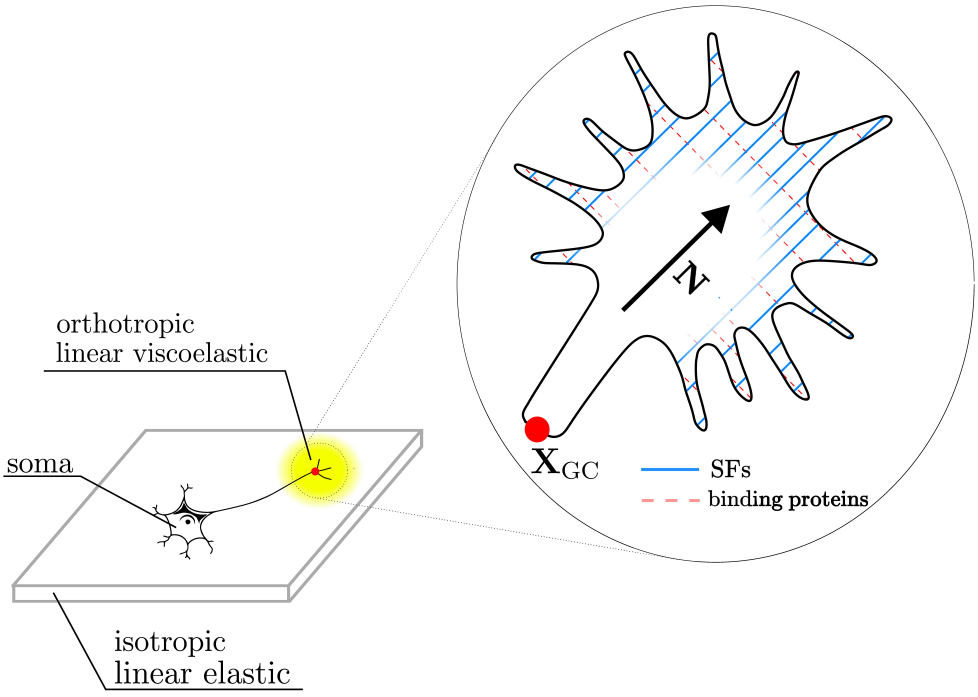

Figure 2.3: Growth cone model representation.

in literature [4]. Then, we will deduce its value by solving the tubulin-driven axon growth model presented in Section 2.4.

We clarify that in our model the path followed by the growth cone does not coincide with the axon. The axonal shaft is indeed identified as the end-to-end segment from soma to axon tip (see Fig. 2.4) and it assembles at each instant t depending on the position of the growth cone. This assumption is based on biological observations and allows to simplify the model. Indeed, it has been experimentally observed [18, 20, 21] that neurons actively regulate the tension along the axon in order to maintain a certain rest value [18]. This is made by straightening the axonal shaft over time (see Fig. 1.5). We just assume this process is instantaneous with the axon that reassembles at each time instant t. Considering the axon as coincident with the GC trajectory would also lead to some difficulties in modelling the tubulin transport as illustrated in Section 2.4. Moreover, axons maintain a shape that differs much from a straight line just when they grow on micro-patterned substrates with specific geometries [20, 25–29, 35, 57]. In all the other cases, modelling axons as straight segments is consistent with the biological

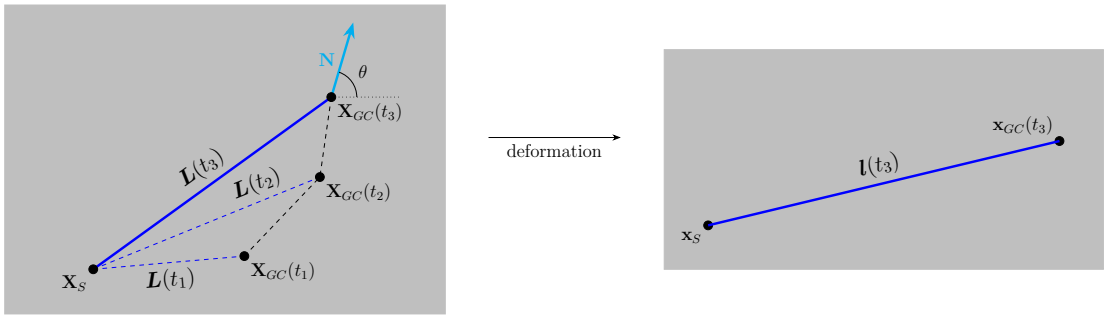

Lagrangian frame Eulerian frame

Figure 2.4: Representation of the neuron in the Lagrangian and Eulerian frames. The black dashed line is the path followed by the GC. The blue dashed line is the axon defined at a previous time instant. The solid blue line is the axon at the current time t.

evidence.

We now write in mathematical terms what we above-mentioned. We first define the vectors that link the soma to the axon tip in both the Lagrangian and Euclidean configurations:

$$\boldsymbol{L}(t) = \mathbf{X}_{\mathrm{GC}}(t) - \mathbf{X}_S, \qquad \boldsymbol{l}(t) = \mathbf{x}_{\mathrm{GC}}(t) - \mathbf{x}_S, \tag{2.21}$$

where $\mathbf{X}_S$ and $\mathbf{x}_S$ are the positions of the soma in the Lagrangian and Eulerian frame, respectively. The axon length at time t is

$$L(t) = |\boldsymbol{L}(t)|. \tag{2.22}$$

The Lagrangian length and the Euclidean one coincide when the applied deformation is null.

2.2.2 GC and axon orientations

The axon orientation is denoted by the angle $\varphi(t)$ formed by the vector $L(t)$ that represents the axon and the x axis (see Fig. 2.5). This angle will be used in the next sections and it will come in handy for the statistical analysis of the model results in Section 4. The fact that the orientation angle of the growth cone and the orientation of the axon may differ is consistent with the biological phenomenology. Indeed, the growth cone is a very motile structure that changes direction quickly and its role is to steer the axon in order to change the growth direction.

Theorem 1. *If the growth cone reaches an equilibrium direction θ_{eq}, for a time that is large enough, the following equality holds*

$$\varphi_{eq} := \lim_{t\to\infty} \varphi(t) = \theta_{eq}. \tag{2.23}$$

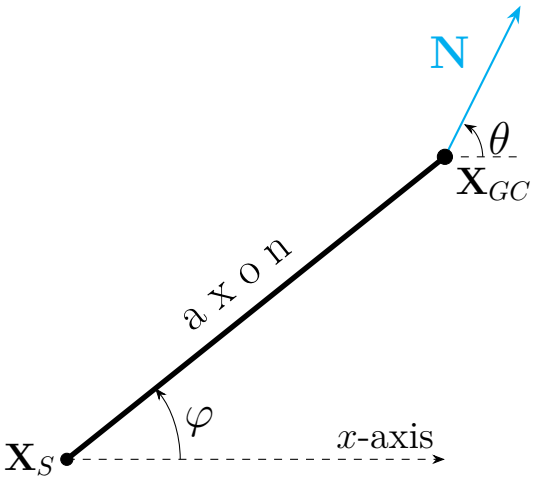

Figure 2.5: Orientation angles of the axon and the growth cone.

Proof. We refer to Fig. 2.6 where we set as $\mathbf{X}_S$ and $\mathbf{X}_{\text{GC}}$ the soma and the growth cone position respectively. The point P is the spot where the GC reaches the equilibrium orientation θ_{eq}, from that point on the growth cone moves along the straight line b and its orientation does not change because it has reached the equilibrium value. Referencing to Fig. 2.6, we define the angle β as the difference between the GC equilibrium angle and the axon direction:

$$\beta(t) \coloneqq \theta_{\text{eq}} - \varphi(t). \tag{2.24}$$

We consider the triangle $\overset{\triangle}{\mathbf{X}_S H \mathbf{X}_{\text{GC}}}$ and define $p = \overline{P\mathbf{X}_{\text{GC}}}$, $k = \overline{HP}$ and $u = \overline{\mathbf{X}_S H}$. We then apply the law of sines to get

$$\frac{\sin\varphi}{p+k} = \frac{\sin\beta}{u} \qquad \Rightarrow \qquad \sin\beta = \frac{u}{p+k}\sin\varphi. \tag{2.25}$$

We can now write

$$\sin\varphi = \sin\left(\theta_{\text{eq}} - \beta\right) = \sin\theta_{\text{eq}}\cos\beta - \sin\beta\cos\theta_{\text{eq}} \tag{2.26}$$

and by substituting Eq. (2.25) in the previous equality, we get

$$\sin\beta\left[1 + \frac{u}{p+k}\cos\theta_{\text{eq}}\right] = \frac{u}{p+k}\sin\theta_{\text{eq}}\cos\beta \tag{2.27}$$

that finally leads to

$$\tan\beta = \frac{\sin\theta_{\text{eq}}}{\frac{p+k}{u} + \cos\theta_{\text{eq}}}. \tag{2.28}$$

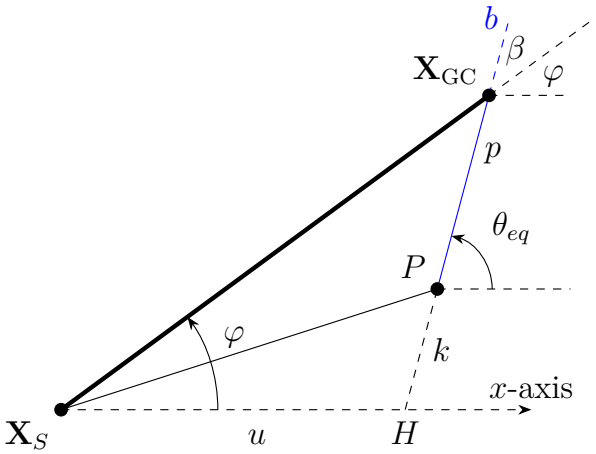

Figure 2.6: Geometrical proof of Eq. (2.23)

For sufficiently large times ($t \to \infty$), the axon continues to grow leading the distance $p \to \infty$. Thus, the term $\tan\beta \to 0$ and consequently $\beta \to 0$. We finally obtain the following asymptotic result

$$\lim_{t\to\infty} \beta(t) = \lim_{t\to\infty} (\theta_{\mathrm{eq}} - \varphi(t)) = 0. \tag{2.29}$$

Thus defining $\varphi_{\mathrm{eq}} \coloneqq \lim_{t\to\infty} \varphi(t)$ we have Eq. (2.23).

□

2.3 Reorientation model

In this section, the model for the growth cone reorientation is presented. The aim is to develop a model that can reproduce the dependence of the reorientation of the growth cone on the frequency and the strain amplitude of the applied deformation. Indeed, in the case of neurons, also the strain amplitude is reported to play an important role in the cell reorientation timing and final angle [4]. In order to do so, we follow what done in [1] by introducing a linear viscoelastic model. An extension to the non-linear frame is presented in [2, 58].

As already mentioned in Section 2.2, the substrate alone is modelled as an isotropic linear elastic material while the region where the growth cone is located is modelled as orthotropic and linear viscoelastic as a consequence of the GC-substrate interaction. The biaxiality in the mechanical behaviour is given by the alignment direction of the stress fibers $\mathbf{N}$ and the orthogonal direction $\mathbf{N}_\perp$ along which the binding proteins are placed.

The other assumption we make is treating the growth cone as a Maxwell viscoelastic material with a single relaxation time. The viscoelastic response of

the cellular structure is due to the time required by the acto-myosin network to reorganize itself, and to the continuous rearrangement process of the FAs. The latter ones attach and detach repeatedly to the substrate to minimize the stress perceived by the growth cone, especially if subject to a continuous external deformation. The higher is the frequency of the cyclic stretch applied, the faster the growth cone's cytoskeleton rearranges as reported in biological observations. In this scenario, the growth cone behaves elastically. On the contrary, the GC shows its viscous characteristics for lower frequency regimes when the cytoskeleton rearrangement time is lower than the deformation period.

We now write down the evolution equation for the growth cone orientation following what has been done in [1]. We start by defining the work done by the stress on the growth cone due to the SFs alignment process, which in the linear frame is $\mathcal{L} \coloneqq \mathbb{T}(t|\theta) : \mathbb{E}(t)$, where $\mathbb{T}(t|\theta)$ is the Cauchy stress tensor given the previous orientations θ and $\mathbb{E}$ is the infinitesimal strain tensor characterizing the linear terms of the externally imposed deformation. The evolution of the orientation angle θ can be related to the changes in the work $\mathcal{L}$ using the Lagrangian mechanics and neglecting the inertial terms. The following equation holds:

$$K\lambda_\theta \frac{\mathrm{d}\theta}{\mathrm{d}t} = -\frac{\partial \mathcal{L}}{\partial \theta} \tag{2.30}$$

where K is the Young modulus of the GC-substrate material and λ_θ is the time the growth cone needs to reorient itself. Hence, the product $K\lambda_\theta$ can be seen as a viscous-like coefficient measuring cell resistance to realignment. By substituting the definition of $\mathcal{L}$ in Eq. (2.30) we get the dynamics equation for the orientation angle

$$\frac{\mathrm{d}\theta(t)}{\mathrm{d}t} = -\frac{1}{K\lambda_\theta}\frac{\partial \mathbb{T}}{\partial \theta}(t|\theta) : \mathbb{E}. \tag{2.31}$$

The latter equation tells us that θ, and hence the growth cone, tend to assume a value for which the variation of the stress $\mathbb{T}$ with respect to θ is null or orthogonal to the deformation given by $\mathbb{E}$.

In order to close the model we need a constitutive relation for $\mathbb{T}$. In the viscoelastic frame, the model reads

$$\mathbb{T}(t|\theta) = \int_{-\infty}^{t} \mathcal{C}(\theta(\tau); t-\tau)\left[\mathbb{E}(t) - \mathbb{E}(\tau)\right] d\tau \tag{2.32}$$

in which we referred to the relaxation kernel as $\mathcal{C}$ that takes into account the memory effects of the viscoelastic material. We assume an exponential dependence on the term $t-\tau$ with a single relaxation time λ. This parameter can be interpreted as the time necessary for the cytoskeleton to disassemble and reassemble in order to change the spatial configuration of the growth cone. Hence, the relaxation kernel writes

$$\mathcal{C}(\theta(\tau)|t-\tau) = \frac{1}{\lambda}\mathcal{C}_0(\theta(\tau))e^{-(t-\tau)/\lambda} \tag{2.33}$$

where $\mathcal{C}_0(\theta(t))$ is the fourth-order elasticity tensor (or stiffness tensor). Then Eq. (2.32) becomes

$$\mathbb{T}(t|\theta) = \int_{-\infty}^{t} \frac{1}{\lambda}\mathcal{C}_0(\theta(\tau))e^{-(t-\tau)/\lambda}\left[\mathbb{E}(t) - \mathbb{E}(\tau)\right] d\tau \tag{2.34}$$

and the final differential form of its constitutive equation is

$$\lambda\frac{\mathrm{d}\mathbb{T}}{\mathrm{d}t}(t|\theta) + \mathbb{T}(t|\theta) = \mathbf{C}_0(t|\theta)\frac{\mathrm{d}\mathbb{E}}{\mathrm{d}t}(t), \tag{2.35}$$

where Eq. (2.35) the functional $\mathbf{C}_0$ is defined as

$$\mathbf{C}_0(t|\theta) \coloneqq \int_{-\infty}^{t} e^{-(t-\tau)/\lambda}\mathcal{C}_0(\theta(\tau))\, d\tau. \tag{2.36}$$

2.3.1 Energy minimization

In the literature, some works have focused on mathematical models in which the equilibrium orientation angle of the cells coincides with the minimum strain or minimum stress direction [33]. However, these models do not precisely reproduce cell reorientation behaviour. Indeed, it has been demonstrated that models based on energy minimization give results that are in better agreement with the biological evidence [1, 3, 10, 30]. Taking that into account, our model relies on the fact that the growth cone orientation is driven by the minimization of a general elastic energy density $\mathcal{U}$. Indeed, it can be proven [1] that in both the high and low frequency regime the Eq. (2.31) reduces to the following

$$\frac{\mathrm{d}\theta(t)}{\mathrm{d}t} \propto -\frac{\partial\mathcal{U}}{\partial\theta} = \frac{\partial\mathbb{T}}{\partial\theta} : \mathbb{E}. \tag{2.37}$$

As already stated, in the range of strain amplitudes tested in [4], PDMS has been proven to have a linear elastic behaviour [41]. Hence, we hereafter work in the linear approximation by considering just the linear terms of the deformation characterized by the strain tensor $\mathbb{E}$. For this reason, the specific form of the elastic energy density for the growth cone that is valid for our model assumes the following form

$$\mathcal{U} = \mathcal{U}_{\mathrm{iso}}(I_1) + \mathcal{U}_{\mathrm{ortho}}(I_4) + \mathcal{U}_{\mathrm{mix}}(I_1,\, I_4) \tag{2.38}$$

where where $\mathcal{U}_{\mathrm{iso}}$ is the purely isotropic contribution, the term $\mathcal{U}_{\mathrm{ortho}}$ represents the orthotropic contribution, while $\mathcal{U}_{\mathrm{mix}}$ gives the coupling effects of isotropy and anisotropy. In the linear approximation, all the invariants that give higher-order terms are neglected, and thus all the terms in Eq. (2.38) depend just on the invariants of $\mathbb{E}$ which give linear terms, i.e.

$$I_1 \coloneqq \mathrm{tr}\mathbb{E}, \qquad I_4 \coloneqq \mathbf{N}\cdot\mathbb{E}\mathbf{N}. \tag{2.39}$$

Since the first invariant does not depend on the orientation θ, as $\dfrac{\partial \mathcal{U}_{\text{iso}}}{\partial \theta} = 0$ the term $\mathcal{U}_{\text{iso}}$ can be neglected in our discussion. Then, the final form of the elastic energy will be

$$\begin{aligned} \mathcal{U} &= \mathcal{U}_{\text{ortho}}(I_4) + \mathcal{U}_{\text{mix}}(I_1,\, I_4) \\ &= \frac{1}{2} K_{\parallel} \left(\mathbf{N} \cdot \mathbb{E}\mathbf{N}\right)^2 + 2K_{14} \left(\operatorname{tr} \mathbb{E}\right) \left(\mathbf{N} \cdot \mathbb{E}\mathbf{N}\right). \end{aligned} \tag{2.40}$$

where $K_{\parallel}$ is a coefficient related to the stiffness along the SFs direction and K_{14} weights the coupling term. We remark that, depending on the amplitude stretching ranges we work with, we can obtain an equivalent result to what is given in Eq. (2.40) also by considering the substrate as nonlinear. The general elastic strain energy density would be dependent on the eight invariants of the tensor $\mathbb{C}$. By assuming, when possible, to work in the small deformations limit the invariants of $\mathbb{C}$ can be approximated with the invariants of the strain tensor $\mathbb{E}$ and with some further simplifications a final energy form that is very similar to the one in Eq. (2.40) can be written. An example of this procedure can be seen in [1, 2].

Recalling the explicit forms of $\mathbb{E}$ and $\mathbf{N}$ defined in Eq. (2.14) and Eq. (2.40), respectively, Eq. (2.40) becomes

$$\begin{aligned} \mathcal{U} = &\frac{1}{2} K_{\parallel} (\varepsilon_x \cos^2\theta + \varepsilon_y \sin^2\theta)^2 \\ &+\ 2K_{14} (\varepsilon_x + \varepsilon_y)(\varepsilon_x \cos^2\theta + \varepsilon_y \sin^2\theta). \end{aligned} \tag{2.41}$$

The derivative of $\mathcal{U}$ with respect to the orientation angle is

$$\begin{aligned} \frac{\partial \mathcal{U}}{\partial \theta} = &2K_{\parallel} \sin\theta \cos\theta (\varepsilon_y - \varepsilon_x)(\varepsilon_x \cos^2\theta + \varepsilon_y \sin^2\theta) \\ &+\ 4K_{14} (\varepsilon_x + \varepsilon_y)(\varepsilon_y - \varepsilon_x) \sin\theta \cos\theta \end{aligned} \tag{2.42}$$

and the equilibrium condition $\dfrac{\partial \mathcal{U}}{\partial \theta} = 0$ reads

$$2(\varepsilon_y - \varepsilon_x) \cos\theta \sin\theta \left[K_{\parallel} \varepsilon_x \cos^2\theta + K_{\parallel} \varepsilon_y \sin^2\theta + 2K_{14} (\varepsilon_x + \varepsilon_y) \right] = 0. \tag{2.43}$$

Considering the interval $[0,\, \pi]$, Eq. (2.43) is satisfied under one of the following conditions on the interval:

$$\sin\theta = 0 \quad \Rightarrow \quad \theta_{\text{eq}} = 0, \pi \tag{2.44}$$

$$\cos\theta = 0 \quad \Rightarrow \quad \theta_{\text{eq}} = \frac{\pi}{2}, \tag{2.45}$$

$$K_{\parallel}\varepsilon_x \cos^2\theta + K_{\parallel}\varepsilon_y \sin^2\theta + 2K_{14}(\varepsilon_x + \varepsilon_y) = 0$$

$$\cos^2\theta_{\text{eq}} = \frac{2K_{14}(\varepsilon_x + \varepsilon_y) + K_{\parallel}\varepsilon_y}{K_{\parallel}(\varepsilon_y - \varepsilon_x)}. \tag{2.46}$$

Equations (2.44) and (2.45) give the *parallel* and *perpendicular* orientation, respectively. Equation (2.46) leads to the definition of the so called *oblique equilibrium*.

By substituting the relation $\varepsilon_y = -r\varepsilon_x$, the Eq. (2.46) becomes

$$\cos^2\theta_{\text{eq}} = \frac{K_{\parallel}r + 2K_{14}(r-1)}{K_{\parallel}(1+r)}. \tag{2.47}$$

With further computations, we obtain the final form of the oblique solutions:

$$\cos^2\theta_{\text{eq}} = \frac{1}{2} + \mathcal{K}\left(\frac{1}{2} - \frac{1}{r+1}\right) \tag{2.48}$$

where we have introduced the parameter

$$\mathcal{K} = \frac{K_{\parallel} + 4K_{14}}{K_{\parallel}} = 1 + 4\frac{K_{14}}{K_{\parallel}} \tag{2.49}$$

that embodies all the mechanical characteristics of the growth cone-substratum media. What we have just obtained is consistent with the results reported in [1, 2, 30]. From Eq. (2.48) it is clear that the parameter r is fundamental to determine the final equilibrium angle of the growth cone. This parameter is easily tunable in biaxial experiments and controlled by imposing different deformations to the substratum or by using different clamps for stretching it. A complete study on the incidence of r on the cell orientation angle is made in [30], even if the study has not been conducted on neuron-type cells.

Equilibrium orientations and stability

Now we are going to exploit the stability of the equilibrium angles given in Eq. (2.44), Eq. (2.45) and Eq. (2.48). We demonstrate that the existence and stability of such orientations depend on the sign of $\mathcal{K}$ and the value of r. For the Thesis purpose, we are interested in discussing the case $\mathcal{K} > 1$, indeed this case holds always true in our specific case considering Eq. (2.49). The other cases can be deduced from [1].

We first need to introduce the parameter $\rho \coloneqq \dfrac{\mathcal{K}+1}{\mathcal{K}-1}$ and then set the conditions of existence for the oblique equilibria. Of course, since

$$0 \leq \cos^2\theta_{\text{eq}} \leq 1 \tag{2.50}$$

the oblique equilibrium angle exists if $\frac{1}{\rho} < r < \rho$. The parallel and perpendicular angles, instead, always exist.

In order to conduct the stability study, we write down the second-order derivative of our energy $\mathcal{U}$ with respect to θ

$$\begin{aligned}\frac{\partial^2 \mathcal{U}}{\partial \theta^2} = {} & 2\varepsilon_x^2(r+1)\left[K_\parallel \cos^2\theta(1+r) + 2K_{14}(1-r) - K_\parallel r\right]\left(\cos^2\theta - \sin^2\theta\right) \\ & + 4\varepsilon_x^2(r+1)^2 K_\parallel \cos^2\theta \sin^2\theta.\end{aligned} \tag{2.51}$$

and set the general stability condition as follows

$$\left.\frac{\partial^2 \mathcal{U}}{\partial \theta^2}\right|_{\theta=\theta_{\mathrm{eq}}} > 0. \tag{2.52}$$

Considering $\mathcal{K} > 1$, the stability analysis gives the following results (reported also in Fig. 2.7):

- $\theta_{eq} = 0$ is stable if $r > \rho$;
- $\theta_{eq} = \frac{\pi}{2}$ is stable if $r < \frac{1}{\rho}$;
- the oblique equilibrium angles are always stable.

2.3.2 Stochastic term

Cells are living beings. That means that their movement can not be uniquely given by a deterministic equation. Indeed, cellular crawling and axonal pathfinding as well are characterized by intrinsic randomness. Each neuron can react differently to external stimuli even if some common general behaviour can be extrapolated from the experimental results. This is reflected in an uncertainty in the experimental results. In all the works analyzed, the equilibrium angle is not unique, but it is given as a range of possible values.

Mathematically, we assume that randomness characterizes the orientation angle rather than the growth cone position. Another option could be adding the uncertainty also on the growth cone speed term $V(t)$. We modelled the randomness in the neuron reorientation process by adding a stochastic term to Eq. (2.31). We then obtain a new stochastic differential equation

$$\frac{\mathrm{d}\theta(t)}{\mathrm{d}t} = -\frac{1}{K\lambda_\theta}\frac{\partial \mathbb{T}}{\partial \theta}(t|\theta) : \mathbb{E} + \sqrt{\frac{\sigma^2}{\lambda_\theta}}\xi = -\frac{1}{K\lambda_\theta}\frac{\partial \mathcal{U}}{\partial \theta} + \sqrt{\frac{\sigma^2}{\lambda_\theta}}\xi \tag{2.53}$$

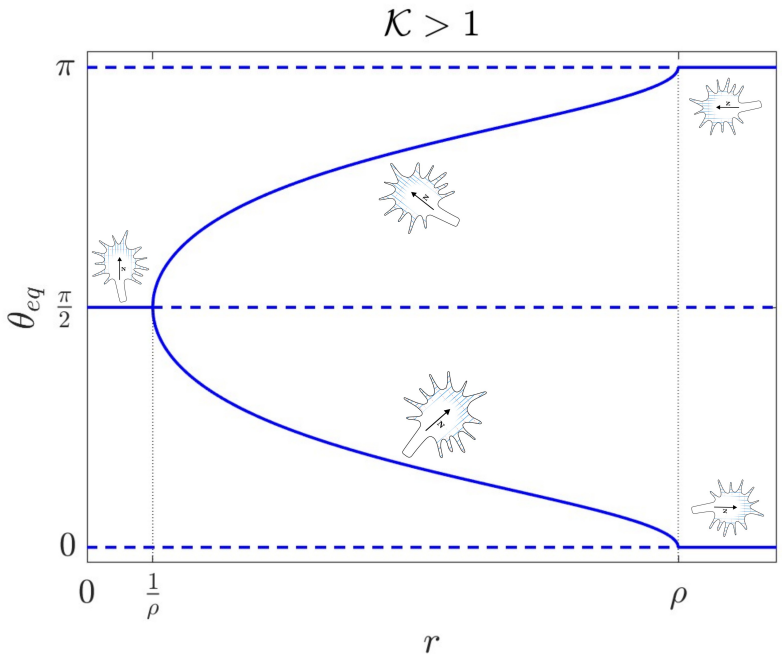

Figure 2.7: Bifurcation diagram for the case $\mathcal{K} > 1$. The solid line represents the stable equilibrium while the dashed ones are the unstable equilibrium.

where σ is a parameter representing the stochastic angular fluctuation and $\xi \sim \mathcal{N}(0,1)$. The latter equation can be properly written as an Itô process [59]:

$$\mathrm{d}\theta = -\frac{1}{K\lambda_\theta}\frac{\partial \mathcal{U}}{\partial \theta}\,\mathrm{d}t + \sqrt{\frac{\sigma^2}{\lambda_\theta}}\,\mathrm{d}W_t \tag{2.54}$$

where W_t is the stochastic variable that defines a Wiener process. This stochastic process, also known as Brownian motion, is the most commonly used in modelling the behaviour of living beings. This variable can be numerically approximated with $\mathrm{d}W_t = \sqrt{\mathrm{d}t}\,\mathcal{N}(0,1)$ as stated in [60].

2.4 Axon growth model

In this section, we are going to present the model for the axonal growth. We consider the one-dimensional model developed in [48] which is an extension to the one previously presented in [46, 61]. In the previous Chapter, we explained how the protrusion of new microtubules in the growth cone leads to an effective elongation of the axon. The model tries to replicate this scheme and to ideally set the tubulin concentration as the main and only variable responsible for neuron

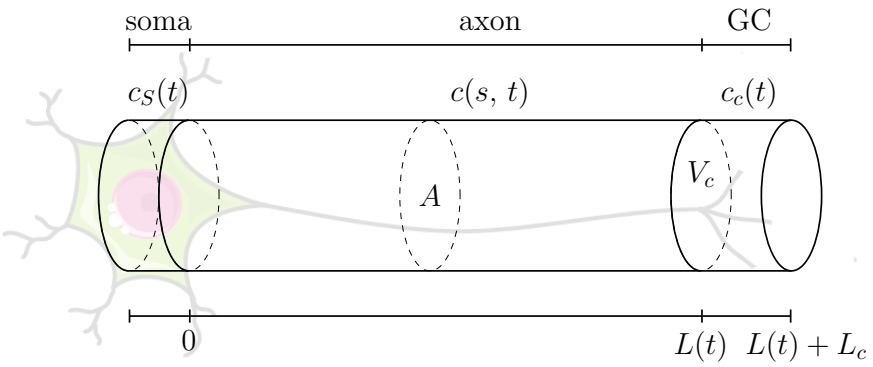

Figure 2.8: One-dimensional compartment model for tubulin-driven axon growth

growth. Moreover, we assume tubulin molecules small enough to consider them as a homogeneous continuum.

We follow the classical division of the neuron by splitting it into soma, axonal shaft and the growth cone located at the axon tip. We treat each part as a compartment in a one-dimensional frame (see Fig. 2.8). We are going to use the coordinate s directed along the axon direction which is given at each instant time by the angle $\varphi(t)$. The soma is placed at $s = 0$ while the tip of the axon is at $s = L(t)$. The growth cone is assumed to have characteristic length L_c and volume V_c. The axonal shaft cross-sectional area is A and is assumed constant. The tubulin concentration in the soma, along the axon and in the growth cone are denoted by $c_S(t)$, $c(s,t)$ and $c_c(t)$, respectively. The production of the tubulin takes place only in the soma, while its degradation occurs in the neurite and in the growth cone with a constant rate g. All the parameters that will appear in this section are listed in Table 2.1.

We start by writing down the conservation of mass equation along the axon in the general section $(s_1,\, s_2)$ in the Lagrangian frame of the substrate:

$$\frac{\mathrm{d}}{\mathrm{d}t}\int_{s_1}^{s_2} Ac(x,t)\ \mathrm{d}s = A\left[F(s_1) - F(s_2)\right] - \int_{s_1}^{s_2} Agc(s,t)\ \mathrm{d}s, \tag{2.55}$$

where $F[\,\mathrm{mol/ms^2}]$ is the flux per unit area of tubulin which is defined as $F = c\mathrm{v}$. We can rewrite a constitutive equation for the flux according to the Fick's law [48] by setting

$$F = ac - D\frac{\partial c}{\partial s}. \tag{2.56}$$

Substituting Eq. (2.56) in Eq. (2.55) and differentiating lead to the classic advection-diffusion-reaction equation for c

$$\frac{\partial c}{\partial t} + a\frac{\partial c}{\partial s} - D\frac{\partial^2 c}{\partial s^2} = -gc \quad \text{for} \quad 0 < s < L(t). \tag{2.57}$$

Parameter	Meaning	Unit
a	tubulin active transport velocity	m/s
D	tubulin diffusion coefficient	m^2/s
g	tubulin degradation rate	s^{-1}
L_c	GC length	m
L_0	initial axon length	m
r_g	tubulin polymerization rate	$m^4/s\,mol$
$\tilde{r}_g$	GTP reaction polymerization rate	s^{-1}
c_∞	equilibrium tubulin concentration in the GC	mol/m^3
A	axon cross-sectional area	m^2
v	tubuline velocity	m/s
V_c	GC volume	m^3
$\tilde{s}_g$	microtubules disassembly rate	s^{-1}
$\rho A_g k L_c$	portion of the assembly microtubules that may undergo disassembly	mol

Table 2.1: Parameters used in the one-dimesional axonal growth model

The conservation of mass Eq. (2.55) should also hold in the growth cone compartment. While the flux in $s = L(t) + L_c$ is null, the one over the boundary $s = L(t)$ from the left to the right is not. In order to write down this flux, we define

$$c^- \coloneqq c(L(t)^-, t) = \lim_{j \to 0} c(L(t) - j, t). \tag{2.58}$$

and then we define the derivative of the concentration right behind $s = L(t)$ as

$$\partial_s c^- \coloneqq \lim_{j \to 0} \left.\frac{\partial c}{\partial s}\right|_{L(t)-j}. \tag{2.59}$$

The total flux that arrives at the growth cone from the axon (seen by an observer who's moving with the boundary $s = L(t)$) is

$$A\left(ac^- - D\partial_s c^- - L'(t)c^-\right). \tag{2.60}$$

We referred to $L'(t)$ as the speed of the axon growth. The conservation of mass for the growth cone reads

$$\begin{aligned} &\underbrace{\frac{\mathrm{d}\left(V_c c_c\right)}{\mathrm{d}t}}_{\text{mass increase per unit time}} = \\ &= \underbrace{A\left(ac^- - D\partial_s c^- - L'(t)c^-\right)}_{\text{flux in}} - \underbrace{gV_c c_c}_{\text{degradation}} - \underbrace{\tilde{r}_g V_c c_c}_{\text{assembly}} + \underbrace{\tilde{s}_g \rho A_g k L_c}_{\text{disassembly}}. \end{aligned} \tag{2.61}$$

The ODE that models the axon growth speed is now introduced:

$$V(t) = \frac{\mathrm{d}L(t)}{\mathrm{d}t} = r_g \left(c_c(t) - c_\infty\right). \tag{2.62}$$

Finally, we rewrite Eq. (2.61) by making some algebra and substituting Eq. (2.62) in it. Thus, the final form of the conservation of mass for the growth cone reads

$$L_c \frac{\mathrm{d}c_c}{\mathrm{d}t} = ac^- - D\partial_s c^- - r_g(c_c - c_\infty)c^- - gL_c c_c - \tilde{r}_g L_c c_c + \tilde{r}_g L_c c_\infty. \tag{2.63}$$

Since we are dealing with a diffusion equation, we expect the solution for $c(x,t)$ to be smooth. Hence, it is natural to impose the continuity in $s = 0$ and $s = L(t)$. In particular, we set $c^- = c_c(t)$ for every time t.

2.5 Complete model

In this section, we are simply going to write down all the equations that make up our model for neuron growth and reorientation. In this way, a general view is given of the variables involved and how they are linked.

$$
\begin{cases}
\dfrac{\mathrm{d}\mathbf{X}_{\mathrm{GC}}(t)}{\mathrm{d}t} = V(t)\mathbf{N}(t), \\
\mathbf{N}(t) = \left[\cos\theta(t),\, \sin\theta(t)\right]^{\top}, \\
\dfrac{\mathrm{d}\theta(t)}{\mathrm{d}t} = -\dfrac{1}{K\lambda_\theta}\dfrac{\partial \mathbb{T}}{\partial \theta}(t|\theta) : \mathbb{E} + \sqrt{\dfrac{\sigma^2}{\lambda_\theta}}\xi, \\
\lambda\dfrac{\mathrm{d}\mathbb{T}}{\mathrm{d}t}(t|\theta) + \mathbb{T}(t|\theta) = \mathbf{C}_0(t|\theta)\dfrac{\mathrm{d}\mathbb{E}}{\mathrm{d}t}(t), \\
\dfrac{\partial c}{\partial t} + a\dfrac{\partial c}{\partial s} - D\dfrac{\partial^2 c}{\partial s^2} = -gc \qquad 0 < s < L(t), \\
L_c\dfrac{\mathrm{d}c_c}{\mathrm{d}t} = ac^- - D\partial_s c^- - \left(r_g c_c + \tilde{r}_g L_c\right)(c_c - c_\infty), \\
V(t) = \dfrac{\mathrm{d}L(t)}{\mathrm{d}t} = r_g\,(c_c(t) - c_\infty), \\
\\
\mathbf{N}(0) = \mathbf{N}_0, \\
\mathbf{X}_{\mathrm{GC}}(0) = \mathbf{X}^0_{\mathrm{GC}}, \\
\theta(0) = \theta_0, \\
\mathbb{T}(0) = \mathbf{0}, \\
\mathbf{C}_0(0) = \mathbf{0}, \\
c(0,\, t) = c_S(t) \qquad t \geq 0, \\
c(L(t),\, t) = c_c(t) \qquad t > 0, \\
c(s,\, 0) = c_0(s) \qquad 0 \leq s \leq L_0, \\
L(0) = L_0, \\
c_c(0) = c_0(L_0).
\end{cases}
\tag{2.64}
$$

Chapter 3

Numerical implementation

The mathematical model proposed in Chapter 2 can not be solved analytically, hence a numerical implementation is needed. In this Chapter, we describe the different schemes used in order to discretize the equations of the model both in space and time. Once the discretization has been done, the model has been implemented in MATLAB ®. In algorithm 1 we list all the steps necessary to solve the complete model. Specifically, in Section 3.1 we deal with the discretization of the reorientation equations of the model, i.e. Eq. (2.31) and Eq. (2.35). Instead, in Section 3.2 we give the numerical form of the axonal growth model given in Eq. (2.57), Eq. (2.62) and Eq. (2.63).

3.1 Reorientation model discretization

The numerical implementation of the growth cone reorientation model given in Section 2.3 is here tackled following what has been done in [1]. We are first going to discretize Eq. (2.20). The time discretization is performed through the explicit Euler method thanks to its ease of implementation. The time interval is set equal to Δt. The position of the growth cone at time $t^n = n\Delta t$ is approximated with $\mathbf{X}_{\mathrm{GC}}^n \approx \mathbf{X}_{\mathrm{GC}}(t^n)$. The explicit scheme reads:

$$\mathbf{X}_{\mathrm{GC}}^{n+1} = \mathbf{X}_{\mathrm{GC}}^n + \Delta t V^n \mathbf{N}^n \tag{3.1}$$

where V^n is the axon growth velocity at time t^n obtained from the resolution of the tubulin-driven axonal growth model whose discretization will be later discussed. Instead, $\mathbf{N}^n$ is the growth cone orientation at time t^n depending on the orientation angle $\theta(t^n)$ at the same instant. In order to update the value of the orientation angle, we are now going to discretize Eq. (2.31). The value of the angle at time $t^n = n\Delta t$ is approximated with $\theta^n \approx \theta(t^n)$. The term $\dfrac{\partial \mathbb{T}}{\partial \theta}$ is instead substituted

using a first-order centred finite-differences scheme. Considering the component T_{xx} and T_{yy} of $\mathbb{T}$, the discretization of Eq. (2.31) reads

$$\theta^{n+1} = \theta^n - \frac{\Delta t}{K\lambda_\theta}\left[\frac{T^n_{xx}(\theta+\Delta\theta) - T^n_{xx}(\theta-\Delta\theta)}{2\Delta\theta} - r\frac{T^n_{yy}(\theta+\Delta\theta) - T^n_{yy}(\theta-\Delta\theta)}{2\Delta\theta}\right]\varepsilon^n_x. \tag{3.2}$$

Considering that we start our simulations from the undeformed state, at time $t = 0$ we have $\varepsilon^0_x = 0$, $T^0_{xx} = 0$, $T^0_{yy} = 0$ and $\mathbf{C}_0$ identically equal to 0. The explicit Euler scheme is used also in the approximation of time derivatives present in the constitutive Eq. (2.35). For the sake of simplicity, we report the discretized equation just for the component T_{xx} computed at time t^{n+1}. Hence, the approximated value T^{n+1}_{xx} will be used to compute θ^{n+2} following the advancement scheme in Eq. (3.2). Supposing $r = 0$, the explicit time-marching numerical method is

$$T^{n+1}_{xx} = T^n_{xx}\left(1 - \frac{\Delta t}{\lambda}\right) + \frac{1}{\lambda}(\mathbf{C}^n_0)_{xxxx}\,\dot{\varepsilon}^n_x. \tag{3.3}$$

The trapezoidal rule can be used to approximate the integral term present in the definition of $\mathbf{C}_0$. The integral, considering $r = 0$, is discretized in the following way:

$$\begin{aligned}
(\mathbf{C}^n_0)_{xxxx} &= \int_{-\infty}^{t^n} e^{(t^n-\tau)/\lambda}\,(\mathcal{C}_0(\theta))_{xxxx}\,\mathrm{d}\tau \\
&= \int_{-\infty}^{t^{n-1}} e^{(t^n-\tau)/\lambda}\,(\mathcal{C}_0(\theta))_{xxxx}\,\mathrm{d}\tau + \int_{t^{n-1}}^{t^n} e^{(t^n-\tau)/\lambda}\,(\mathcal{C}_0(\theta))_{xxxx}\,\mathrm{d}\tau \\
&= e^{-(t^n-t^{n-1})/\lambda}(\mathbf{C}^{n-1}_0)_{xxxx} + \int_{t^{n-1}}^{t^n} e^{(t^n-\tau)/\lambda}\,(\mathcal{C}_0(\theta))_{xxxx}\,\mathrm{d}\tau \\
&\approx e^{-(t^n-t^{n-1})/\lambda}(\mathbf{C}^{n-1}_0)_{xxxx} \\
&\quad + \frac{1}{2}\left(t^n - t^{n-1}\right)\left[(\mathcal{C}_0)_{xxxx}(\theta^n) - e^{-(t^n-t^{n-1})/\lambda}(\mathcal{C}_0)_{xxxx}(\theta^{n-1})\right].
\end{aligned} \tag{3.4}$$

All the results can be straightforwardly extended in the case $r \neq 0$ and for the component T_{yy}.

3.2 Axonal growth model discretization

In Section 2.4 we presented the tubulin-driven model for the axonal growth. We recall that the model is nonlinear and consists of a coupled set of a PDE and two ODE. The PDE describes the transport process of free tubulin from the soma to the growth cone. It is defined on a one-dimensional domain with a moving boundary,

which is itself part of the solution. This makes the numerical implementation a little delicate. In order to work on a constant spatial domain, we perform a spatial scaling of the model as reported in [46, 48, 49]. After that, we approximate the system using the method of lines, i.e. we introduce a first spatial discretization in order to transform the PDE into an ODE. Finally, we perform a time discretization and we obtain the fully implementable system.

3.2.1 Spatial scaling

As the axon grows, the domain of the PDE expands since it is defined as the interval $[0,\ L(t)]$. We want to prevent this problem in order to be able to implement a method in which a constant number of spatial computational cells can be used regardless of the axon length and neglecting the axon orientation. To do so, we scale the growing domain to the constant interval [0,1] (see Fig. 3.1). The scaling is done with respect to the axon length $L(t)$ and reads

$$y \coloneqq \frac{s}{L(t)}, \qquad \frac{\partial y}{\partial s} = \frac{1}{L(t)}, \qquad \frac{\partial y}{\partial t} = -\frac{s l'(t)}{L^2(t)} = -\frac{y l'(t)}{L(t)} \tag{3.5}$$

with $s \in [0, L(t)]$ and $y \in$ [0,1]. Considering the tubulin concentration on the y-domain $\bar{c}(y,t) \coloneqq c(yL(t), t)$, we get

$$\frac{\partial c}{\partial t} = \frac{\partial \bar{c}}{\partial t} - \frac{y l'(t)}{L(t)} \frac{\partial \bar{c}}{\partial y}, \qquad \frac{\partial c}{\partial t} = \frac{1}{L(t)} \frac{\partial \bar{c}}{\partial y}, \qquad \frac{\partial^2 c}{\partial s^2} = \frac{1}{L^2(t)} \frac{\partial^2 \bar{c}}{\partial y^2}. \tag{3.6}$$

By substituting Eq. (3.5) and Eq. (3.6) in Eq. (2.57), Eq. (2.62) and Eq. (2.63), we can write down the transformed dynamic model for the axonal growth:

$$\begin{cases} \dfrac{\partial \bar{c}}{\partial t} + \alpha(y, c_c, l) \dfrac{\partial \bar{c}}{\partial y} - \dfrac{D}{L^2} \dfrac{\partial^2 \bar{c}}{\partial y^2} = -g\bar{c}, \quad 0 < y < 1,\ t > 0 \\ \\ \dfrac{\mathrm{d}c_c}{\mathrm{d}t} = \dfrac{(a - gL(t))}{L(t)} c_c - \dfrac{D}{L(t) l} \partial_y \bar{c}^- - \dfrac{(r_g c_c + \tilde{r_g} L(t))}{L(t)} (c_c - c_\infty), \quad t > 0 \\ \\ \dfrac{\mathrm{d}l}{\mathrm{d}t} = r_g (c_c - c_\infty), \quad t > 0 \\ \\ \bar{c}(0,t) = c_S(t), \quad t \geq 0 \\ \bar{c}(1,t) = c_c(t), \quad t > 0 \\ \bar{c}(y,0) = c_0(yL_0), \quad 0 \leq y \leq 1 \\ c_c(0) = c_0(L_0) \\ L(0) = L_0 \end{cases} \tag{3.7}$$

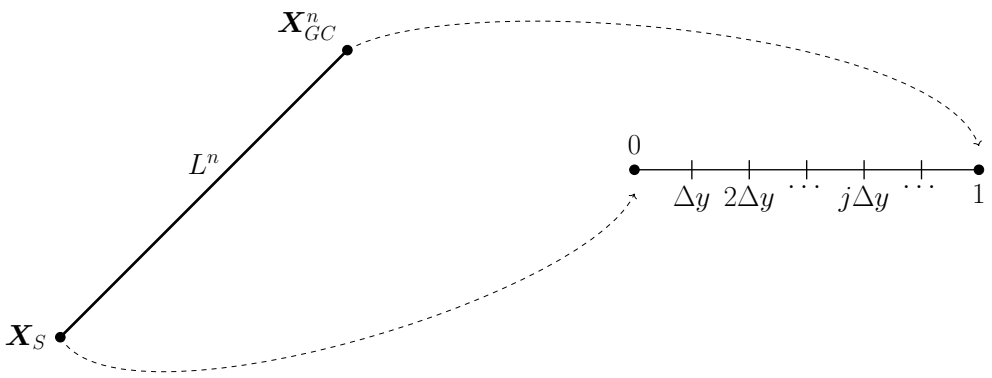

Figure 3.1: Scaling and discretization of the axon at time $t = t^n$. The transformation allows to pass from the growing domain $[0, L(t)]$ to the fixed interval [0,1] as shown by the dashed arrows.

where we defined $\alpha(y, c_c, L) \coloneqq \dfrac{a - yL'(t)}{L(t)} = \dfrac{a - yr_g(c_c - c_\infty)}{L}$. It is fundamental to understand the difference between the scaling process we have just applied and the deformation that we apply to the substrate. The passage from the reference configuration to the deformed one is a physical fact. It happens in reality and the axon length changes due to the deformation. Indeed, the axon is stretched as the substrate is. The spatial scaling is instead just a mathematical tool. There is no actual change in the axon length when we scale the domain into the interval [0,1]. It is just a trick that we use in order to have a fixed domain on which we can compute the solution of the model numerically by maintaining the cell size constant regardless of the axon length. So at each time step, we consider the axon length in the deformed configuration, we map it to the domain [0,1], we compute in MATLAB ®the tubulin concentration, we map the values back to the original domain and finally, we get the growth axon speed.

3.2.2 Spatial and time discretization

We find an approximate solution to the model by applying the method of lines. We first introduce the spatial discretization to rewrite the PDE of the system as an ODE. Let us divide the y-interval [0,1] into M computational cells. Each cell has size $\Delta y \coloneqq 1/M$. The edges of the cells are identified by the points $y_j = j\Delta y$ with $j = 0, \ldots, M$ and at each point the tubulin concentration is approximated by $\bar{C}_j \approx \bar{c}(y_j, t)$. According to the boundary conditions, $\bar{C}_0$ and $\bar{C}_M$ should be respectively interpreted as $c_S(t)$ and $c_c(t)$.

The approximation of the spatial derivatives is made using second-order central finite differences, while for the term $\partial_y \bar{c}^-$ a one-sided second-order approximation is used. The following relations hold

$$\begin{aligned} \frac{\partial \bar{c}(y_j,\cdot)}{\partial y} &\approx \frac{\bar{C}_{j+1}-\bar{C}_{j-1}}{2\Delta y}, \\ \frac{\partial^2 \bar{c}(y_j,\cdot)}{\partial y^2} &\approx \frac{\bar{C}_{j+1}-2\bar{C}_j+\bar{C}_{j-1}}{\Delta y^2}, \\ \partial_y \bar{c}^- &\approx \frac{3\bar{C}_M-4\bar{C}_{M-1}+\bar{C}_{M-2}}{2\Delta y}. \end{aligned} \tag{3.8}$$

For what concerns the time discretization, we use an explicit Euler method. As a remark, the time step is denoted by Δt and the general time instant t by $t^n \coloneqq n\Delta t$. The concentration along the axon is numerically approximated with $\bar{C}_j^n \approx \bar{c}(y_j, t^n)$ for $j = 1, \dots, M-1$. Similarly, the tubulin concentration in the growth cone and the axon length are approximated with $C_c^n \approx c_c(t^n)$ and $L^n \approx l(t^n)$. Each time derivative is substituted by formulas like

$$\frac{\partial \bar{c}(y_j,t^n)}{\partial t} \approx \frac{\bar{C}_j^{n+1}-\bar{C}_j^n}{\Delta t}. \tag{3.9}$$

We now write down the complete explicit time marching numerical method that has been implemented in MATLAB ®. We substitute Eq. (3.8) and Eq. (3.9) in Eq. (3.7) to get

$$\begin{aligned} C_c^{n+1} &= C_c^n\left[1+\frac{\Delta t}{L_c}\left(a-gL_c-\frac{3D}{2\Delta y L^n}\right)\right] \\ &\quad -\frac{\Delta t}{L_c}\left(r_g C_c^n+\tilde{r_g}L_c\right)\left(C_c^n-c_\infty\right)+\frac{\Delta t D}{2\Delta y L^n L_c}\left(4\bar{C}_{M-1}^n-\bar{C}_{M-2}^n\right), \\ L^{n+1} &= L^n + r_g \Delta t\left(C_c^n - c_\infty\right) \\ \mathbf{C}^{n+1} &= \mathbf{A}\mathbf{C}^n \end{aligned} \tag{3.10}$$

where

$$\mathbf{A} \coloneqq \begin{bmatrix} 1 & 0 & 0 & \dots & 0 \\ A_{2,1} & A & A_{2,3} & \ddots & \vdots \\ 0 & \ddots & \ddots & \ddots & 0 \\ 0 & \ddots & A_{M-1,M-2} & A & A_{M-1,M} \\ 0 & \cdots & \cdots & 0 & 1 \end{bmatrix} \quad \mathbf{C}^n \coloneqq \begin{bmatrix} \bar{C}_1^n \\ \bar{C}_2^n \\ \vdots \\ \bar{C}_M^n \end{bmatrix}. \tag{3.11}$$

The coefficients on the diagonal of $\mathbf{A}$ are

$$\begin{aligned} A &= 1 - \Delta t \left[\frac{2D}{\left(L^n \Delta y\right)^2} + g \right] \\ A_{j,j-1} &= \Delta t \left[-\frac{\alpha(y_j, C_c^n, L^n)}{2\Delta y} + \frac{D}{\left(L^n \Delta y\right)^2} \right] \\ A_{j,j+1} &= \Delta t \left[\frac{\alpha(y_j, C_c^n, L^n)}{2\Delta y} + \frac{D}{\left(L^n \Delta y\right)^2} \right] \end{aligned} \tag{3.12}$$

and the imposed Dirichlet boundary conditions at each time step are $\bar{C}_0^{n+1} = C_s^{n+1}$ and $\bar{C}_M^{n+1} = C_c^{n+1}$.

In order to prevent numerical oscillations and let the method converge to the solution, we must impose some condition on the choice of the discretization parameters Δt and Δy. In this perspective, we recall the CFL condition Δt and the cell Pèclet condition for Δy:

$$\Delta t \leq \frac{\Delta y^2 L_{\min}^2}{2D}, \qquad \Delta y \leq \frac{2D}{(a + r_g c_\infty) L_{\min}} \tag{3.13}$$

where $L_{\min}$ is the minimal axon length that can be achieved. The same value of the time discretization parameter Δt is used for both the implementation of the reorientation part of the model and the axonal outgrowth one.

Algorithm 1 Algorithm which solves the discretized version of the complete model presented in Eq. (2.64)

Reorientation input: $\mathbf{N}_0$, $\boldsymbol{X}_{\mathrm{GC}}^0$, f, ε, $\mathbb{T}(0)$, $\mathbf{C}_0(0)$
Axonal outgrowth input: L_0, c_0, $c_c(0)$, c_S
Using the second equation of the system (3.10) we get the initial outgrowth velocity
for $n = 0,1,\ldots,N$ **do**
    Update $\mathbf{X}_{\mathrm{GC}}$ in the Lagrangian configuration using Eq. (3.1)
    Compute the new GC orientation θ from Eq. (3.2)
    Compute the polarization $\mathbf{N}$
    Solve the tubulin-driven diffusion system Eq. (3.10)
    Update the growth speed V
    Update the stress tensor $\mathbb{T}$ using Eq. (3.3)
    Update $\mathbf{C}_0$ using Eq. (3.4)
end

Chapter 4

Results

After introducing the entire model for the process of axonal pathfinding in response to cyclic stretch, we are finally ready to present the numerical results obtained implementing in MATLAB ®the numerical scheme proposed in Chapter 3. The numeric discretization parameters Δt and Δy are set in order to satisfy the condition given in Eq. (3.13) and their values have been reported in the caption of each of the simulations shown in this Chapter.

In the first part of this Chapter, we present the parameter estimation for both the axonal elongation process and the reorientation of the growth cone. We will give all the values of the parameters collected from the experiments present in the literature. Subsequently, in Section 4.2 we use these parameters to test the sensitivity of our model. We are first going to test the axonal growth model given in Section 2.4 and then the reorientation model shown in Section 2.3.

Finally, in Section 4.3 we perform the numerical simulations for the entire model and we compare the results to the biological evidence given in the literature.

4.1 Parameter estimation

Axonal outgrowth model parameters

The values of the model parameters introduced in Section 2.4 are collected from the literature. The transport of tubulin and other cellular components along the axon has been widely tested. Despite that, this phenomenon is still not fully understood and experiments have been carried out on different types of neurons and cells [62–65]. Hence, it is not possible to determine a unique value for each of the parameters that are shown in our model. Still, we can provide some ranges of values within which the parameters can fall to be considered biologically valid. The complete list of suitable intervals for the axonal outgrowth is given in Table 4.1.

Parameter	Interval	Unit
a	0.5-3	$10^{-8}\,\mathrm{m/s}$
D	1-25	$10^{-12}\,\mathrm{m^2/s}$
g	1-200	$10^{-7}\,\mathrm{s^{-1}}$
L_c	1-20	$10^{-6}\,\mathrm{m}$
r_g	2.3	$10^{-7}\,\mathrm{m^4/s\,mol}$
$\tilde{r_g}$	0.053	$\mathrm{s^{-1}}$
c_∞	11.90	$10^{-3}\,\mathrm{mol/m^3}$
c_S	0-4c_∞	$10^{-3}\,\mathrm{mol/m^3}$

Table 4.1: Parameter values intervals for the axonal outgrowth model given in [48].

Before we choose the exact parameter values to assign to match the experimental evidence, in Section 4.2.1 we will study how the different parameters can affect the axonal growth. In particular, we will focus on the length of the axonal shaft L. In all the simulations that will be performed, we suppose the axon to be initially comparable to the dimension of the growth cone. Hence its initial value is set as $L_0 = 10\,\mu\mathrm{m}$. The tubulin concentration in the soma will be instead $c_S = 2c_\infty$ and it is supposed to remain constant in time. Since the axon is initially very short, we can assume that the initial tubulin concentration along the shaft is constant and equal to the tubulin concentration in the soma, giving $c(s,0) = 2c_\infty \,\forall s \in (0, L_0)$. For the same reason, we set the initial tubulin concentration in the growth cone equal to the concentration in the soma, i.e. $c_c(0) = 2c_\infty$. All the other parameters may vary and in Section 4.2.1 we will finally set all their values in order to get numerical results consistent with the experiments presented in [4].

Reorientation model parameters

Let us now introduce all the parameter values used to run the numerical simulations concerning the reorientation part of our model presented in Section 3.1. We start by defining all the mechanical properties of the substrate. We refer to the experiments conducted in [4]. They used 20×60×1 mm PDMS strips (Sylgard 184, 10:1) that were cured for 2 h at 80 °C. Considering the specific preparation condition, the material is reported to have a Young modulus $E = 2.05\,\mathrm{MPa}$ [43] and a Poisson's ratio $\nu = 0.495$ [66]. As said in the previous Chapters, the substrate is cyclically pulled by two lateral clamps. Since the region of interest where the neurons are analyzed is positioned in the central part of the substratum away from the lateral clamps (see Fig. 2.2), we can assume the uniaxial stretching condition. The strain

f (Hz)	0.05	0.15	0.25	0.25	0.25
ε (%)	10	10	10	2	5

Table 4.2: Values of stretching frequency and amplitude used in the experiments conducted in [4].

imposed along the x-direction takes the following sinusoidal form

$$\varepsilon_x(t) = \frac{1}{2}\varepsilon\left[1 - \cos\left(2\pi f t\right)\right] \tag{4.1}$$

while on the y-axis the strain is freely determined by the mechanical characteristics of the substrate because we are considering a uniaxial stretch. Thus, we can write $\varepsilon_y = -r\varepsilon_x$ and set $r = \nu = 0.495$. All the combinations of stretching frequency and amplitude tested are listed in Table 4.2.

We recall that, based on our model, we have determined that there are three equilibrium angles that exist in the first quadrant of the circumference. These angles, in the interval $[0, \pi)$ include one parallel to the stretching direction, one perpendicular, and one oblique. It is important to note that the corresponding angles can be found in the other quadrants due to symmetry reasons. According to biological pieces of evidence presented in [4], neurons tend to reorient themselves primarily along angles within the interval $[60° - 90°]$, and this pattern is symmetrically evident in the other quadrants as well. Therefore, we can assume that the oblique equilibrium is stable while the other two equilibria are unstable, as shown in Fig. 2.7. We have then set the oblique equilibrium angle to coincide with the medium value of the interval $[60°, 90°]$ obtaining $\theta_{\text{eq}} = 75°$, and given that $r = 0.495$, we have determined that $\mathcal{K} = 2.56$ using Eq. (2.48).

Considering Eq. (2.31), we now focus on the term K which is the Young modulus of the GC-substrate material. Due to the difficulty of determining this parameter experimentally, we follow the approach taken in [1] and introduce a new parameter, denoted as $\hat{K}_{\parallel}$, where

$$\hat{K}_{\parallel} = K_{\parallel} + 4K_{14} = K_{\parallel}\mathcal{K}.$$

Here, $K_{\parallel}$ relates to the stiffness of the GC-substrate material along the SFs direction. By setting $K = \hat{K}_{\parallel}$ and utilizing the simplified version of the energy density, the term $K_{\parallel}$ simplifies with the other terms present in Eq. (2.31) and Eq. (2.35). Therefore, in our work, the value of $K_{\parallel}$ does not directly influence the model results. We arbitrarily set $K_{\parallel} = 1$.

The growth cone viscous relaxation time has been measured to be below $10s$ in [67], while the change in its direction and the consequent steering of the axon requires a time in the order of minutes, according to [68]. The simulation will be performed using biologically plausible values. We set the growth cone relaxation

time $\lambda = 1\,\mathrm{s}$ and the time required to reorient $\lambda_\theta = 60\,\mathrm{s}$. These values give numerical results in good agreement with experimental evidence reported in [4].

Stochastic term

In this section, we will compute the value of the stochastic angular fluctuation σ present in Eq. (2.53). We first introduce $g = g(\theta, t)$ as the probability density function (PDF) of the growth cone orientation. The probability density function we are using is defined on $\theta \in [0, \pi)$. The dynamics of g is given by the Fokker-Planck equation [59], whose equilibrium solution in our specific case is

$$g^\infty(\theta) = C \exp\left[-\frac{1}{4\bar{\sigma}^2}(1+\nu)^2\cos^4\theta - \frac{1}{4\bar{\sigma}^2}(1+\nu)(S-2\nu)\cos^2\theta - \frac{1}{4\bar{\sigma}^2}\nu(\nu-S)\right]. \tag{4.2}$$

where $S = (\mathcal{K}-1)(1-r)$ and $\bar{\sigma}^2 = \dfrac{\sigma^2}{2\varepsilon_x^2}$. The definition of $\bar{\sigma}$ is valid in the high-frequency regime which is indeed our case of interest. It clearly shows how the higher the strain, the more focused the response to the reorientation. Hence we obtain more peaked distribution than the ones with a lower stretch amplitude.

At this point, we introduce the definition of circular average on the interval $[0, \pi)$

$$\bar{\theta}_l(t) \coloneqq \int_0^\pi \theta\, g^\infty(t, \theta)\, d\theta \tag{4.3}$$

and we compute the value of σ such that $\bar{\theta}_l$ is equal to the oblique equilibrium angle given in Section 4.1, i.e. we set $\bar{\theta}_l = \theta_{\mathrm{eq}} = 75°$. We then set the amplitude of the applied strain $\varepsilon = 10\%$, since it is the value used in the experiments conducted in [4] which we would like to numerically reproduce with our model. Using MATLAB ®, we find that the optimal choice for the angular dispersion parameter is $\sigma = 0.0095$. In Fig. 4.1 we display the equilibrium PDF g^∞ for different stretching amplitudes ε. As we predicted, the distribution becomes more peaked with increasing strain level, in correspondence with the oblique equilibrium angles of the first two quadrants of the circumference. This implies that for the higher frequency rate, the deterministic term will significantly influence the dynamics of θ. Conversely, for lower strain amplitudes, the stochastic term has greater significance compared to the deterministic one. Thus, growth cones are inclined to follow orientations that deviate from the equilibrium.

4.2 Sensitivity analysis

This section is dedicated to the sensitivity analysis of the different parts that make up our model. We are going to vary some of the values of the parameters and then

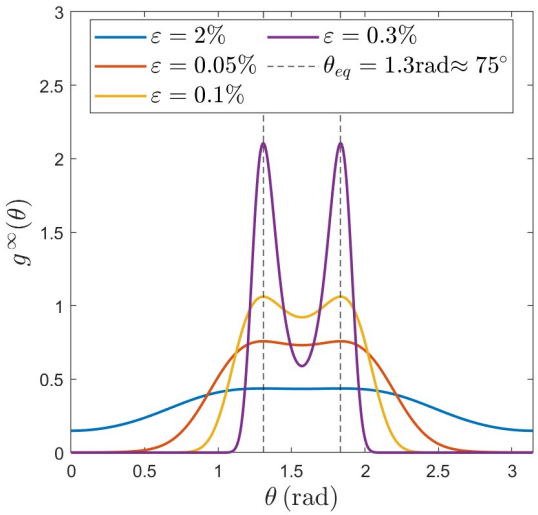

Figure 4.1: Plot of the equilibrium PDF g^∞ depending on different values of the stretching amplitude ε with fixed $\sigma = 0.0095$ and $r = 0.495$.

discuss how the simulations are affected by these variations. This will allow us to finally determine the best values to use in the simulations of the entire model that will be performed in Section 4.3.

4.2.1 Axonal outgrowth parameters

We start by varying the tubulin active transport velocity a (see Fig. 4.2a). As we can imagine, the higher the transport of the tubulin along the axonal shaft is, the longer the resulting axon will be. This is due to the fact that with a higher transport velocity, more tubulin arrives from the soma to the growth cone leading to a higher assembly rate for the new microtubules. We can observe that, an increase in the values of a leads to an increase in the length of the axonal extension, following a linear behaviour. The result is similar if we vary the diffusion coefficient D, as done in Fig. 4.2b. In this case, we can see how for lower values of D, a small increment in its value can lead to a considerable increase in the length of the neurite. As D becomes larger, the axonal extension increment gets smaller. The other parameter we decided to vary is the length of the growth cone L_c (see Fig. 4.2c). A longer growth cone leads to a larger amount of volume where the tubulin can be stored and then polymerized. So, the longer the growth cone, the longer the axonal shaft is. That behaviour is well captured by our model, even though 50 µm and 100 µm are extreme values that cannot be observed in nature and have been simulated just to display the role of the GC length in our model. Finally, we varied the value of the tubulin degradation rate g. From what we reported in Fig. 4.2d, we can state

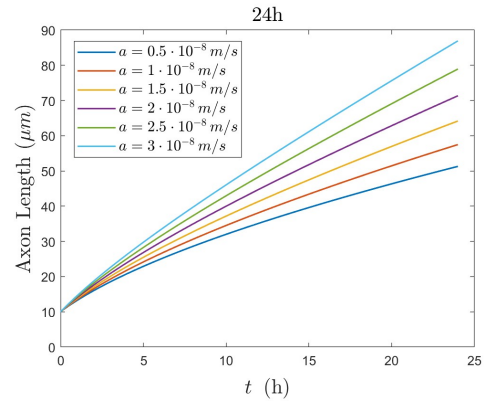

(a) $D = 1 \cdot 10^{-12}$, $g = 5 \cdot 10^{-7}$, $L_c = 4\,\mu m$, $\Delta y = 0.05$, $\Delta t = 0.1\,s$

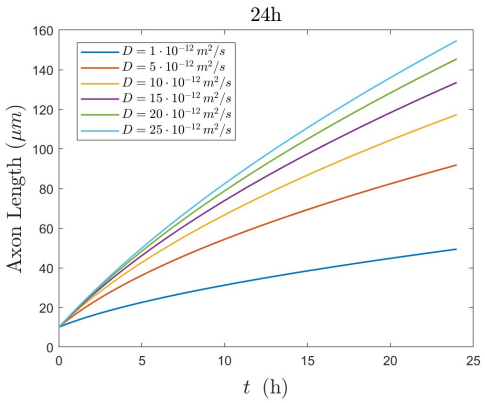

(b) $a = 0.5 \cdot 10^{-8}$, $g = 5 \cdot 10^{-7}$, $L_c = 4\,\mu m$, $\Delta y = 0.1$, $\Delta t = 0.02\,s$

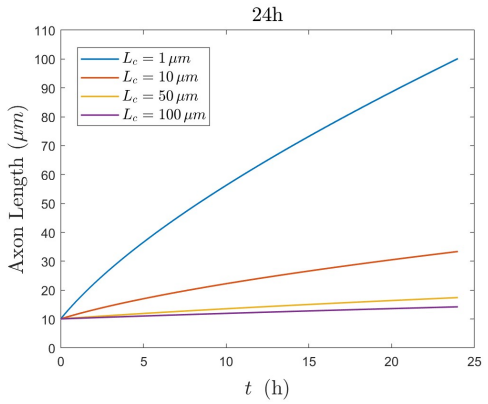

(c) $D = 1 \cdot 10^{-12}$, $g = 5 \cdot 10^{-7}$, a=$0.5 \cdot 10^{-8}$, $\Delta y = 0.05$, $\Delta t = 0.1\,s$

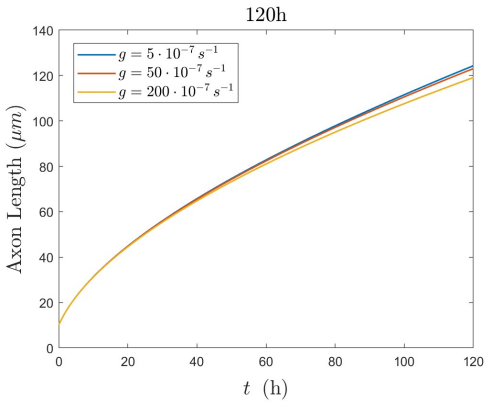

(d) $D = 1 \cdot 10^{-12}$, $a = 0.5 \cdot 10^{-8}$, $L_c = 4\,\mu m$, $\Delta y = 0.05$, $\Delta t = 0.1\,s$

Figure 4.2: Parametric sweep for the tubulin driven axon outgrowth model. The initial conditions are: $L_0 = 10$, $c_S = 2c_\infty$, $c(s,0) = 2c_\infty \, \forall s \in (0, L_0)$, $c_c(0) = 2c_\infty$.

that the importance of this parameter becomes more evident as the simulation time increases. Indeed, in the 24 h simulation, no differences have been noted. With 120 h simulated, the difference becomes slightly visible even though a large change in the value of g corresponds to a very small change in the axonal length. We can suppose that for longer times simulations, these differences become more evident. We can, instead, state that by increasing the value of g, the length of the neurite decreases. This is consistent with the fact that if the degradation rate of the tubulin is higher, there is less free tubulin available in both the axon and the GC to be polymerized into the new microtubules. We can conclude that D is the parameter that mostly affects the axon growth rate among the four discussed.

Parameter	Value	Unit
a	0.5	$10^{-8}\,\mathrm{m/s}$
D	1	$10^{-12}\,\mathrm{m^2/s}$
g	5	$10^{-7}\,\mathrm{s^{-1}}$
L_c	4	µm
r_g	2.3	$10^{-7}\,\mathrm{m^4/s\,mol}$
$\tilde{r}_g$	0.05	$\mathrm{s^{-1}}$
c_∞	11.90	$10^{-3}\,\mathrm{mol/m^3}$
c_S	$2c_\infty$	$10^{-3}\,\mathrm{mol/m^3}$
L_0	5	µm

Table 4.3: Parameter values used for the simulation shown in Figs. 4.3 and 4.4

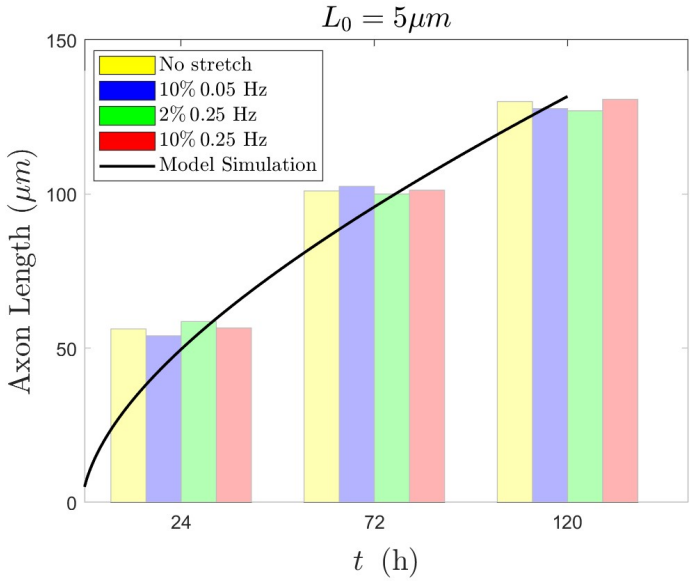

Figure 4.3: Comparison between the length of the axon obtained by our simulation (solid line) and some of the experimental evidence given in [4] (coloured vertical bars). The data are reported after 24 h, 72 h and 120 h from the beginning of the experiment. For the simulation, we set $\Delta y = 0.02$, $\Delta t = 0.005$ and used the parameters in Table 4.3.

We now want to find the parameter values that better fit the experimental data presented in [4]. In the experiments, no significant difference has been observed in the length of the neuron growth under cyclic loading and the control ones. This led us to not include any tension-related term in the axonal growth model. We performed a simulation of an axon growing for 120 h by considering an initial

neurite length of $L_0 = 5\,\mu\text{m}$. The tubulin concentration in the soma is $c_S = 2c_\infty$ and constant in time. The initial conditions for the tubulin concentration along the axon and in the growth cone are the same as the previously presented simulations: $c(s,0) = 2c_\infty \, \forall s \in (0, L_0)$ and $c_c(0) = 2c_\infty$. By using the parameter values listed in Table 4.3 we obtain the results shown in Fig. 4.3, in terms of axon length, and Fig. 4.4 in terms of tubulin concentration in space and time. In particular in Fig. 4.3 a comparison between experimental evidence and our model result is given. We can see how the model fits the data given by [4] at different times of the axonal elongation process. From the same simulation, we plotted the tubulin concentration profile along the axon after 120 h (see Fig. 4.4a) and the history of the tubulin concentration in the growth cone (see Fig. 4.4b). We can see how the tubulin concentration gradually decreases as we move toward the GC and its maximum value is in correspondence with the soma. At the axon termination, we have the lowest value corresponding with the free tubulin concentration present in the growth cone. This is consistent with the fact that the flux of tubulin goes from the soma to the axon tip. For what concerns the concentration of free tubulin in the growth cone we can notice how it rapidly decreases to reach the equilibrium value c_∞ as we expected. We recall that the more free tubulin is present in this area, the more microtubules are assembled and so the higher is the axonal elongation.

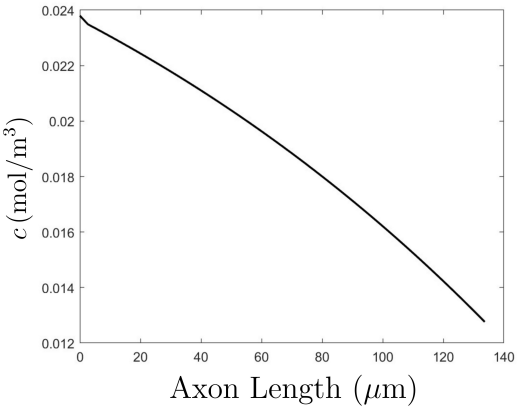

(a) Free tubulin concentration profile along the axonal shaft after 120 h

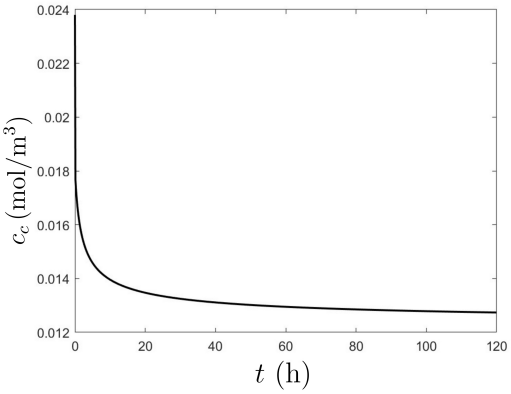

(b) Time evolution of the free tubulin concentration in the growth cone

Figure 4.4: Free tubulin concentration profiles resulting from our model. We used the parameters in Table 4.3 and we set $\Delta y = 0.02$ and $\Delta t = 0.005$.

4.2.2 Reorientation parameters

In this section, the numerical results for the reorientation of the sole growth cone are given. In this phase, we don't consider any stochastic term. Hence the dynamics

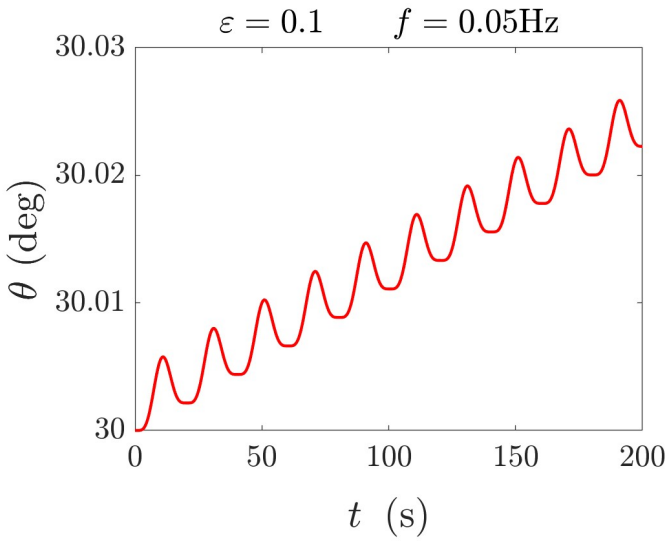

Figure 4.5: Time evolution of θ for a very short period according to Eq. (2.31) and Eq. (2.35). The starting angle is $\theta_0 = 30°$. The other parameters used in the simulation are: $r = 0.495$, $\lambda = 1\,\mathrm{s}$, $\lambda_\theta = 60\,\mathrm{s}$ and $\Delta t = 0.1s$.

of the orientation angle θ is solved according to Eq. (2.31) and Eq. (2.35). In all the simulations $\theta_0 = 30°$ is the starting orientation angle, while both the stress tensor $\mathbb{T}$ and the functional $\mathbf{C}_0$ have been set identically equal to 0 at $t = 0$ because we start the simulation from the undeformed state. We also fixed the biaxiality ratio $r = 0.495$.

We first analyze Fig. 4.5, where the reorientation process of the growth cone has been simulated for a very short period imposing a cyclic deformation with frequency $f = 0.05\,\mathrm{Hz}$ and strain amplitude $\varepsilon = 10\%$. We can see how the dynamics of θ displays an oscillatory behaviour, as expected, because we are applying a periodic deformation to the substrate. Consequently, the orientation angle gradually increases through small oscillations until it reaches the predicted orientation. The magnitude and the frequency of such oscillations depend on the characteristics of the cyclic stretch imposed on the sample. However, when considering larger simulation periods these oscillations become harder to distinguish because of graphical reasons.

Let us now consider the numerical results given in Fig. 4.6, where we simulated the growth cone reorientation process for longer periods such as 24 h and 120 h. We first analyze the case where the frequency is fixed at value $f = 0.25\,\mathrm{Hz}$ and the stretching amplitude varies. In the simulations, we have included also the strains tested in [4] (2%, 5% and 10%). From Fig. 4.6a we can see that the higher the strain rate is, the faster the reorientation process occurs. Indeed, for $\varepsilon = 30\%$ the

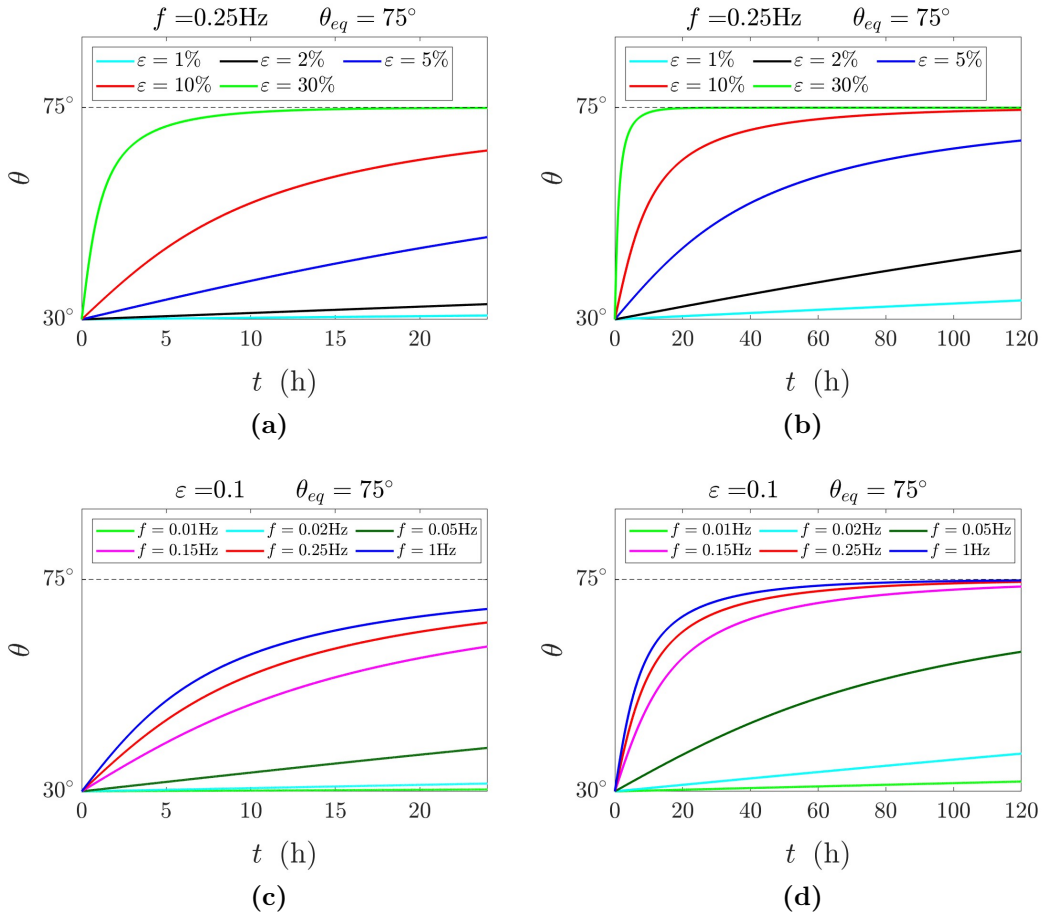

Figure 4.6: Time evolution of θ starting from $\theta_0 = 30°$. In (a)-(b) the frequency is fixed and the strain varies. In (c)-(d) the stretching amplitude is fixed and various frequencies have been tested. In all the simulations $r = 0.495$, $\lambda = 1\,\mathrm{s}$, $\lambda_\theta = 60\,\mathrm{s}$ and $\Delta t = 0.1s$.

equilibrium angle is reached after just 10 h. For lower values of ε, e.g. 10% and 5%, it is necessary to wait around 120 h in order to see the growth cone reaching the oblique equilibrium $\theta_{\mathrm{eq}} = 75°$ (see Fig. 4.6b). Instead, for very low values of the strain rate the reorientation process takes longer times. Even after 120 h, there is just a slight difference between the final angle and the initial one. This leads to having in fact no visible reorientation during the experimental observation periods. The numerical results are thus in good agreement with what is presented in [4]. Indeed, in [4] data were collected after 24 h, 72 h and 120 h of stretching. With a frequency of $f = 0.25\,\mathrm{Hz}$, neurons showed no significant reorientation when $\varepsilon = 2\%$. At $\varepsilon = 10\%$, a large number of neurons aligned themselves to angles

between 60° and 90° or their symmetric counterparts in other quadrants within just 24 hours. After 120 h, all the cells resulted aligned in that direction. The reorientation process was also observed for $\varepsilon = 5\%$, albeit at a slower rate, resulting in some neurons not aligning to the equilibrium direction.
We now consider the simulations in which the strain rate is fixed at $\varepsilon = 10\%$ and various frequencies are tested. Also in this case the values used in [4] for the stretching frequency have been included (0.05 Hz, 0.15 Hz and 0.25 Hz). Considering Fig. 4.6c is clear that higher frequencies induce reorientation with a characteristic time that decreases with the frequency. However, the higher the frequencies become, the less significant the acceleration of the reorientation process is. We can indeed notice how after around 60 h the behaviour for the higher frequencies tested is substantially the same and they both led the growth cone to reach the final reorientation angle after 120 h. The results are consistent with the biological evidence in [4]. Considering $f = 0.05\,\text{Hz}$ the reorientation process takes place in a shorter time compared to what occurs with higher frequency values as $f = 0.15\,\text{Hz}$ and $f = 0.25\,\text{Hz}$.
Another interesting phenomenon that can be seen from our simulations is the presence of a minimum threshold under which the cyclic stretch does not induce any significant response in the growth cone orientation. This happens also with other cell types [1]. In our case, the threshold value can be quantified around $f = 0.017\,\text{Hz}$. This frequency sets the transition from the low-frequency regime to the high-frequency one. Since we have that $\lambda_\theta \gg \lambda$, the transition is mostly affected by λ_θ and happens when $\lambda_\theta f \approx 1$. In the high-frequency regime the relaxation time, i.e. λ_θ, is much longer than the oscillation period T of the cyclic deformation. So, the reorganization process of the cell is slower than the period of the imposed strain. The growth cone response in this case is elastic and it reorients itself by minimizing the energy. On the contrary, in the low-frequency regime, the reorientation process becomes viscous. The period of the imposed deformation is longer than λ_θ and therefore the growth cone adapts to the imposed strain and does not reorient significantly on the time scale of the experiment. Based on our simulations, it is evident that there is no significant reorientation of the growth cone even after 120 h when the frequency is at 0.01 Hz, which falls under the low-frequency regime. Additionally, we observed that for a frequency of 0.02 Hz, which is only slightly above the minimum threshold, the reorientation process takes longer than the experimental observation period. In contrast, all frequencies tested in the study by Lin et al. (2020) belong to the high-frequency regime, where the growth cone successfully reorients itself to reach the equilibrium angle.

4.3 Complete model simulations

Now everything is ready to present the simulation results of the entire neuron reorientation and axonal outgrowth model given in Eq. (2.64). Ideally, it would be possible to simulate the growth of all neurons distributed on the substrate simultaneously. However, for computational reasons, we chose to simulate the growth of each individual neuron independently, assuming that each of them is positioned at the centre of the substrate. The two approaches are equivalent since the mechanical behaviour of the substrate in the testing region is uniform as shown in Fig. 2.2. Furthermore, we remark that the chosen approach neglects the possibility of neurons coming into contact, during their growth and reorientation process, which is something not included in the mathematical model.

Recalling that the soma is fixed, we set for each of the neurons simulated

$$\mathbf{X}_S = (0,0), \qquad L_0 = 5\,\mu\text{m}, \qquad \theta_0 \in U(0,\, 2\pi), \tag{4.4}$$

where U in this case is the continuous uniform distribution. In this way, we can faithfully reproduce the random initial distribution of neurites' orientations. Consequently, the initial conditions assigned to the growth cone position and orientation are

$$\mathbf{N}_0 = \Big[\cos\theta_0,\, \sin\theta_0\Big]^\top, \qquad \mathbf{X}_{\text{GC}}(0) = L_0\mathbf{N}_0, \tag{4.5}$$

and the neurite at time $t = 0$ is the end-to-end segment from $\mathbf{X}_S$ to $\mathbf{X}_{\text{GC}}(0)$ (see. Fig. 4.7a - green line). Initially, the orientation of the axon and the growth cone coincide, i.e. $\theta_0 = \varphi_0$.

We begin by presenting a comparison of the simulated growth cone dynamics in Fig. 4.7 when the random term is included versus when it is not. We recall that in our model, the axon does not coincide with the path followed by the growth cone, but it is the segment that links the soma to the growth cone and we suppose that it instantly reforms at each instant. When comparing Fig. 4.7a and Fig. 4.7b, we can notice that in the case without the random term, the trajectory followed by the growth cone is smoother. On the contrary, the addition of the random term makes the path followed by the cone less regular, thus simulating the crawling process of the cell structure. The final orientation of both the growth cone and the axon differs as well in the two cases, even though they are similar. Indeed, the random term can both speed up or slow down the reorientation process, thereby replicating the natural variability of the single neuron behaviour.

In order to validate the model, we made some statistics on the simulations and compared them to the experimental results reported in [4]. At first, we considered that the phenomenon of growth occurred with constant velocity, ignoring the tubulin-driven axonal growth model. The velocity considered is $V = 4 \cdot 10^{-10}\,\text{m/s}$

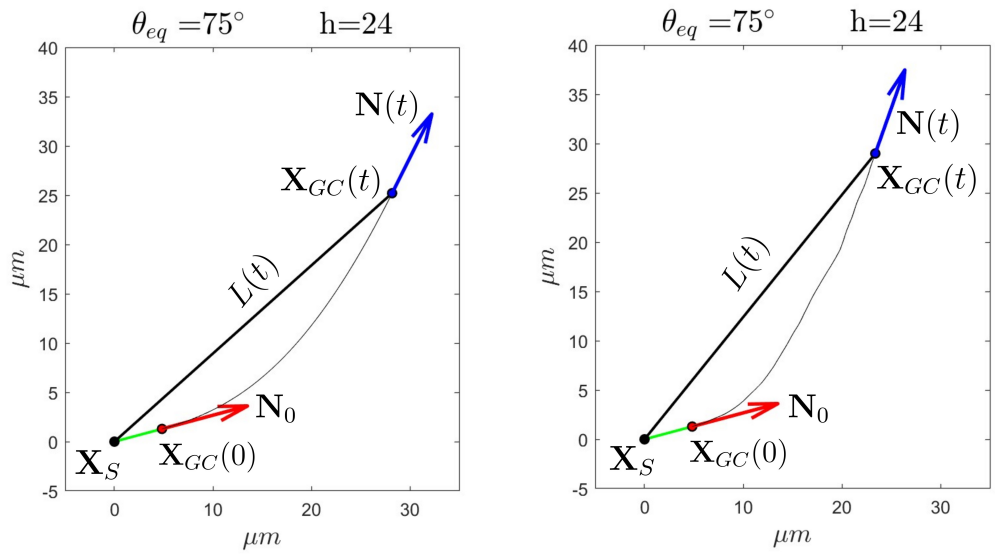

(a) No random term added **(b)** Random term added

Figure 4.7: Simulations of axon growth and reorientation for 24 h when no random term is considered and when it is. The thicker green line is the axon at initial time $t = 0$. The thin line is the path followed by the growth cone according to Eq. (2.20). The initial orientation angle is $\theta_0 = \pi/12$, the growth velocity is supposed to be constantly equal to $V = 4 \cdot 10^{-10}\,\mathrm{m/s}$. We have set $f = 0.25\,\mathrm{Hz}$, $\varepsilon = 10\%$ and $\Delta t = 0.1s$.

which is simply an average of the experimental instant velocities reported in [4] at 24, 72 and 120 h. We included the random term while keeping other parameters as listed in Table 4.3. To obtain statistically valid results, we simulated the reorientation process and growth of 100 different neurons with the initial conditions given in Eq. (4.4) and Eq. (4.5). We set $\Delta t = 0.1\,\mathrm{s}$ and reported the results at 24, 72 and 120 h. The combinations of values for the stretching frequency and amplitude investigated are the ones listed in Table 4.2. In order to easily compare the numerical results with the experimental ones, we used circular histograms to represent the statistics of our model. The same representation method has been used by Lin et al. in [4] where they analysed the reorientation process of 100 neurons and they summarized the results as circular histograms. Specifically, Fig. 4.8 and Fig. 4.9 respectively highlight how variations in either the strain amplitude or the frequency affect neuron reorientation. In all cases, the circle has been divided into 12 slices measuring 30° each. Then at 24, 72 and 120 h they counted how many axons fell into each of the slices and generated the relative circular histograms.

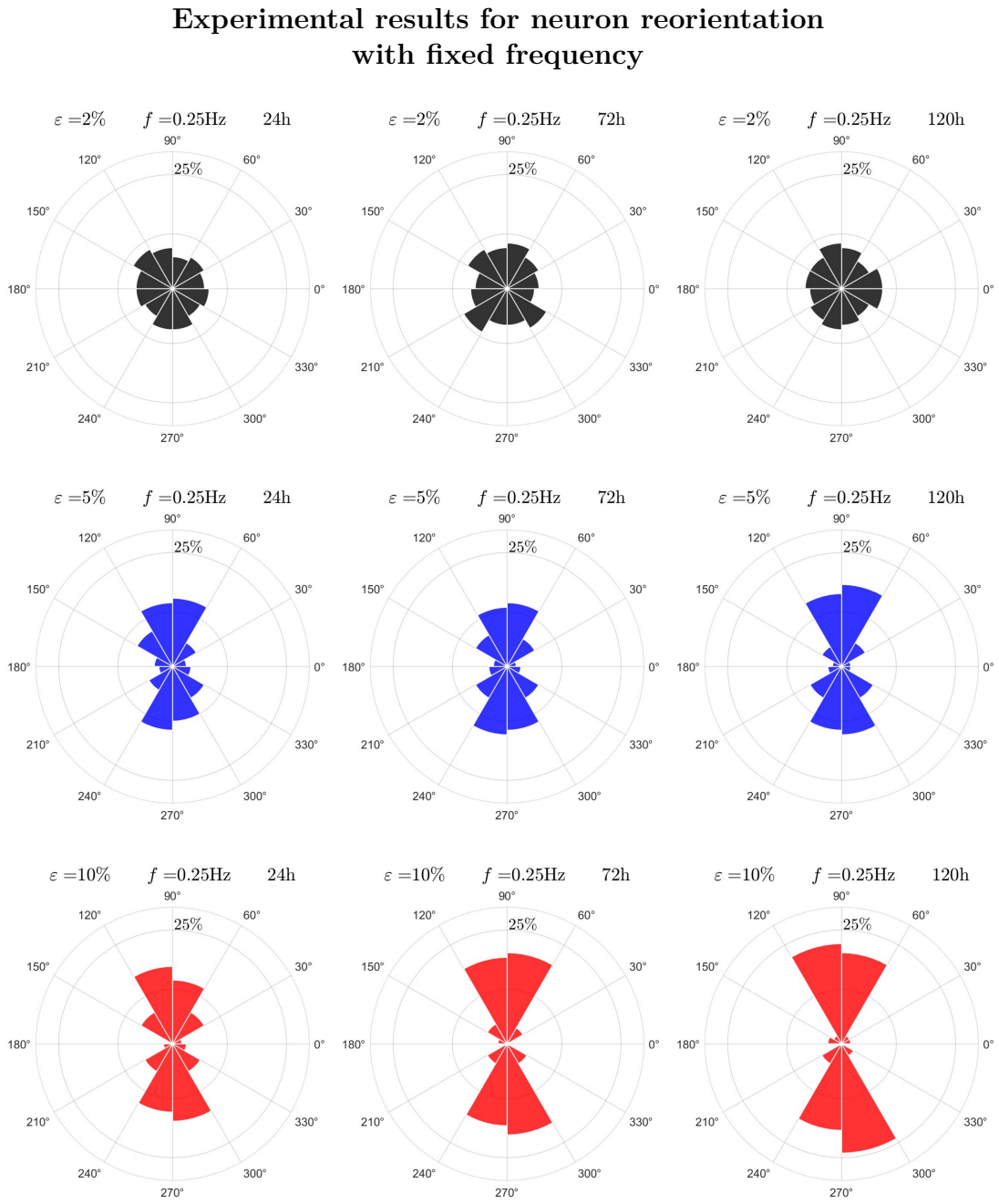

Figure 4.8: Statistical results of neuron reorientation taken from the experiments conducted by Lin et al. in [4] when the frequency is fixed equal to $f = 0.25\,\text{Hz}$ and different strain amplitudes are considered. A sample of $N = 100$ neurons has been analysed in the experiments. The histogram bars represent the percentage of neurons whose orientation angle falls into the specific slice of the circle.

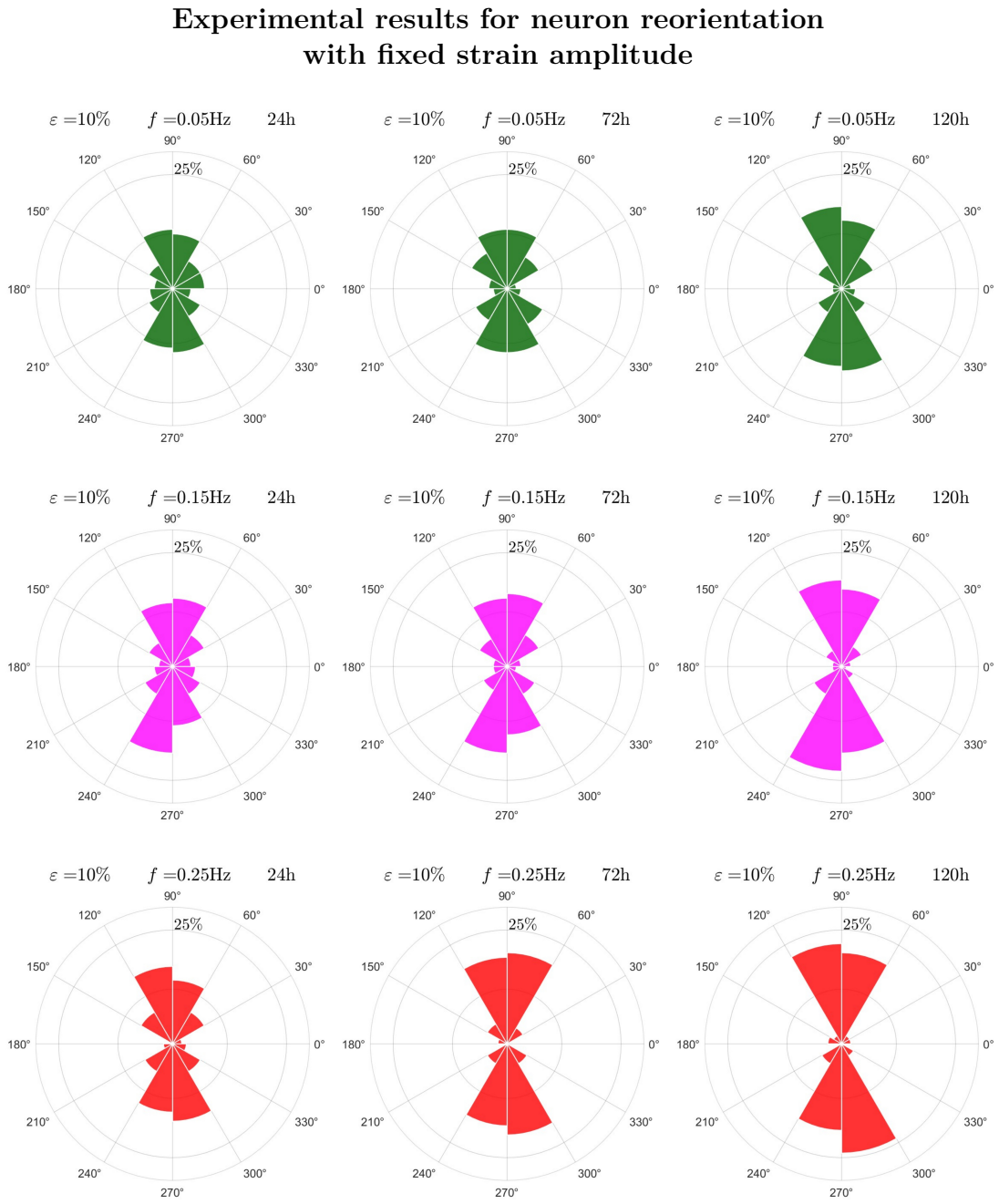

Figure 4.9: Statistical results of neuron reorientation taken from the experiments conducted by Lin et al. in [4] when the strain amplitude is fixed equal to $\varepsilon = 10\%$ and different frequencies are considered. A sample of $N = 100$ neurons has been analysed in the experiments. The histogram bars represent the percentage of neurons whose orientation angle falls into the specific slice of the circle.

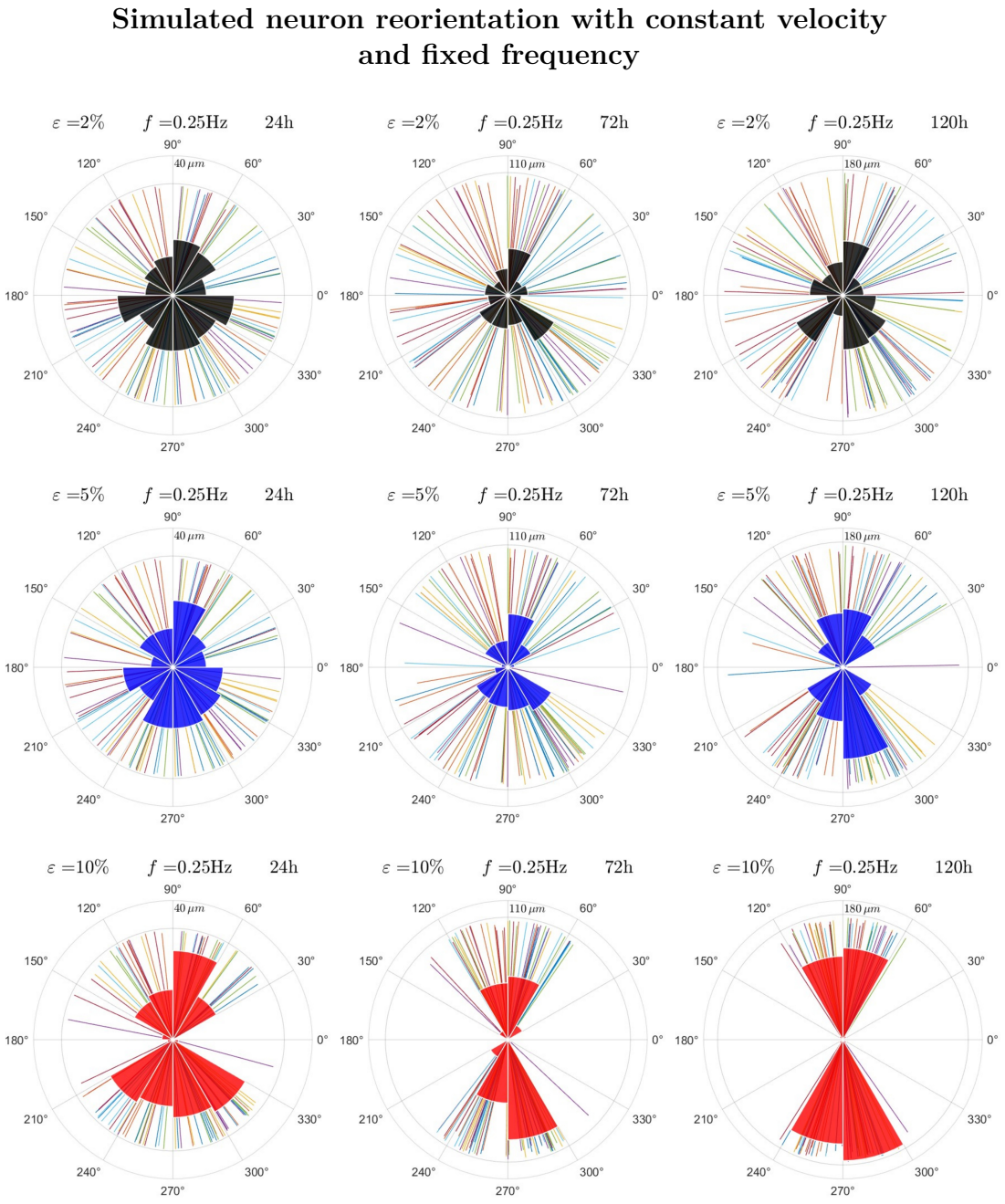

Figure 4.10: Statistical results of neuron reorientation at different strain amplitudes and at constant frequency. The random term is included, the growth velocity is constant with value $V = 4 \cdot 10^{-10}\,\mathrm{m/s}$, $\lambda = 1\,\mathrm{s}$, $\lambda_\theta = 60\,\mathrm{s}$ and $\Delta t = 0.1\,\mathrm{s}$. The statistics are made on 100 simulated neurons.

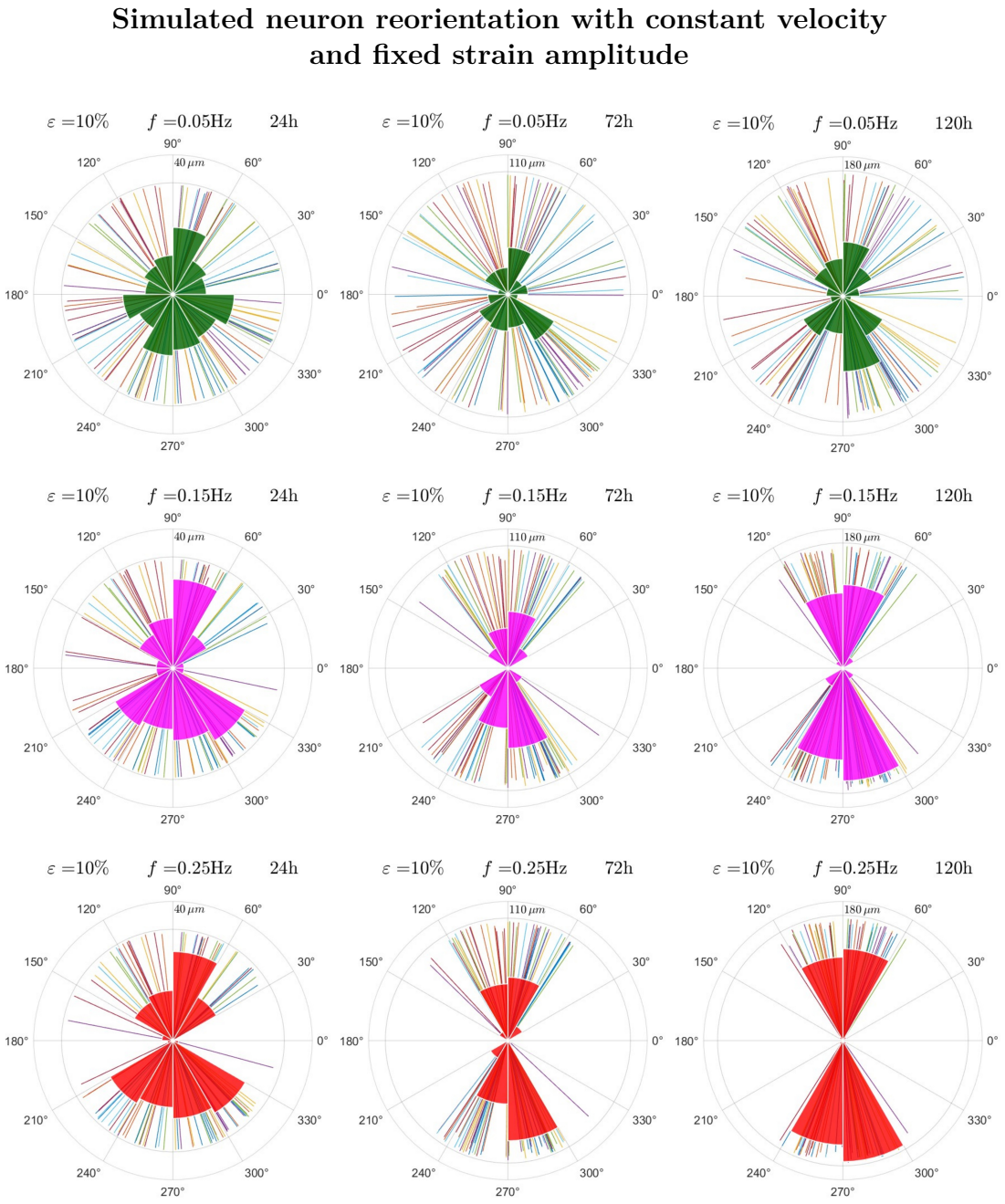

Figure 4.11: Statistical results of neuron reorientation at different frequencies and at constant stretching amplitude. The random term is included, the growth velocity is constant with value $V = 4 \cdot 10^{-10}\,\mathrm{m/s}$, $\lambda = 1\,\mathrm{s}$, $\lambda_\theta = 60\,\mathrm{s}$ and $\Delta t = 0.1\,\mathrm{s}$. The statistics are made on 100 simulated neurons.

We applied the same procedure to our model on a sample of $N = 100$ simulated neurons. The resulting circular histograms with the resulting simulated axons of the model are given in Fig. 4.10 and Fig. 4.11. At a first sight, the numerical simulations appear to be in good agreement with the experimental observation in Figs. 4.8 and 4.9. The reorientation process is well simulated and clearly visible from the histograms. Indeed, simulated neurons tend to align perpendicularly with respect to the main stretch direction. The different behaviours at different frequencies and amplitudes are mimicked as well: increasing either the strain amplitude or the frequency, the reorientation process becomes faster.
Finally, we observed that the absence of reorientation, biologically observed for small strains, can be reproduced in the model. Indeed, at 2% strain rate, the distribution of the neurons' orientation angles stays uniform along the circumference even after 120 hours of cyclic deformation. The qualitative discrepancies that we can point out are: axons appear to be longer than the ones observed in the experiments. For example, after 120 h the simulated neurons are around 60 µm longer than the real neurons tested in [4]. Furthermore, we remark that the reorientation process is not finely reproduced for the lowest of the frequency values tested. Indeed, when $f = 0.05\,\mathrm{Hz}$ despite the simulated neurons reorienting over time, the entire process occurs much more slowly compared to experimental observations.

To further investigate the numerical results, let us introduce the *order parameter* defined as

$$\langle \cos 2\varphi \rangle = \frac{1}{N} \sum_{i=1}^{N} \cos 2\varphi_i \tag{4.6}$$

where N is the total number of neurons and φ_i if the orientation angle of the i-th axon. The value of this parameter can span from -1 to 1: a random orientation of the sample corresponds to 0, a fully coherent parallel orientation gives 1 and a fully perpendicular one equals -1. We computed the order parameters for the simulations in Fig. 4.10 and Fig. 4.11 and plotted their time evolution in Fig. 4.15. As anticipated, we observe a monotonically decreasing trend in the computed order parameter, in line with the experimental data. However, it is noticeable that the model tends to overestimate the order parameter values, particularly over extended simulation periods such as 72 and 120 h. This implies that the reorientation process is simulated faster than it occurs in reality. A possible way to overcome this problem is to decrease the time needed by the growth cone to change its orientation, i.e. decrease the value of λ_θ. The other option that we will implement further in this work is to drop the assumption that the axon growth velocity is constant. Indeed, we saw in Section 4.2.1 how with the tubulin-driven axonal growth model neurons tend to progressively decrease their growth rate as time passes. Consequently, the axon reorientation process also experiences a slowdown when coupled with the tubulin-driven axonal outgrowth, resulting in simulation outcomes more in line with experimental observations. On the contrary, when the strain amplitudes are

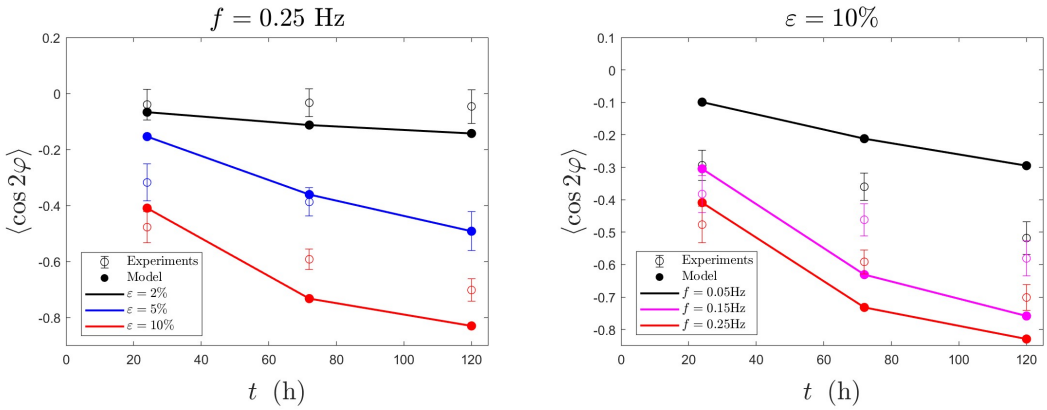

Figure 4.12: Evolution of order parameters for the simulated neuron cells on the substrate subjected to cyclic stretch with different values of frequency and amplitude. The axon outgrowth velocity is supposed to be constant. The empty circles are experimental data from [4] with error bars representing the standard deviation, and the solid curves are the simulation results of our model.

5% or 10% and for shorter periods such as 24 h, there is an underestimation of the order parameter. This might be attributed to the axon's orientation angle φ not having sufficient time to align with that assumed by the growth cone θ. Nonetheless, we can state that the model performs well in replicating differences in strain amplitude with a high stretching frequency, but it seems to have difficulty in accurately capturing the different behaviours when varying the frequency value.

At this point, we perform simulations assuming that the velocity is no longer constant but determined by the axonal growth model outlined in Section 2.4. Thus, we will simulate the complete model as presented in Eq. (2.64). Similarly to the previous case, 100 different neurons with random initial orientations have been simulated, and the results have been compared to those presented in [4] reproduced in Fig. 4.8 and Fig. 4.9. The parameters for the axonal outgrowth used are listed in Table 4.3. As previously done, all the statistics are given as circular histograms in Fig. 4.13 and Fig. 4.14. In comparison to the previous situation, it can be observed that the inclusion of the axonal growth model via tubulin diffusion successfully results in neurons reaching a length around 110 µm after 120 h. This is consistent with the experimental data reported in [4]. Hence, the addition of the tubulin-driven model to the reorientation process allowed us to overcome the overestimation of the neurons' length that we previously had obtained when we used a constant value for the axonal outgrowth velocity.

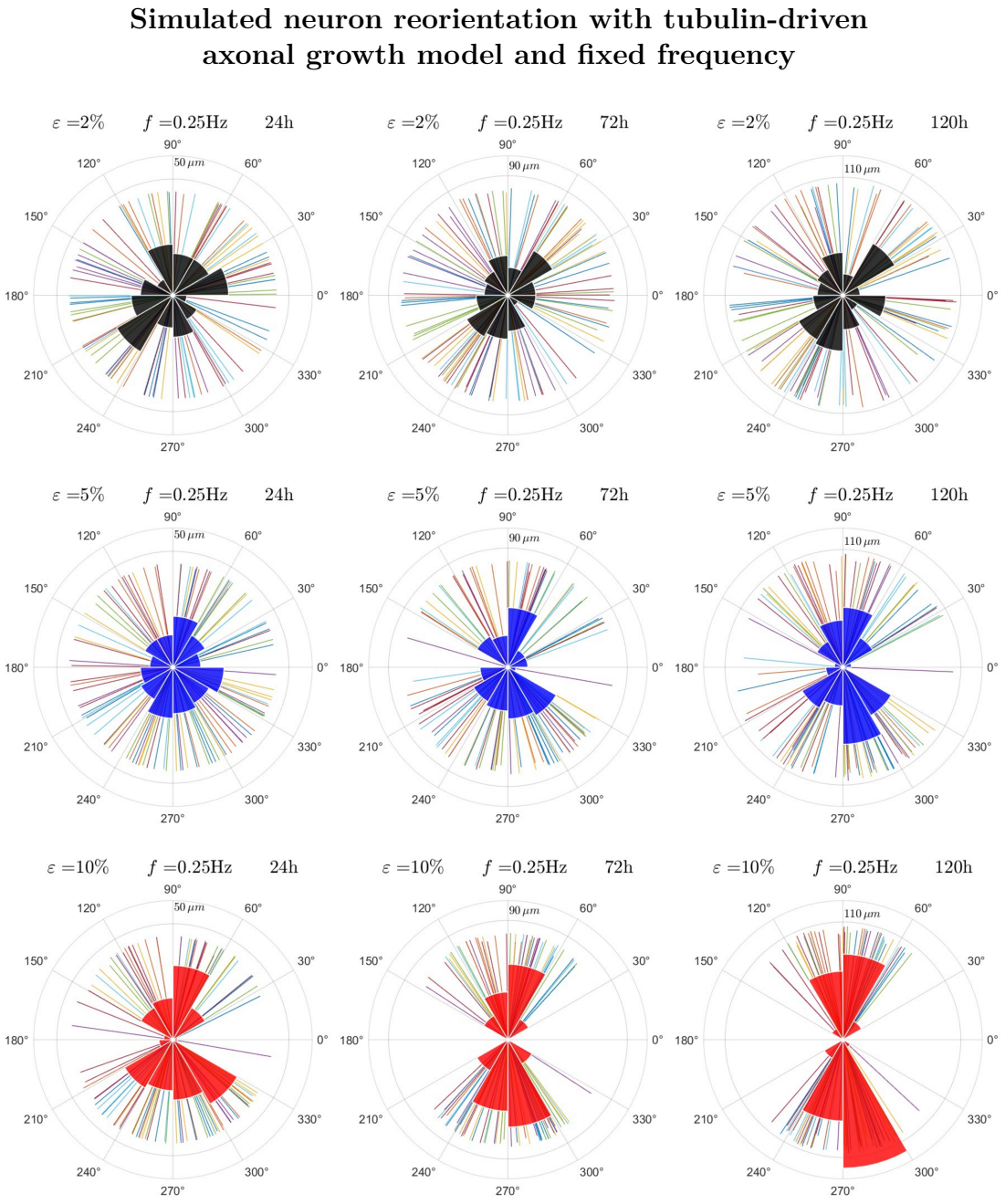

Figure 4.13: Statistical results of neuron reorientation at different stretching amplitudes and at constant frequency when the tubulin-driven axonal growth model is implemented. The random term is included, $\lambda = 1\,\text{s}$, $\lambda_\theta = 60\,\text{s}$, $\Delta x = 0.1$ and $\Delta t = 0.1\,\text{s}$. The statistics are made on 100 simulated neurons.

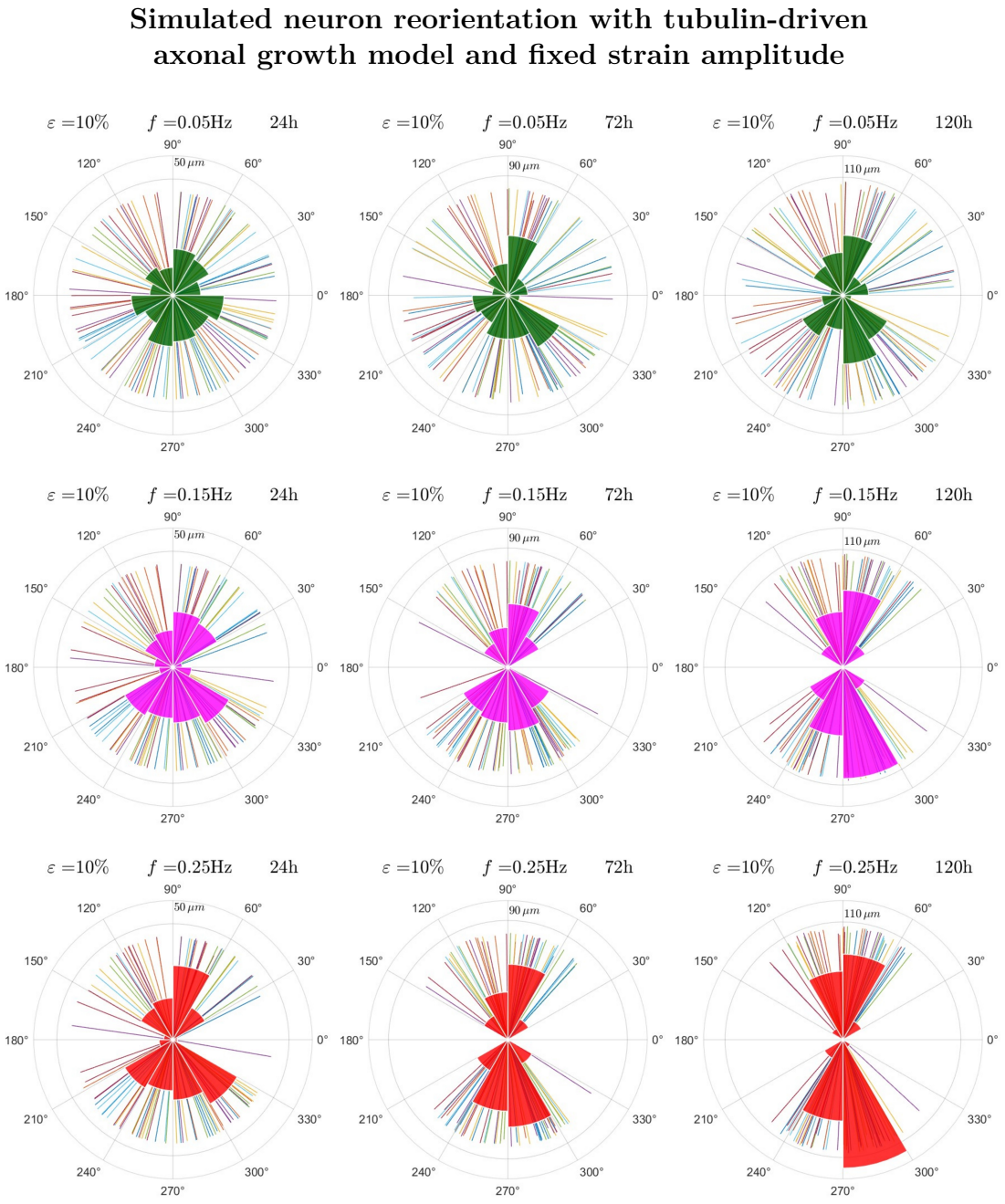

Figure 4.14: Statistical results of neuron reorientation at different frequencies and at constant stretching amplitude when the tubulin-driven axonal growth model is implemented. The random term is included, $\lambda = 1\,\mathrm{s}$, $\lambda_\theta = 60\,\mathrm{s}$, $\Delta x = 0.1$ and $\Delta t = 0.1\,\mathrm{s}$. The statistics are made on 100 simulated neurons.

If we compare the numerical results given in Figs. 4.13 and 4.14 with the histograms computed from the experiments in Figs. 4.8 and 4.9, we can state that when analyzed in its entirety, the model effectively predicts the behaviour of neurons exposed to dynamic stimuli. However, we can still observe that when using a low frequency ($f = 0.05\,\text{Hz}$) the model struggles to produce results faithful to the experimental data (compare Fig. 4.14 and Fig. 4.9). Although the reorientation process takes place, it is not simulated quickly enough, which ultimately results in a broader angular distribution of the axons' orientation. Let us now refer to Fig. 4.15 to make a deeper analysis of the order parameters defined in Eq. (4.6). We first notice that at 24 h the reorientation process is underestimated with order parameters that are higher than the experimental ones. As already anticipated, the fact that the orientation of the growth cone and the axon differs may lead to a delay in the axon reaching the equilibrium orientation in a short time. However, for longer periods, in most of the numerical tests performed, the simulation results are in good agreement with what is reported in [4]. The model has been able to fit the different behaviours between the 0.15 Hz case and the 0.25 Hz one after 72 and 120 hours. The model has been also able to mimic the absence of the reorientation when $\varepsilon = 2\%$ and $f = 0.25\,\text{Hz}$. Conversely, the model lacks in finely reproducing what happens in the experiments when the strain amplitude is equal to 5% and in the case of a relatively low frequency $f = 0.05\,\text{Hz}$.

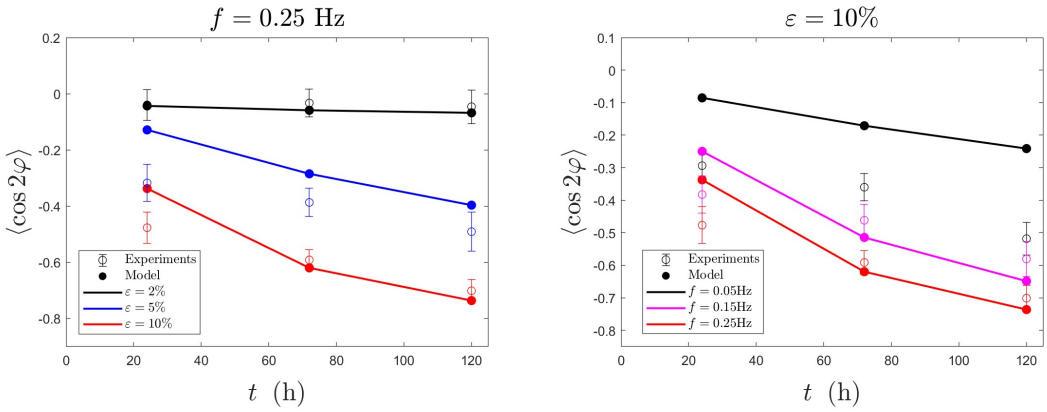

Figure 4.15: Evolution of order parameter for the simulated neuron cells on the substrate subjected to cyclic stretch with different values of frequency and amplitude. The tubulin-driven axonal outgrowth model has been considered in the simulations. The empty circles are experimental data from [4] with error bars representing the standard deviation, and the solid curves are the simulation results of our model.

Chapter 5

Conclusions and perspectives

The directional alignment and outgrowth of neurons in response to cyclic stretch remains an elusive issue that has not been extensively studied in the literature from both the biological and modelling perspectives yet. This is quite surprising since neuronal cells are constantly exposed to cyclic strain in physiological conditions. Moreover, determining the right directionality of the growth of neural cells is a critical step in nerve regeneration engineering and functional recovery of the nervous systems. It is also true that, due to their peculiar morphology, mathematical modelling of neuron cells is quite challenging, which is why it is a flourishing field for research.

In this dissertation, we presented a new model for the reorientation and growth of neurons in response to cyclic stretching. The model has been created by adapting the linear viscoelastic model for cell reorientation given in [1] and the tubulin-driven axonal outgrowth model in [48]. In our model, the neuron is divided into soma, axonal shaft and growth cone. The externally imposed cyclic stretch triggers the growth cone reorientation that consequently guides the axon. The axonal outgrowth relies instead on the polymerization of free tubulin transported from the soma to the growth cone via a convection-diffusion process. We were able to numerically simulate the neuron reorientation process considering different combinations of stretching frequencies and strain amplitudes. All the results were then validated by comparing the simulation to the experimental evidence in [4]. In particular, our model seems to finely reproduce the neuron behaviours at relatively high-frequency stretching conditions and in the long term. However, more work should be done to improve the reproduction of the reorientation process at low-frequency values and shorter periods.

Our study has been conducted by making some simplifications and has some

limitations that might be interesting to address in future work. We assumed to work considering the substrate's mechanical behaviour as linear. This is quite a strong assumption considering that in some of the experiments, the strain rate values used are considerably high. In order to make our model more reliable in reproducing neuron behaviour under extreme stretching conditions, we can consider dropping this simplification and formulate a new model in the future in which we consider the nonlinearities of the substrate deformation. Such a model could also be written and solved in the Eulerian frame to obtain a more realistic representation of the neurons' behaviour. This would involve considering the changes in growth cone position and orientation in the deformed configuration, as well as how the axon would deform by changing its length, and how the tubulin transport process would be affected by these factors.

We then supposed that the cellular structures do not modify the mechanical behaviour of the substrate alone which remains isotropic. However, we showed how it is acknowledged that the growth cone actually exerts a traction force on the substrate to pull the axon in the axonal guidance process. Hence, to create a more realistic model, the interaction between the neuron and the substrate could be taken into account since it modifies the stresses and strains of the substrate itself. This would require describing the process of adhesion formation and detachment along the axons and the growth cone.

Another simple extension to our model could be to add a tension-dependent term on the axon growth model. In our specific case, this dependency has been excluded just because in the experimental results reported in [4] the cyclic stretch seems not to enhance the outgrowth velocity of neurites. However, we saw how in many other studies tension led to a higher axonal elongation rate. Maybe we can hypothesise that the higher the tension on the axon, the higher the tubulin production in the soma or the higher the polymerization rate in the soma or the faster the transport along the axonal shaft.

Some modifications can be done also from the numerical implementation perspective. In fact, for time discretization we used for the sake of simplicity an explicit Euler method. However, it requires very little time steps Δt to guarantee numerical stability. Since we need to simulate experiments that last for days for a significant number of neuron cells, the computing time required to get our result is quite high. So, a more efficient numerical scheme can be introduced to discretize the model in time. Furthermore, some work should be addressed to rigorously prove the existence and uniqueness of solutions in our model.

In conclusion, the hope is that in the future, further experiments will be carried out to better investigate the reorientation process of neurons subjected to cyclic stretch. By doing so, it will be possible to have a better comprehension of the phenomenon, identify its key mechanisms, and develop more precise mathematical models.

Bibliography

[1] G. Lucci, C. Giverso, and L. Preziosi. «Cell Orientation under Stretch: Stability of a Linear Viscoelastic Model». In: *Mathematical Biosciences* (2021) (cit. on pp. 1, 10, 11, 15–17, 26–30, 37, 45, 53, 65).

[2] G. Lucci and L. Preziosi. «A Nonlinear Elastic Description of Cell Preferential Orientations over a Stretched Substrate». In: *Biomechanics and Modeling in Mechanobiology* 20.2 (Apr. 2021), pp. 631–649. DOI: 10.1007/s10237-020-01406-4 (cit. on pp. 1, 22, 26, 29, 30).

[3] C. Giverso, N. Loy, G. Lucci, and L. Preziosi. «Cell orientation under stretch: A review of experimental findings and mathematical modelling». Unpublished (cit. on pp. 1, 10, 11, 15, 28).

[4] J. Lin, X. Li, J. Yin, and J. Qian. «Effect of Cyclic Stretch on Neuron Reorientation and Axon Outgrowth». In: *Frontiers in Bioengineering and Biotechnology* 8 (Dec. 14, 2020), p. 597867. DOI: 10.3389/fbioe.2020.597867 (cit. on pp. 1, 12, 13, 15, 16, 20, 23, 26, 28, 44–46, 49–57, 60, 61, 64–66).

[5] K. Franze. «The Mechanical Control of Nervous System Development». In: *Development* 140.15 (Aug. 1, 2013), pp. 3069–3077. DOI: 10.1242/dev.079145 (cit. on pp. 1–3).

[6] B. J. Pfister, J. M. Grasman, and J. R. Loverde. «Exploiting Biomechanics to Direct the Formation of Nervous Tissue». In: *Current Opinion in Biomedical Engineering* 14 (June 2020), pp. 59–66. DOI: 10.1016/j.cobme.2020.05.009 (cit. on p. 1).

[7] J.-A. Abraham. «Influence of cyclic mechanical strain on tissues of the central nervous system». PhD thesis. Univ. of Bonn, May 2020 (cit. on pp. 1, 2, 9).

[8] B. J. Pfister, A. Iwata, D. F. Meaney, and D. H. Smith. «Extreme Stretch Growth of Integrated Axons». In: *The Journal of Neuroscience* 24.36 (Sept. 8, 2004), pp. 7978–7983. DOI: 10.1523/JNEUROSCI.1974-04.2004 (cit. on pp. 2, 4, 8).

[9] P. K. Purohit and D. H. Smith. «A Model for Stretch Growth of Neurons». In: *Journal of Biomechanics* 49.16 (Dec. 2016), pp. 3934–3942. DOI: 10.1016/j.jbiomech.2016.11.045 (cit. on p. 2).

[10] J. H.-C. Wang. «Substrate Deformation Determines Actin Cytoskeleton Reorganization: A Mathematical Modeling and Experimental Study». In: *Journal of Theoretical Biology* 202.1 (Jan. 2000), pp. 33–41. DOI: 10.1006/jtbi.1999.1035 (cit. on pp. 2, 15, 28).

[11] S. Shah, J. Chetta, and B. Bober. «Axonal Transport and Neuromechanics:» in: *Molecular and Cellular Biomechanics*. Ed. by Bradley Layton. Pan Stanford, Apr. 3, 2015, pp. 99–126. DOI: 10.1201/b18093-7 (cit. on p. 3).

[12] K. Franze. «Integrating Chemistry and Mechanics: The Forces Driving Axon Growth». In: *Annual Review of Cell and Developmental Biology* 36.1 (Oct. 6, 2020), pp. 61–83. DOI: 10.1146/annurev-cellbio-100818-125157 (cit. on pp. 3, 4, 6).

[13] D. V. Lowery L. A.and Vactor. «The Trip of the Tip: Understanding the Growth Cone Machinery». In: *Nature Reviews Molecular Cell Biology* 10.5 (May 2009), pp. 332–343. DOI: 10.1038/nrm2679 (cit. on pp. 4, 5).

[14] H. Oliveri and A. Goriely. «Mathematical Models of Neuronal Growth». In: *Biomechanics and Modeling in Mechanobiology* 21.1 (Feb. 2022), pp. 89–118. DOI: 10.1007/s10237-021-01539-0 (cit. on pp. 4, 13).

[15] P. Lamoureux, R. Buxbaum, and S. Heidemann. «Direct evidence that growth cones pull». In: *Nature* 340.6229 (July 1989), pp. 159–162. DOI: 10.1038/340159a0 (cit. on p. 4).

[16] P. Weiss. «NERVE PATTERNS: THE MECHANICS OF NERVE GROWTH». In: *Dynamics of Development: Experiments and Inferences*. Elsevier, 1968, pp. 445–485. DOI: 10.1016/B978-1-4832-2919-5.50026-X (cit. on p. 6).

[17] D. Bray. «Axonal Growth in Response to Experimentally Applied Mechanical Tension». In: *Developmental Biology* 102.2 (1984), pp. 379–389. DOI: 10.1016/0012-1606(84)90202-1 (cit. on p. 6).

[18] T. J. Dennerll, P. Lamoureux, R. E. Buxbaum, and S. R. Heidemann. «The Cytomechanics of Axonal Elongation and Retraction.» In: *Journal of Cell Biology* 109.6 (Dec. 1, 1989), pp. 3073–3083. DOI: 10.1083/jcb.109.6.3073 (cit. on pp. 6–8, 13, 23).

[19] J. Zheng, P. Lamoureux, V. Santiago, T. Dennerll, R. Buxbaum, and S. Heidemann. «Tensile Regulation of Axonal Elongation and Initiation». In: *The Journal of Neuroscience* 11.4 (Apr. 1, 1991), pp. 1117–1125. DOI: 10.1523/JNEUROSCI.11-04-01117.1991 (cit. on p. 6).

[20] D. Zhang, H. Suo, J. Qian, J. Yin, J. Fu, and Y. Huang. «Physical Understanding of Axonal Growth Patterns on Grooved Substrates: Groove Ridge Crossing versus Longitudinal Alignment». In: *Bio-Design and Manufacturing* 3.4 (Dec. 2020), pp. 348–360. DOI: 10.1007/s42242-020-00089-1 (cit. on pp. 7, 10, 15, 23).

[21] J. Rajagopalan, A. Tofangchi, and M. T. A. Saif. «Drosophila Neurons Actively Regulate Axonal Tension In Vivo». In: *Biophysical Journal* 99.10 (Nov. 2010), pp. 3208–3215. DOI: 10.1016/j.bpj.2010.09.029 (cit. on pp. 7, 8, 23).

[22] D. Koch, W. J. Rosoff, J. Jiang, H. M. Geller, and J. S. Urbach. «Strength in the Periphery: Growth Cone Biomechanics and Substrate Rigidity Response in Peripheral and Central Nervous System Neurons». In: *Biophysical Journal* 102.3 (Feb. 2012), pp. 452–460. DOI: 10.1016/j.bpj.2011.12.025 (cit. on p. 9).

[23] D. E. Koser et al. «Mechanosensing Is Critical for Axon Growth in the Developing Brain». In: *Nature Neuroscience* 19.12 (Dec. 2016), pp. 1592–1598. DOI: 10.1038/nn.4394 (cit. on pp. 9, 14).

[24] Y.-J. Chang, C.-J. Tsai, F.-G. Tseng, T.-J. Chen, and T.-W. Wang. «Micropatterned Stretching System for the Investigation of Mechanical Tension on Neural Stem Cells Behavior». In: *Nanomedicine: Nanotechnology, Biology and Medicine* 9.3 (Apr. 2013), pp. 345–355. DOI: 10.1016/j.nano.2012.07.008 (cit. on p. 10).

[25] J. M. Vensi Basso, I. Yurchenko, M. Simon, D. J. Rizzo, and C. Staii. «Role of Geometrical Cues in Neuronal Growth». In: *Physical Review E* 99.2 (Feb. 11, 2019), p. 022408. DOI: 10.1103/PhysRevE.99.022408 (cit. on pp. 10, 23).

[26] J. P. Sunnerberg, M. Descoteaux, D. L. Kaplan, and C. Staii. «Axonal Growth on Surfaces with Periodic Geometrical Patterns». In: *PLOS ONE* 16.9 (Sept. 23, 2021). Ed. by Etienne Dague, e0257659. DOI: 10.1371/journal.pone.0257659 (cit. on pp. 10, 23).

[27] F. Johansson, P. Carlberg, N. Danielsen, L. Montelius, and M. Kanje. «Axonal Outgrowth on Nano-Imprinted Patterns». In: *Biomaterials* 27.8 (Mar. 2006), pp. 1251–1258. DOI: 10.1016/j.biomaterials.2005.07.047 (cit. on pp. 10, 23).

[28] H. Suo, Z. Wang, G. Dai, J. Fu, J. Yin, and L. Chang. «Polyacrylonitrile Nerve Conduits With Inner Longitudinal Grooved Textures to Enhance Neuron Directional Outgrowth». In: *Journal of Microelectromechanical Systems* 27.3 (June 2018), pp. 457–463. DOI: 10.1109/JMEMS.2018.2810097 (cit. on pp. 10, 23).

[29] W. Li, Q. Y. Tang, A. D. Jadhav, A. Narang, W. X. Qian, P. Shi, and S. W. Pang. «Large-Scale Topographical Screen for Investigation of Physical Neural-Guidance Cues». In: *Scientific Reports* 5.1 (Mar. 2, 2015), p. 8644. DOI: 10.1038/srep08644 (cit. on pp. 10, 23).

[30] A. Livne, E. Bouchbinder, and B. Geiger. «Cell Reorientation under Cyclic Stretching». In: *Nature Communications* 5.1 (May 30, 2014), p. 3938. DOI: 10.1038/ncomms4938 (cit. on pp. 10, 11, 15, 28, 30).

[31] R. De, A. Zemel, and S. A. Safran. «Dynamics of Cell Orientation». In: *Nature Physics* 3.9 (Sept. 2007), pp. 655–659. DOI: 10.1038/nphys680 (cit. on pp. 10, 15).

[32] R. Kaunas. «Sarcomeric Model of Stretch-Induced Stress Fiber Reorganization». In: *Cell Health and Cytoskeleton* (Dec. 2010), p. 13. DOI: 10.2147/CHC.S14984 (cit. on pp. 10, 15).

[33] U. Faust, N. Hampe, W. Rubner, N. Kirchgeßner, S. Safran, B. Hoffmann, and R. Merkel. «Cyclic Stress at mHz Frequencies Aligns Fibroblasts in Direction of Zero Strain». In: *PLoS ONE* 6.12 (Dec. 16, 2011). Ed. by Markus J. Buehler, e28963. DOI: 10.1371/journal.pone.0028963 (cit. on pp. 10, 15, 28).

[34] J. A. Abraham, C. Linnartz, G. Dreissen, R. Springer, S. Blaschke, M. A. Rueger, G. R. Fink, B. Hoffmann, and R. Merkel. «Directing Neuronal Outgrowth and Network Formation of Rat Cortical Neurons by Cyclic Substrate Stretch». In: *Langmuir* 35.23 (June 11, 2019), pp. 7423–7431. DOI: 10.1021/acs.langmuir.8b02003 (cit. on pp. 10, 11).

[35] F. Haq, C. Keith, and G. Zhang. «Neurite Development in PC12 Cells on Flexible Micro-Textured Substrates under Cyclic Stretch». In: *Biotechnology Progress* 22.1 (Feb. 3, 2006), pp. 133–140. DOI: 10.1021/bp0501625 (cit. on pp. 11, 23).

[36] Bernadette Brady, Gerard King, Ross T. Murphy, and Declan Walsh. «Myocardial Strain: A Clinical Review». In: *Irish Journal of Medical Science (1971 -)* 192.4 (Aug. 2023), pp. 1649–1656. DOI: 10.1007/s11845-022-03210-8 (cit. on p. 11).

[37] Arianna Carnevale, Emiliano Schena, Domenico Formica, Carlo Massaroni, Umile Giuseppe Longo, and Vincenzo Denaro. «Skin Strain Analysis of the Scapular Region and Wearables Design». In: *Sensors* 21.17 (Aug. 26, 2021), p. 5761. DOI: 10.3390/s21175761 (cit. on p. 11).

[38] S. Higgins, J. . Lee, L. Ha, and J. Y. Lim. «Inducing Neurite Outgrowth by Mechanical Cell Stretch». In: *BioResearch Open Access* 2.3 (June 2013), pp. 212–216. DOI: 10.1089/biores.2013.0008 (cit. on p. 11).

[39] Y. Ishibashi, K. Uesugi, and K. Morishima. «Effect of Mechanical Stimulation on Neurite Outgrowth of Dorsal Root Ganglion Neurons toward Integrative Mechanobiologic Nerve Bridge». In: Sapporo, Japan: IEEE, Dec. 2016, pp. 797–802. DOI: 10.1109/SII.2016.7844097 (cit. on p. 11).

[40] F. Schneider, T. Fellner, J. Wilde, and U. Wallrabe. «Mechanical Properties of Silicones for MEMS». In: *Journal of Micromechanics and Microengineering* 18.6 (June 1, 2008), p. 065008. DOI: 10.1088/0960-1317/18/6/065008 (cit. on p. 12).

[41] T. K. Kim, J. K. Kim, and O. C. Jeong. «Measurement of Nonlinear Mechanical Properties of PDMS Elastomer». In: *Microelectronic Engineering* 88.8 (Aug. 2011), pp. 1982–1985. DOI: 10.1016/j.mee.2010.12.108 (cit. on pp. 12, 20, 28).

[42] J. D. Glover, C. E. McLaughlin, M. K. McFarland, and J. T. Pham. «Extracting Uncrosslinked Material from Low Modulus Sylgard 184 and the Effect on Mechanical Properties». In: *Journal of Polymer Science* 58.2 (2020), pp. 343–351. DOI: 10.1002/pol.20190032 (cit. on p. 12).

[43] I. D. Johnston, D. K. McCluskey, C. K. L. Tan, and M. C. Tracey. «Mechanical Characterization of Bulk Sylgard 184 for Microfluidics and Microengineering». In: *Journal of Micromechanics and Microengineering* 24.3 (Mar. 1, 2014), p. 035017. DOI: 10.1088/0960-1317/24/3/035017 (cit. on pp. 12, 44).

[44] R. Bernal, P. A. Pullarkat, and F. Melo. «Mechanical Properties of Axons». In: *Physical Review Letters* 99.1 (July 3, 2007), p. 018301. DOI: 10.1103/PhysRevLett.99.018301 (cit. on p. 13).

[45] M. O'Toole, P. Lamoureux, and K. E. Miller. «A Physical Model of Axonal Elongation: Force, Viscosity, and Adhesions Govern the Mode of Outgrowth». In: *Biophysical Journal* 94.7 (Apr. 2008), pp. 2610–2620. DOI: 10.1529/biophysj.107.117424 (cit. on pp. 13, 14).

[46] D. R. McLean and B. P. Graham. «Mathematical Formulation and Analysis of a Continuum Model for Tubulin-Driven Neurite Elongation». In: *Proceedings of the Royal Society of London. Series A: Mathematical, Physical and Engineering Sciences* 460.2048 (Aug. 8, 2004), pp. 2437–2456. DOI: 10.1098/rspa.2004.1288 (cit. on pp. 13, 14, 32, 39).

[47] B. P. Graham, K. Lauchlan, and D. R. Mclean. «Dynamics of Outgrowth in a Continuum Model of Neurite Elongation». In: *Journal of Computational Neuroscience* 20.1 (Feb. 2006), pp. 43–60. DOI: 10.1007/s10827-006-5330-3 (cit. on pp. 13, 14).

[48] S. Diehl, E. Henningsson, A. Heyden, and S. Perna. «A One-Dimensional Moving-Boundary Model for Tubulin-Driven Axonal Growth». In: *Journal of Theoretical Biology* 358 (Oct. 2014), pp. 194–207. DOI: 10.1016/j.jtbi.2014.06.019 (cit. on pp. 13, 14, 16, 17, 32, 33, 39, 44, 65).

[49] S. Diehl, E. Henningsson, and A. Heyden. «Efficient Simulations of Tubulin-Driven Axonal Growth». In: *Journal of Computational Neuroscience* 41.1 (Aug. 2016), pp. 45–63. DOI: 10.1007/s10827-016-0604-x (cit. on pp. 13, 14, 39).

[50] M. P. V. Veen and J. V. Pelt. «Neuritic Growth Rate Described by Modeling Microtubule Dynamics». In: *Bulletin of Mathematical Biology* 56.2 (), pp. 249–273 (cit. on p. 13).

[51] P. K. Purohit. «Tension Dependent Growth and Retraction of Neurites». In: *Procedia IUTAM* 12 (2015), pp. 185–192. DOI: 10.1016/j.piutam.2014.12.020 (cit. on pp. 13, 14).

[52] J. A. García-Grajales, A. Jérusalem, and . Goriely. «Continuum Mechanical Modeling of Axonal Growth». In: *Computer Methods in Applied Mechanics and Engineering* 314 (Feb. 2017), pp. 147–163. DOI: 10.1016/j.cma.2016.07.032 (cit. on p. 14).

[53] H. Oliveri, K. Franze, and A. Goriely. «Theory for Durotactic Axon Guidance». In: *Physical Review Letters* 126.11 (Mar. 15, 2021), p. 118101. DOI: 10.1103/PhysRevLett.126.118101 (cit. on p. 14).

[54] I. Yurchenko, J. M. Vensi Basso, V. S. Syrotenko, and C. Staii. «Anomalous Diffusion for Neuronal Growth on Surfaces with Controlled Geometries». In: *PLOS ONE* 14.5 (May 6, 2019). Ed. by Keng-Hwee Chiam, e0216181. DOI: 10.1371/journal.pone.0216181 (cit. on p. 15).

[55] Y.C. Fung. *A first course in continuum mechanics / Y.C. Fung*. eng. Englewood: Prentice-Hall, 1969 (cit. on p. 17).

[56] S. Forte, L. Preziosi, and M. Vianello. «Meccanica dei Continui». ita. In: *Meccanica Dei Continui*. Vol. 114. Italy: Springer Milan, 2019. ISBN: 9788847039841 (cit. on p. 17).

[57] I. Yurchenko, M. Farwell, D. D. Brady, and C. Staii. «Neuronal Growth and Formation of Neuron Networks on Directional Surfaces». In: *Biomimetics* 6.2 (June 16, 2021), p. 41. DOI: 10.3390/biomimetics6020041 (cit. on p. 23).

[58] J. Merodio and R.W. Ogden. «The Influence of the Invariant on the Stress–Deformation and Ellipticity Characteristics of Doubly Fiber-Reinforced Non-Linearly Elastic Solids». In: *International Journal of Non-Linear Mechanics* 41.4 (May 2006), pp. 556–563. DOI: 10.1016/j.ijnonlinmec.2006.02.001 (cit. on p. 26).

[59] N. Loy and L. Preziosi. «A Statistical Mechanics Approach to Describe Cell Reorientation Under Stretch». eng. In: *Bulletin of mathematical biology* 85.7 (2023), pp. 60–60 (cit. on pp. 32, 46).

[60] T. Sauer. «Numerical Solution of Stochastic Differential Equations in Finance». In: *Handbook of Computational Finance*. Ed. by Jin-Chuan Duan, Wolfgang Karl Härdle, and James E. Gentle. Berlin, Heidelberg: Springer Berlin Heidelberg, 2012, pp. 529–550. DOI: 10.1007/978-3-642-17254-0_19 (cit. on p. 32).

[61] B. P. Graham and A. Van Ooyen. «Compartmental Models of Growing Neurites». In: *Neurocomputing* 38–40 (June 2001), pp. 31–36. DOI: 10.1016/S0925-2312(01)00463-5 (cit. on p. 32).

[62] Peter W. Baas, C. Vidya Nadar, and Kenneth A. Myers. «Axonal Transport of Microtubules: The Long and Short of It: Axonal Transport of Microtubules». In: *Traffic* 7.5 (May 2006), pp. 490–498 (cit. on p. 43).

[63] M. Caplow and L. Fee. «Dissociation of the Tubulin Dimer Is Extremely Slow, Thermodynamically Very Unfavorable, and Reversible in the Absence of an Energy Source». In: *Molecular Biology of the Cell* 13.6 (June 2002). Ed. by Guido Guidotti, pp. 2120–2131. DOI: 10.1091/mbc.e01-10-0089 (cit. on p. 43).

[64] C. H. Keith. «Slow Transport of Tubulin in the Neurites of Differentiated PC12 Cells». In: *Science, New Series* 235.4786 (1987), pp. 337–339. eprint: 1698602 (cit. on p. 43).

[65] J. T. Kevenaar and C. C. Hoogenraad. «The Axonal Cytoskeleton: From Organization to Function». In: *Frontiers in Molecular Neuroscience* 8 (Aug. 14, 2015). DOI: 10.3389/fnmol.2015.00044 (cit. on p. 43).

[66] A. Müller, M. C. Wapler, and U. Wallrabe. «A Quick and Accurate Method to Determine the Poisson's Ratio and the Coefficient of Thermal Expansion of PDMS». In: *Soft Matter* 15.4 (2019), pp. 779–784. DOI: 10.1039/C8SM02105H (cit. on p. 44).

[67] T. Betz, D. Koch, D. Lim, and J. A. Käs. «Stochastic Actin Polymerization and Steady Retrograde Flow Determine Growth Cone Advancement». In: *Biophysical Journal* 96.12 (June 2009), pp. 5130–5138. DOI: 10.1016/j.bpj.2009.03.045 (cit. on p. 45).

[68] A. Tamada, S. Kawase, F. Murakami, and H. Kamiguchi. «Autonomous Right-Screw Rotation of Growth Cone Filopodia Drives Neurite Turning». In: *Journal of Cell Biology* 188.3 (Feb. 8, 2010), pp. 429–441. DOI: 10.1083/jcb.200906043 (cit. on p. 45).

[69] A. Colombi, S. Falletta, M. Scianna, and L. Scuderi. «An Integro-Differential Non-Local Model for Cell Migration and Its Efficient Numerical Solution». In: *Mathematics and Computers in Simulation* 180 (Feb. 2021), pp. 179–204. DOI: 10.1016/j.matcom.2020.08.020.

[70] S. Biringen. «A Note on the Numerical Stability of the Convection-Diffusion Equation». In: *Journal of Computational and Applied Mathematics* 7.1 (Mar. 1981), pp. 17–20. DOI: 10.1016/0771-050X(81)90002-4.

[71] H. E. Pettermann and A. DeSimone. «An Anisotropic Linear Thermo-Viscoelastic Constitutive Law: Elastic Relaxation and Thermal Expansion Creep in the Time Domain». In: *Mechanics of Time-Dependent Materials* 22.4 (Nov. 2018), pp. 421–433. DOI: 10.1007/s11043-017-9364-x.

[72] H. E. Pettermann, C. Cheyrou, and A. DeSimone. «Modeling and Simulation of Anisotropic Linear Viscoelasticity: Direction Dependent Time–Temperature-Shift Functions». In: *Mechanics of Time-Dependent Materials* 25.4 (Dec. 2021), pp. 679–689. DOI: 10.1007/s11043-020-09468-8.

[73] L. M. Wang and E. Kuhl. «Viscoelasticity of the Axon Limits Stretch-Mediated Growth». In: *Computational Mechanics* 65.3 (Mar. 2020), pp. 587–595. DOI: 10.1007/s00466-019-01784-2.

[74] M. Imura, S. Yamada, K. Yamamoto, Y. Morita, and E. Nakamachi. «Development of a Three-Dimensional Cell Culture System for the Enhancement of Nerve Axonal Extension by Cyclic Stretch Stimulation». In: *Journal of Biomechanical Science and Engineering* 15.4 (2020), pp. 20-00094-20–00094. DOI: 10.1299/jbse.20-00094.

[75] K. Xu, X. Liu, X. Li, J. Yin, P. Wei, J. Qian, and J. Sun. «Effect of Electrical and Electromechanical Stimulation on PC12 Cell Proliferation and Axon Outgrowth». In: *Frontiers in Bioengineering and Biotechnology* 9 (Oct. 21, 2021), p. 757906. DOI: 10.3389/fbioe.2021.757906.

[76] H. Oliveri, R. De Rooij, E. Kuhl, and A. Goriely. «Rheology of Growing Axons». In: *Physical Review Research* 4.3 (Aug. 12, 2022), p. 033125. DOI: 10.1103/PhysRevResearch.4.033125.

[77] K. E. Miller and D. C. Samuels. «The Axon as a Metabolic Compartment: Protein Degradation, Transport, and Maximum Length of an Axon». In: *Journal of Theoretical Biology* 186.3 (June 1997), pp. 373–379. DOI: 10.1006/jtbi.1996.0355.

[78] J. A. Galbraith and P. E. Gallant. «Axonal Transport of Tubulin and Actin». In: *Journal of Neurocytology* 29 (2000), pp. 889–911.

[79] J. A. Galbraith, T. S. Reese, M. L. Schlief, and P. E. Gallant. «Slow Transport of Unpolymerized Tubulin and Polymerized Neurofilament in the Squid Giant Axon». In: *Proceedings of the National Academy of Sciences* 96.20 (Sept. 28, 1999), pp. 11589–11594. DOI: 10.1073/pnas.96.20.11589.

[80] P. C. Kerstein, R. H. Nichol IV, and T. M. Gomez. «Mechanochemical Regulation of Growth Cone Motility». In: *Frontiers in Cellular Neuroscience* 9 (July 7, 2015). DOI: 10.3389/fncel.2015.00244.

[81] R. W. Gundersen and J. N. Barrett. «Characterization of the Turning Response of Dorsal Root Neurites toward Nerve Growth Factor.» In: *Journal of Cell Biology* 87.3 (Dec. 1, 1980), pp. 546–554. DOI: 10.1083/jcb.87.3.546.

[82] E. M. Craig. «Model for Coordination of Microtubule and Actin Dynamics in Growth Cone Turning». In: *Frontiers in Cellular Neuroscience* 12 (Oct. 31, 2018), p. 394. DOI: 10.3389/fncel.2018.00394.

[83] D Bray and K Chapman. «Analysis of Microspike Movements on the Neuronal Growth Cone». In: *The Journal of Neuroscience* 5.12 (Dec. 1, 1985), pp. 3204–3213. DOI: 10.1523/JNEUROSCI.05-12-03204.1985.

[84] T. Betz, D. Koch, Y.-B. Lu, K. Franze, and J. A. Käs. «Growth Cones as Soft and Weak Force Generators». In: *Proceedings of the National Academy of Sciences* 108.33 (Aug. 16, 2011), pp. 13420–13425. DOI: 10.1073/pnas.1106145108.

[85] J. Aletta and L. Greene. «Growth Cone Configuration and Advance: A Time-Lapse Study Using Video- Enhanced Differential Interference Contrast Microscopy». In: *The Journal of Neuroscience* 8.4 (Apr. 1, 1988), pp. 1425–1435. DOI: 10.1523/JNEUROSCI.08-04-01425.1988.

[86] I D Johnston, D K McCluskey, C K L Tan, and M C Tracey. «Mechanical Characterization of Bulk Sylgard 184 for Microfluidics and Microengineering». In: *Journal of Micromechanics and Microengineering* 24.3 (Mar. 1, 2014), p. 035017. DOI: 10.1088/0960-1317/24/3/035017.